# The Triassic Period

**Chapter** · January 2020

DOI: 10.1016/B978-0-12-824360-2.00025-5



**4 authors**, including:

James Ogg
Purdue University
**297** PUBLICATIONS **22,407** CITATIONS
SEE PROFILE

M. J. Orchard
Natural Resources Canada
**280** PUBLICATIONS **7,162** CITATIONS
SEE PROFILE

H. Jiang
China University of Geosciences
**64** PUBLICATIONS **3,534** CITATIONS
SEE PROFILE

J.G. Ogg and Z.-Q. Chen
With contributions by M.J. Orchard and H.S. Jiang

Chapter 25

# The Triassic Period

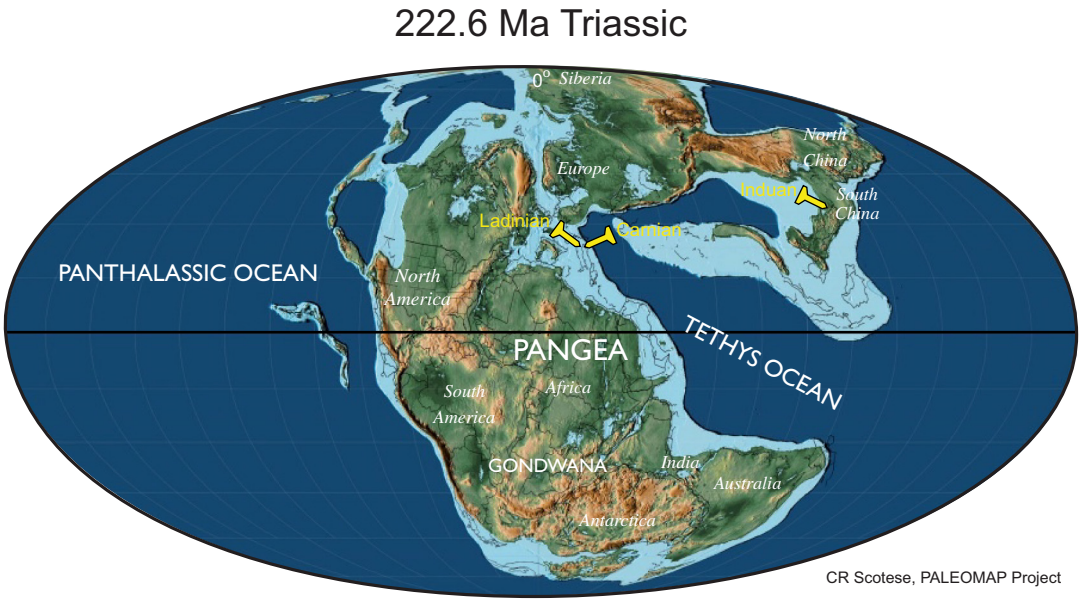


## Chapter outline



**Abstract**

The Triassic is bound by two mass extinctions that coincide with vast outpourings of volcanic flood basalts. The Mesozoic begins with a gradual recovery of plant and animal life after the end-Permian mass extinction. Conodonts and ammonoids are the main correlation tools for marine deposits. The Pangea supercontinent has no known glacial episodes during the Triassic, but the modulation of its monsoonal climate by Milankovitch cycles left sedimentary signatures useful for high-resolution scaling. Dinosaurs begin to dominate the terrestrial ecosystems in latest Triassic. In contrast to the rapid evolution and pronounced environmental changes that characterize the Early Triassic through Carnian, the Norian–Rhaetian of the Late Triassic was an unusually long interval of stability in Earth history.

**Geologic Time Scale 2020. DOI:** https://doi.org/10.1016/B978-0-12-824360-2.00025-5

Our understanding of the Triassic underwent a revolution during the past two decades. Collaborations among geochemists, paleomagnetists, paleontologists, and other stratigraphers have concentrated on its exciting boundary intervals but have also enabled compilation of a comparatively detailed bio-mag-geochem-cyclostratigraphy scale for much of the Triassic (Fig. 25.1). High-precision radioisotopic dates and cyclostratigraphic studies, coupled with enhanced methods for global correlation and detailed compilations of geochemical oscillations, have revealed a startling inequality in duration of Triassic subdivisions and in the paces of evolutionary and environmental change. The latest Permian through Early Triassic has been revealed as an extraordinary interval of pronounced environmental stress and extraordinarily rapid evolutionary turnover that one author has termed "The Worst of Times" (Wignall, 2015). In contrast, the Norian of Late Triassic spans nearly three times the duration of the entire Early Triassic without any significant events.

This knowledge and the inevitable new questions and debates have been partially summarized in review articles and special volumes. In particular, the books *Triassic Time Scale* (Lucas, 2010a) and *The Late Triassic World: Earth in a Time of Transition* (Tanner, 2018) contain separate papers on every main stratigraphic topic (e.g., history and status of chronostratigraphy, biostratigraphy of different marine and terrestrial groups, magnetic polarity time scale, radioisotopic age database). Reviews of the history, subdivisions, biostratigraphic zonations, and correlation of individual Triassic stages are compiled in several sources, including *Albertiana* newsletters of The International Commission on Triassic Stratigraphy (https://albertiana-sts.org/), Tozer (1967, 1984), Lucas (2018a), and Tong et al. (2019).

Portions of the following text, especially on the historical background for subdivisions, have been modified from the chapters on Triassic in GTS2012 and GTS2016 (Ogg, 2012; Ogg et al., 2016). As with any review and synthesis, this one compiled in Sept 2019 will quickly become outdated as new major breakthroughs are published.

## 25.1 History and subdivisions

The *Trias* of von Alberti (1834) united a trio of formations widespread in southern Germany—a lower Buntsandstein (colored sandstone), Muschelkalk (clam limestone), and an upper Keuper (nonmarine reddish beds). These continental and shallow-marine formations were difficult to correlate beyond Germany; therefore most of the traditional stages (Anisian, Ladinian, Carnian, Norian, Rhaetian) were named from ammonoid-rich successions of the Northern Calcareous Alps of Austria. However, the stratigraphy of these Austrian tectonic slices proved unsuitable for establishing formal boundary stratotypes, or even deducing the sequential order of the stages (Tozer, 1984). For example, the Norian was originally considered to underlie the Carnian stage, but after a convolute scientific-political debate (reviewed in Tozer, 1984), the Norian was established as the younger stage. Over 50 different stage names have been proposed for subdividing the Triassic (tabulated in Tozer, 1984). European stratigraphers commonly use substages with geographic names, whereas North American stratigraphers prefer a generic lower/middle/upper nomenclature (e.g., Fassanian Substage versus Lower Ladinian).

The Subcommission on Triassic Stratigraphy (International Commission on Stratigraphy) adopted seven standard Triassic stages in 1991 (Visscher, 1992), but the general lack of unambiguous historical precedents for placement of Triassic stage boundaries slowed the establishment of formal Global Boundary Stratotype Section and Points (GSSPs) (Fig. 25.1). As of December 2019, only three stages (Induan, Ladinian, Carnian) have GSSPs; and four stages (Olenekian, Anisian, Norian, Rhaetian) lack an international definition.

The traditional definitions for these stages (and substages) were based on lowest occurrences of ammonoid genera within exposures in the Alpine, Himalayan and Mediterranean regions. Current candidates for the GSSPs for the yet-to-be-defined global stages have focused on utilizing the phosphatic teeth of the enigmatic conodonts as the primary markers, which provide a more widespread method of correlation than ammonoids. However, the possible offsets of the lowest occurrences of preferred conodont markers from the traditional ammonoid zones that had defined the stages, disagreements on the taxonomy of the potential marker conodonts along lineages, and their possible diachroneity in interregional appearances are among the factors that have contributed to the delays in formalizing the GSSPs for the remaining half of the Triassic stages and for standardized recognition of substages. Other factors include difficulties in finding suitable sections that have multiple methods for global correlation and in achieving reliable correlations between tropical Tethyan and cooler Boreal marine realms (e.g., review by Konstantinov and Klets, 2009). As with the majority of the stage boundaries in the geologic time scale that have not yet been formally defined, the controversies lie in the details on how to achieve useful and reliable global correlations.

### 25.1.1 The Permian–Triassic Boundary

#### *25.1.1.1 End-Permian ecological catastrophes and defining the base of the Mesozoic*

The Paleozoic terminated in a complex environmental catastrophe and mass extinction of life. This sharp evolutionary division led Phillips (1840, 1841) to introduce Mesozoic (*middle life*, with Triassic at the base) between the Paleozoic

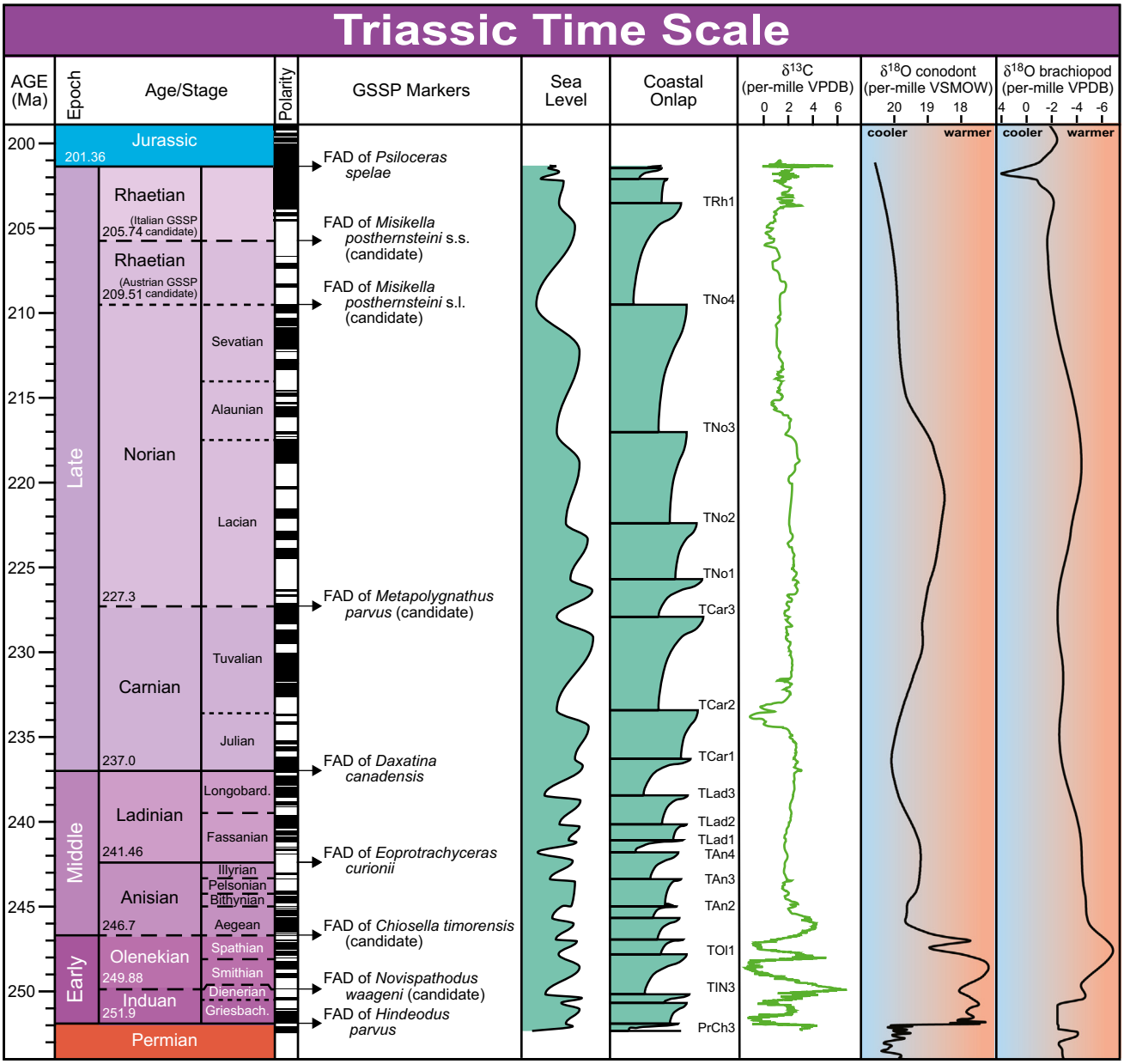


**FIGURE 25.1** Triassic overview. Main markers or candidate markers for GSSPs of Triassic stages are a FAD of ammonoid or conodont taxa as detailed in the text. ("Age" is the term for the time equivalent of the rock-record Stage.) See text for Rhaetian stage boundary options. Magnetic polarity scales from marine sediments are a composite of several syntheses, including Hounslow and Muttoni (2010) and Maron et al. (2015, 2019) with estimated calibrations to the magneto-cyclostratigraphy from thick lacustrine strata in the Newark Basin that span the late Carnian through Rhaetian (Kent and Olsen, 1999; Kent et al., 2017). These magnetic polarity scales are enlarged and detailed in Figs. 25.5– 25.7. Coastal onlap and schematic sea-level curve with labels for selected major sequence boundaries are modified from Haq (2018). See also review in Simmons et al. (2020, Ch. 13: Phanerozoic eustasy, this book). The $\delta^{13}C$ curve is a merger of generalized trends with relative magnitudes (see Cramer and Jarvis 2020, Ch. 11: Carbon isotope stratigraphy, this book), including Early Triassic from Sun et al (2012) and portions of Ladinian through Rhaetian from Muttoni et al. (2014). The Triassic $\delta^{18}O$ curve (inverted scale) is a statistical fit of conodont-apatite data (Grossman and Joachimski, 2020, Ch. 10: Oxygen isotope stratigraphy, this book) including Early Triassic from Sun et al (2012) and Middle and Late Triassic trend from Trotter et al. (2015) and of brachiopod carbonate data. The vertical scale of this diagram is standardized to match the vertical scales of the stratigraphic summary figure at the beginning of each Phanerozoic chapter. The vertical scale of this diagram is standardized to match the vertical scales of the first stratigraphic summary figure in all other Phanerozoic chapters. *FAD*, First-appearance datum; *GSSP*, Global Boundary Stratotype Section and Point; *VPDB*, Vienna PeeDee Belemnite $\delta^{13}C$ and $\delta^{18}O$ standard; *VSMOW*, Vienna Standard Mean Ocean Water $\delta^{18}O$ standard.

(*old life*, ending with the Permian) and Kainozoic (*recent life*, after the Cretaceous). The latest Permian to earliest Triassic events include the progressive disappearance of up to 80% of marine genera, pronounced negative carbon-isotope and strontium-isotope anomalies, the massive flood basalts of the Siberian Traps, widespread anoxic oceanic conditions, a major sea-level regression, and exposure of shelves followed by a major transgression, a "chert gap" and "coal gap," and replacement of reefal ecosystems with microbial-dominated carbonate precipitation (e.g., reviews by Holser and Magaritz, 1987; Erwin, 1993, 2006; Kozur, 1998; Hallam and Wignall, 1999; Erwin et al., 2002; Wignall, 2007; Knoll et al., 2007; Metcalfe and Isozaki, 2009a; Korte et al., 2010; Chen et al., 2014, 2019; Wignall, 2015; Shen et al., 2019; and many other compilations). The majority of ecosystems did not fully recover early Middle Triassic (middle-late Anisian) (Chen and Benton, 2012).

A common hypothesis is that this catastrophe was triggered by the initial phases of the eruption of the Siberian Trap volcanic complex that precipitated a progression of environmental and ecological stresses (e.g., reviews by Erwin, 2006; Chen et al., 2014; Wignall, 2015; Grasby et al., 2016a, 2016b). Most models implicate a release of aerosols and/or carbon dioxide that produced climatic and geochemical impacts on oceanic conditions and on terrestrial systems, although there is not yet a consensus on the relative timing and magnitudes of marine and terrestrial turnovers (e.g., Yin et al., 2007a; Wignall, 2001, 2007; Korte et al., 2010; Isozaki, 2009; Lucas, 2009; Metcalfe and Isozaki, 2009b; Preto et al., 2010). Radioisotopic dating of the Siberian Trap succession and paleontology of intertrap levels correlate well to the dating of the Permian–Triassic boundary interval (Burgess et al., 2014).

The mass disappearance of the Paleozoic fauna and flora, coupled with the widespread occurrence of a major regression-transgression unconformity in most regions, led to a dilemma (Baud, 2014). It was easy to recognize the bleak final act of the Permian, but how should the beginning of the Mesozoic be defined? The base of the Buntsandstein in SW Germany defined the original Trias concept (von Alberti, 1834), but it is a diachronous boundary within continental beds, now assigned to the upper Permian. Similarly, the base of the Werfen Group (base of Tesero Oolite) in the Italian Alps is a diachronous facies boundary. Ammonoids are the common biostratigraphic tool throughout the Mesozoic, and the *Otoceras* ammonoid genus was long considered to be the first "Triassic" form. Therefore Griesbach (1880) assigned the Triassic base to the base of the *Otoceras woodwardi* Zone in the Himalayan region, but this species is only known from the Perigondwana paleomargin of eastern Tethys (e.g., Iran to Nepal). The first occurrence of *Otoceras* species in the Arctic realm (*Otoceras concavum* Zone) was used by Tozer (1967, 1986, 1994) for a Boreal marker of the base of the Triassic but is now known to appear significantly prior to *O. woodwardi* in the Tethyan realm (Krystyn and Orchard, 1996). The progressive evolution of the conodont *Hindeodus* genus through the Permian–Triassic boundary interval provided global correlation markers with no obvious facies dependence; however, conodont biostratigraphy requires special processing and identification experience. Nonbiological correlation markers, such as carbon-isotope excursions or magnetic polarity changes, are conclusive when preserved (e.g., Newell, 1994) but can suffer from diagenetic overprints.

In 2000 the Triassic Subcommission chose the first occurrence of the conodont *Hindeodus parvus* (=*Isarcicella parva* of some earlier conodont studies) within the evolutionary lineage *Hindeodus typicalis–Hindeodus latidentatus–Hindeodus praeparvus–H. parvus–Hindeodus postparvus* as the primary correlation marker for the base of the Mesozoic and Triassic. This biostratigraphic event is the first cosmopolitan correlation level associated with the initial stages of recovery following the end-Permian mass extinctions and environmental changes. Global correlations indicate that this conodont species appears just after the carbon-isotope ($\delta^{13}C_{carb}$) minimum, although its lowest occurrence may be slightly earlier in some local successions (e.g., Payne et al., 2009). This level is slightly lower than the base of the *O. woodwardi* ammonoid zone of the Himalayas. The revised definition for the base-Triassic assigns the *O. concavum* and lowermost portion of *Otoceras boreale* ammonoid zones of the Arctic (the lower part of the "Griesbachian" Substage of Tozer, 1967) into the Permian (e.g., Henderson and Baud, 1997; Baud, 2001, 2014; Baud and Beauchamp, 2001).

In continental settings, the correlated level to this conodont event is close to the disappearance of typical Permian *Dicynodon* tetrapods after an interval of co-occurrence with "Triassic" dicynodont *Lystrosaurus* (Kozur, 1998).

The choice of the first appearance of this conodont to serve as the primary marker for the beginning of the Triassic implies that former traditional concepts of the Permian–Triassic boundary, such as the disappearance of typical Permian marine fauna, rapid facies changes, extensive volcanism, and onset of isotope anomalies, are now assigned to the latest Permian.

### 25.1.1.2 Paleozoic–Mesozoic boundary stratotype (base of Triassic)

The GSSP for the base of the Mesozoic Erathem, the Triassic System, and the Induan Stage is at the base of Bed 27c at a section near Meishan, Zhejiang Province, southern China (Fig. 25.2). This level coincides with the lowest occurrence of conodont *H. parvus* (Yin et al., 2001, 2005). This level was preceded by a pronounced brief negative excursion in carbon isotopes (up to −6‰ $\delta^{13}C_{carb}$ relative to the late-Changhsingian *Clarkina yini* conodont zone) and is within a rapid ~9°C increase in local sea-surface

# Base of the Induan Stage of the Triassic System at Meishan, China

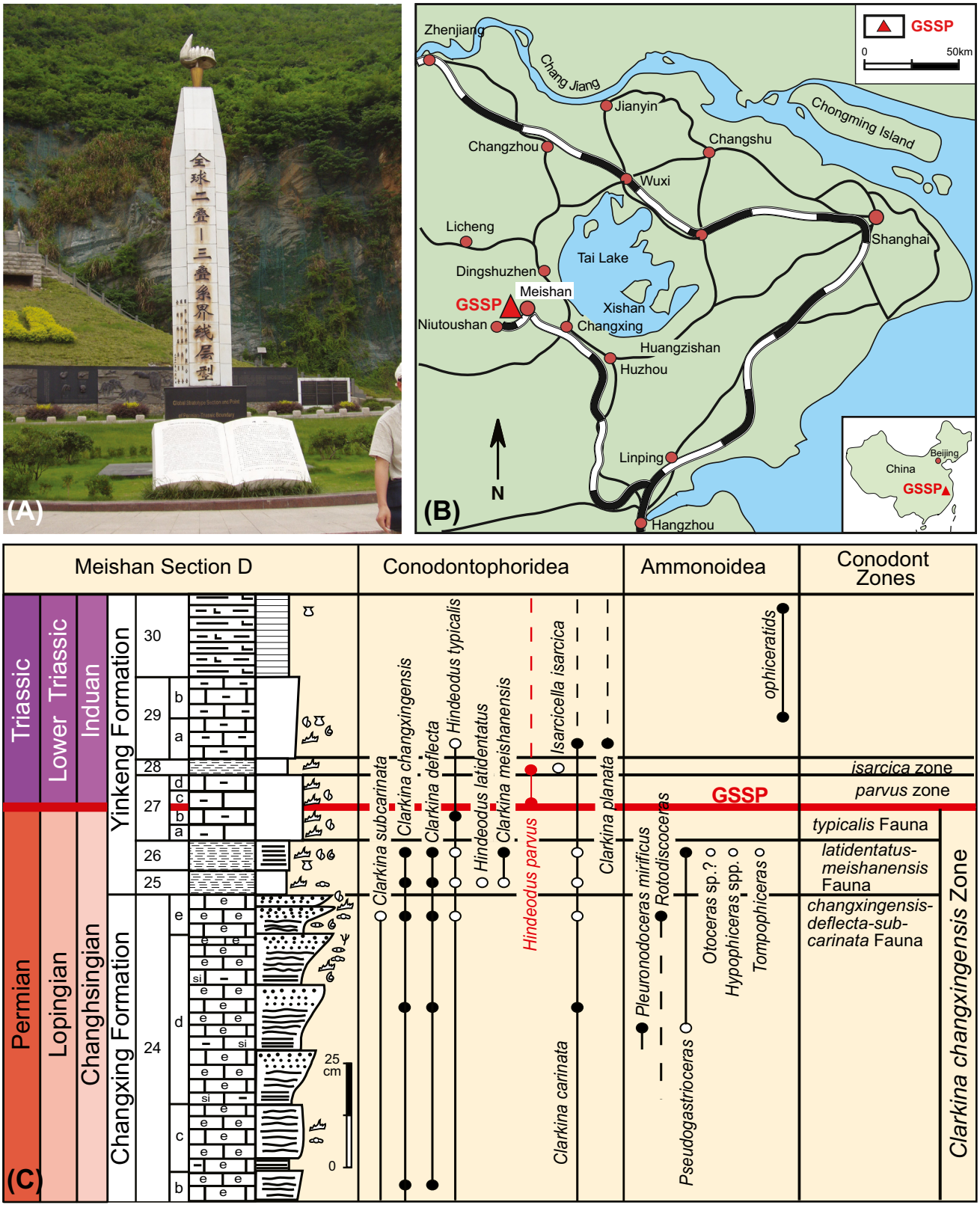


**FIGURE 25.2** GSSP for the base of the Triassic (base of Mesozoic; base of Induan Stage) at the Meishan section, South China. The GSSP level coincides with the lowest occurrence of conodont *Hindeodus parvus* and is within a major negative excursion in carbon isotopes. Note that vertical scale is in centimeters to show details of this boundary interval. Conodont ranges are from the ratified GSSP document (Yin et al., 2001), but later studies have revised the assignments (see Chen et al., 2015, and Fig. 24.6 in Henderson and Shen, 2020, Ch. 24: The Permian Period, this volume). Zircons from the altered volcanic-ash components in Bed 25 and Bed 28 have been dated (e.g., Burgess et al., 2014; Shen et al., 2019). The main end-Permian mass extinction event is at the base of Bed 25. The GSSP is preserved within a GeoPark, with the GSSP site located at the top of the stairs on the right side of the decorative wall behind the monument topped by a statue of the conodont. The GSSP for the base of the Changhsingian Stage (uppermost Permian) is in the lower quarry wall beyond the right side of the photo. *GSSP*, Global Boundary Stratotype Section and Point.

temperature (reviewed by Chen et al., 2015). The underlying Bed 25 is coincident with the main end-Permian mass extinction and has been dated as 251.939 ± 0.031 Ma (Shen et al., 2019).

This Meishan section also hosts the GSSP for the underlying Changhsingian Stage of uppermost Permian and is within a special GeoPark that includes a museum of Earth's history. Indeed, the park-like setting with sculptures and educational exhibitions is probably the most impressive GSSP site worldwide.

This GSSP level is bracketed by volcanic-ash beds, thereby enabling precise radioisotopic ages for both the main end-Permian mass extinction and the base of the Triassic. The former "boundary clay" bentonite (Bed 25) at approximately 18 cm below the GSSP has been sampled extensively as the techniques for Ar/Ar and U/Pb radioisotopic dating evolved in methodology and precision (e.g., Renne et al., 1995; Bowring et al., 1998; Metcalfe et al., 1999; Erwin et al., 2002; Mundil et al., 2001, 2004, 2010; Shen et al., 2010; Burgess et al., 2014). This "boundary clay" is now placed approximately two brief conodont zones below the base of the Triassic. Another volcanic-ash clay approximately 8 cm above the GSSP (Bed 28) enables a narrow bracketing of the age of the Permian–Triassic boundary. Therefore this is one of the few boundary GSSPs that can be precisely dated by radioisotope methods. As techniques and calibrations have evolved, the measured date for this boundary level has progressively shifted to older ages, from c. 248 to c. 252 Ma.

Other important reference sections for the events across the Permian–Triassic boundary are in the Dolomites of Italy (e.g., Broglio Loriga and Cassinis, 1992; Wignall and Hallam, 1992), in the Canadian Arctic (e.g., Tozer, 1967), in the Salt Ranges of Pakistan (e.g., Baud et al., 1996), the Guryul Ravine section in Kashmir (Kapoor, 1996), in sections within Iran (e.g., Kozur, 2007), in marine and terrestrial strata in South China (e.g., Yin et al., 2007b; Metcalfe et al., 2009; Glen et al., 2009), and in terrestrial beds of the Karoo Basin.

## 25.1.2 Subdivisions of the Lower Triassic

A multitude of stage and substage nomenclatures have been applied to the Lower Triassic interval. The Triassic Subcommission adopted the current subdivision into a lower Induan stage and an upper Olenekian stage in 1991. The Induan and Olenekian stages of Kiparisova and Popov (1956, revised in 1964) were named after exposures in the Indus River basin in the Hindustan region of Asia and in the lower reaches of the Olenek River basin of northeast Siberia, respectively.

A suite of four substages is widely used. In an imaginative procedural twist, these Griesbachian, Dienerian, Smithian, and Spathian substages are named after exposures along associated small creeks on Ellesmere and Axel Heiberg islands in the Canadian Arctic, which in turn were named after the Triassic paleontologists—Carl L. Griesbach (1847–1907), Carl Diener (1862–1928), James Perrin Smith (1864–1931), and Leon Spath (1888–1957)—who played important roles in Lower Triassic biostratigraphy (Tozer, 1965). These substages were originally defined by grouping of ammonoid zones.

### *25.1.2.1 Induan*

#### 25.1.2.1.1 Griesbachian and Dienerian substages

The Induan Stage is informally divided into two substages. The lower substage, Griesbachian, is named after Griesbach Creek on northwest Axel Heiberg Island. The definition of the Permian–Triassic boundary implies that the lower portion of the original Griesbachian of Tozer (1965, 1967) is now assigned to the uppermost Permian.

The Dienerian Substage is named after Diener Creek of northwest Ellesmere Island. The Griesbachian/Dienerian boundary is marked by the appearance of Gyronitidae ammonoids. This substage boundary is recognized in Canada and in the Himalayas as the boundary between *Otoceras* and *Meekoceras* ammonoid-bearing beds of Diener (1912) and in the Salt Range of Pakistan at the base of the Lower Ceratite Limestone (Tozer, 1967). In conodont zonations the base of the Dienerian has been placed at the base of the conodont *Sweetospathodus kummeli* Zone.

### *25.1.2.2 Olenekian*

#### 25.1.2.2.1 History, definition, and boundary stratotype candidates

The Olenekian Stage was originally proposed from sections in Arctic Siberia, whereas the stratotype for the preceding Induan stage was in the Hindustan region of Pakistan–India. Neither region has fossiliferous strata spanning their mutual boundary—the Induan in the Olenek River basin is marginal marine to lagoonal, and ammonoids in the transitional interval in the Hindustan region are rare or absent (Zakharov, 1994). The lower Olenekian is marked by the appearance of a diverse ammonoid assemblage of *Hedenstroemia*, *Meekoceras*, *Juvenites*, *Pseudoprospingites*, *Arctoceras*, *Flemingites*, and *Euflemingites*. A sea-level regression caused a scarcity of age-diagnostic conodonts and bivalves during the latest Induan to earliest Olenekian, but the transition seems to be within the lower portion of the *Novispathodus pakistanensis* conodont zone (Zakharov, 1994; Paull, 1997; Orchard and Tozer, 1997). Proposed ammonoid-based biostratigraphic definitions of the stage boundary were the highest occurrence of the ammonoid *Gyronites subdharmus* and the lowest occurrence of the representatives of the *Meekoceras* or *Hedenstroemia* ammonoid genera (Zakharov et al., 2000, 2002). The base of its lower Smithian Substage was originally

defined as the base of a broad *Euflemingites romunderi* ammonoid zone (Tozer, 1965, 1967); then the biostratigraphy was revised to add a *Hedenstroemia hedenstroemi* ammonoid zone (e.g., Orchard and Tozer, 1997). Conodonts were undergoing a pronounced evolutionary radiation at the beginning of the Olenekian, and, even though some taxonomic details remain to be resolved, the widespread distribution and resolution of *Neospathodus* species provide the main method for interregional correlations (Orchard, 2010).

Therefore the base-Olenekian task group selected the lowest occurrence of the conodont *Novispathodus waageni sensu lato* as the primary boundary marker. Correlation of ammonoid and conodont events among paleogeographic provinces indicates the first occurrence of *Neospathodus waageni* is in the lowermost part of the *Rohillites rohilla* ammonoid zone in the Spiti region of the Tethyan realm, is slightly below the lowest occurrence of *Flemingites* and *Euflemingites* ammonoid genera in South China of Tethyan realm, and is in the lower part of *Lepiskites kolyhmensis* Zone of Siberia in the Boreal realm which is just above the regional *Hedenstroemia hedenstromia* Zone (Zakharov et al., 2009). This conodont level is just prior to the peak of the first Triassic positive excursion in $\delta^{13}C_{carb}$, at or just below an upward change from a long-duration reversed-polarity to a brief normal-polarity magnetic zone (LT2r of Hounslow and Muttoni, 2010) at Chaohu, and is just above a widely recognizable sequence boundary (e.g., Krystyn et al., 2007a).

There are two leading candidates for the base-Olenekian GSSP. The West Pingdingshan roadside outcrop near quarries at Chaohu city in the Anhui Province of eastern China has biostratigraphy (with a local *Nov. waageni eowaageni* as the lowest subspecies), carbon isotopes, magnetostratigraphy, and cyclostratigraphy (Tong et al., 2004; Sun et al., 2007; Chinese Triassic Working Group, 2007; Zhao et al., 2007, 2008; Li et al., 2016; Lyu et al., 2018, 2020). A section near Mud (Muth) village in the Spiti valley of northwest India has better ammonoid constraints but lacks the magnetostratigraphy and cyclostratigraphy (Krystyn et al., 2007a, 2007b). A preliminary vote to select Mud as the GSSP was put on hold in 2008 when the *Nov. waageni* conodont marker was identified in strata lower than the proposed GSSP level. An integrated magneto-bio-cyclostratigraphy of another boundary reference section at Daxiakou near the Three Gorges Dam in South China seemed to hint that the lowest occurrence of the conodont marker was ~50 kyr earlier than at the Chaohu GSSP candidate (Zhao et al., 2013; Li et al., 2016). A decision on the base-Olenekian GSSP also requires verifying if these Tethyan-based events can be correlated to the Boreal realm.

#### 25.1.2.2.2 Smithian and Spathian substages

A major environmental and evolutionary event at a global scale occurs within the Olenekian (Algeo et al., 2019a, 2019b; Zhang et al., 2019). The boundary between its two substages, the Smithian and the succeeding Spathian, has been termed the "biggest crisis in Triassic conodont history" (Orchard, 2007a; Goudemand et al., 2008). This boundary is marked by a sudden reduction of ammonoid diversity back to initial Triassic conditions and shift from latitudinal to cosmopolitan distributions (Brayard et al., 2009a), and coincides with a major positive peak in Carbon-13 ($\delta^{13}C_{carb}$) and a cooling climatic shift (e.g., Galfetti et al., 2007a; Goudemand et al., 2019; Algeo et al., 2019a, 2019b).

These two informal substages of the Olenekian Stage were named after the Smith and Spath creeks on Ellesmere Island of the Canadian Arctic. The Spathian Substage is characterized by *Tirolites*, *Columbites*, *Subcolumbites*, *Prohungarites*, and *Keyserlingites* ammonoid genera. In these original stratotypes, the Smithian–Spathian boundary was placed at the base of the *Olenekites pilaticus* ammonoid zone, but there appears to be a missing biostratigraphic interval in the type region (Tozer, 1967; Orchard and Tozer, 1997). The ammonoids recovered in early Spathian with a dramatic evolutionary radiation accompanied by the development of a pronounced latitudinal gradient of diversity (Brayard et al., 2009a). In South China, the FAD of conodont *Nov. pingdingshanensis* was selected as the marker of the base of Spathian (Zhao et al., 2007, 2013; Lyu et al., 2019). The exciting discovery of major geochemical, climatic, and paleontological events that coincide with this substage boundary has led to speculations of concurrent volcanic release of carbon dioxide and/or enhanced storage and preservation of organic matter in the ocean (e.g., Payne and Kump, 2007; Galfetti et al., 2007a, 2007b, 2007c; Algeo et al., 2019b; Grasby et al., 2016b).

### 25.1.3 Subdivisions of the Middle Triassic

#### *25.1.3.1 Anisian*

##### 25.1.3.1.1 History, definition, and boundary stratotype candidates

The Anisian Stage was named after limestone formations near the Enns (=*Anisus*) River at Grossreifling, Austria (Waagen and Diener, 1895). The original Anisian stratotype lacks ammonoids in the lower portion, and lower limit was later clarified in the Mediterranean region (Assereto, 1974). The appearance of a number of ammonoid genera, including *Aegeiceras*, *Japonites*, *Paracrochordiceras*, and *Paradanubites*, may be used to define the base of the Anisian within different regions (e.g., Gaetani, 1993). However, other markers are suggested that may provide a more global correlation value. The lowest occurrence of the *Chiosella timorensis* (or its *sensu stricto* morphotype on its early lineage) conodont slightly precedes the ammonoid level and can be correlated to North American and Asian stratigraphy (Orchard and Tozer, 1997; Orchard, 2010; Chen et al., 2020). Therefore if the lowest

occurrence of *Ch. timorensis* is selected as the global marker, then the uppermost part of the ammonoid *Neopopanoceras haugi* Zone of "latest Olenekian" in the Tethyan realm will slightly overlap the basal Anisian. The boundary interval is close to a peak in carbon-13 ($\delta^{13}C_{carb}$) values. Sea-surface temperatures were reported to have cooled by 4°C during this rise in $\delta^{13}C_{carb}$ (Sun et al., 2012), suggesting a sequestration of carbon dioxide. A shift from reversed-polarity- to normal-polarity-dominated magnetostratigraphy (base of normal-polarity magnetozone MT1n of Hounslow and Muttoni (2010) has been proposed as a primary global boundary marker that can be unambiguously correlated between Boreal and Tethyan faunal realms (Hounslow et al., 2007). However, some stratigraphers wish to retain an ammonoid-based assignment for an Anisian GSSP (and some other Triassic stages/substages) (e.g., discussions posted at Ogg et al., 2020).

Published candidates for the base-Anisian GSSP include locations in Romania, in Albania and two in South China. At Deşli-Caira Hill in north Dobrogea, Romania, the Olenekian–Anisian boundary interval is within a condensed Hallstatt limestone facies with ammonites (Gradinaru et al., 2007). The Kçira section in Albania of reddish nodular limestone has magnetostratigraphy and detailed conodont ranges (Muttoni et al., 1996b, 2019), but has not yet been studied for stable isotope stratigraphy.

In South China, the succession of *Ch. timorensis* and other conodont datums within the boundary interval are interbedded with volcanic-ash beds. Although the individual zircons within each of those beds have a widespread of U–Pb radioisotopic dates, the suites enable estimates of the approximate ages for the various datums with a mean near 247 Ma (Lehrmann et al., 2015; Ovtcharova et al., 2015). The Guandao section in the Nanpanjiang Basin (Guizhou province, South China) has an impressive conodont-magnetic-isotope-cyclo stratigraphy with radioisotopic dates (Lehrmann et al., 2006, 2015; Li et al., 2016, 2018); but the critical Olenekian–Anisian boundary interval is distorted by debris flows and did not yet yield the brief M1n normal-polarity subchron. The Wantou roadcut at Jinya, Fengshan County, Guangxi province in South China has been studied for ammonoid, conodont, and carbon-isotope stratigraphy (Galfetti et al., 2007, 2008), and the main events and trends are bracketed by a succession of a dozen volcanic ashes that have yielded ID-TIMS U–Pb ages (Ovtcharova et al., 2006, 2015). Additional work on that Wantou section has yielded a detailed biomagnetostratigraphy that verified that the M1n polarity subchron is near the first *Ch. timorensis* conodont (Chen et al., 2020).

#### 25.1.3.1.2 Anisian substages

The Anisian Stage has three to four informal substages. Assereto (1974) proposed a stratotype for the Lower Anisian (also called "Aegean" or "Egean") in beds with *Paracrochordiceras* ammonoids at Mount Marathovouno on Chios Island (Aegean Sea, Greece). The Middle Anisian is sometimes subdivided into two substages: a lower "Bithynian," named by Assereto (1974) after the Kokaeli Peninsula (Bithynia) of Turkey, and an upper "Pelsonian," from the Latin name for the region around Lake Balaton in Hungary (Pia, 1930) spanning the *Balatonites balatonicus* ammonoid zone (Assereto, 1974). The Upper Anisian is also called "Illyrian" after the Latin term for Bosnia (Pia, 1930). Southwestern China has continuous Anisian carbonate successions with complete conodont and ammonoid zonations (Enos et al., 2006; Benton et al., 2013; Tong et al. 2019) that have high potential in assisting future decisions on practical inter-regional boundaries of Anisian substages.

### 25.1.3.2 Ladinian

#### 25.1.3.2.1 History, definition, and boundary stratotype candidates

The Ladinian Stage arose after a heated semantic argument of "Was ist norisch?" (Bittner, 1892), when it was realized that most of the strata that had defined a "pre-Carnian" Norian Stage (Mojsisovics, 1869) were actually deposited *after* the Carnian (Mojsisovics, 1893). This debate and the emergence of the Ladinian Stage split the Vienna geological establishment (vividly reviewed by Tozer, 1984). The Ladinian, named after the Ladini inhabitants of the Dolomites region of northern Italy, encompassed the Wengen and Buchenstein beds (Bittner, 1892).

This historical major revision and even partial inversion of the upper Triassic stratigraphy, coupled with uncertainties about correlation potentials and definition of ammonoid zones, contributed to discussions in assigning the basal limit of the Ladinian Stage (e.g., Gaetani, 1993; Brack and Rieber, 1994; Mietto and Manfrin, 1995; Brack et al., 1995; Vörös et al., 1996; Muttoni et al., 1996a; Orchard and Tozer, 1997; Pálfy and Vörös, 1998). The ammonoid contenders for the primary correlation markers were distributed over at least two zones; including the lowest occurrence of representatives of the *Kellnerites* genus, of the *Nevadites* genus, of the *Eoprotrachyceras* genus, of the *Reitziites reitzi* species, and of the *Aplococeras avisianum* species. In addition, the lowest occurrence of the *Budurovignathus* conodont genus was considered.

The base of *Eoprotrachyceras curionii* Zone (lowest occurrence of *Eoprotrachyceras* ammonoid genus, which is the onset of the Trachyceratidae ammonoid family) was eventually preferred. The Bagolino section (eastern Lombardian Alps, Province of Brescia, Northern Italy) was selected for its multiple stratigraphic records, including the bracketing of the boundary interval by dated volcanic ashes (Brack et al., 2005). The Ladinian GSSP at Bagolino is located at the top

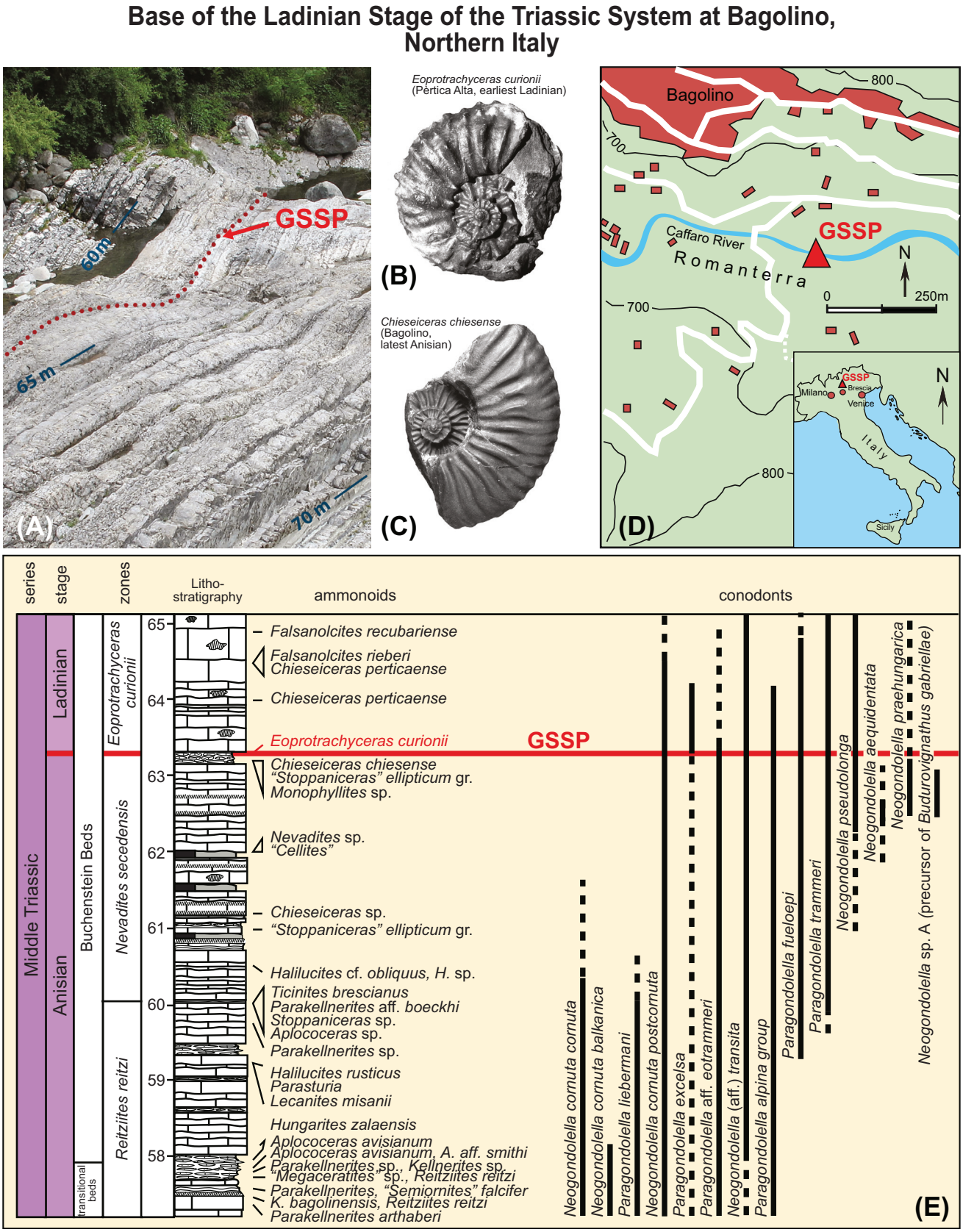


**FIGURE 25.3** GSSP for the base of the Ladinian Stage at Bagolino, Italy. The GSSP level coincides with the lowest occurrence of *Eoprotrachyceras* ammonoid genus (base of *Eoprotrachyceras curionii* Zone). *GSSP*, Global Boundary Stratotype Section and Point. *Photos provided by Peter Brack.*

of a distinct 15–20-cm-thick interval of limestone nodules in a shaly matrix (Chiesense groove), located at approximately 5 m above the base of the Buchenstein Beds (Fig. 25.3). The Ladinian GSSP site is accessible through a geological pathway with explanatory notes and ammonoid casts (Brack, 2010). The *Nevadites secedensis* ammonoid zone of the lowermost Buchenstein Beds, which was historically assigned as Ladinian (e.g., Bittner, 1892), has now become the uppermost zone of the Anisian. Secondary global markers include the lowest occurrence of the conodont *Budurovignathus praehungaricus* and a brief normal-polarity magnetozone (MT8n of Hounslow and Muttoni, 2010; and SC2r.1n of Maron et al., 2019) within the reversed-polarity zone spanning the uppermost Anisian and basal Ladinian. The bracketing U–Pb-dated volcanic ashes indicate a boundary age of approximately 241.5 Ma (Wotzlaw et al., 2018).

#### 25.1.3.2.2 Ladinian substages

Mojsisovics et al. (1895) divided the Ladinian into two substages—Lower or Fassanian (named after Val di Fassa in northern Italy, where it was equated to the Buchenstein Beds and Marmolada Limestone), and Upper or Longobardian (named after the Langobard people of northern Italy, and spanning the Wengen Beds). The substage boundary is approximately at the base of the *Protrachyceras longobardicum* ammonoid zone in the Alpine zonation or the base of *Meginoceras meginae* ammonoid zone in the Canadian zonation.

## 25.1.4 Subdivisions of the Upper Triassic

The Upper Triassic consists of three stages—Carnian, Norian, and Rhaetian—that were originally defined by characteristic ammonoids (Mojsisovics, 1869). However, these units were originally recognized in different locations in the Northern Alps of Austria with uncertain stratigraphic relationships. Indeed, until 1892, Norian units were considered to underlie the Carnian, and it was only after a major geological controversy was the name "Norian" applied to the same units after recognition that they were younger than Carnian (reviewed in Tozer, 1984).

### *25.1.4.1 Carnian*

#### 25.1.4.1.1 History, revised definition, and boundary stratotype candidates

The Carnian stage, either named after localities in the Kärnten (Carinthia) region of Austria, or after the nearby Carnian Alps, was originally applied to Hallsatt Limestone beds bearing ammonoids of *Trachyceras* and *Tropites* (Mojsisovics, 1869). The first occurrence of ammonoid *Trachyceras* (=base of *Trachyceras aon* Zone in Tethys or *Trachyceras desatoyense* in Canada) was the traditional base, although it appears that a *Trachyceras* datum would be asynchronous and not cosmopolitan (e.g., Mietto and Manfrin, 1999). Mojsisovics et al. (1895) included the St. Cassian Beds of northern Italy in a revised Carnian subdivision, therefore the level with lowest occurrence of the cosmopolitan ammonoid *Daxatina* at the Prati di Stuores type locality in the Dolomites (northern Italy) was proposed for the base-Carnian GSSP (Broglio Loriga et al., 1998). This section has relatively rapid sedimentation and proved suitable for multiple types of stratigraphy; therefore it was ratified 10 years later (2008). Three other reference sections with multiple biostratigraphic successions are in Spiti in the Himalaya of northwest India (Balini et al., 1998, 2001), the New Pass section of Nevada in western USA, and the Xingyi section of Guizhou in southwestern China.

The Carnian GSSP at Prati di Stores/Stuores Wiesen is 45 m above the base of the St. Cassian (San Cassiano) Formation (Fig. 25.4) (Mietto et al., 2012). This level was selected to coincide with the lowest occurrence of the ammonoid *Daxatina* (base of *Daxatina canadensis* Subzone, lowest subzone of a broad *Trachyceras* Zone). Secondary markers are the lowest occurrences of the conodont *"Paragondolella" polygnathiformis* and the palynomorphs *Vallasporites ignacii* and *Patinasporites densus* (Mietto et al., 2007). The evolutionary transition from *Daonella* to *Halobia* bivalves is probably near this level (McRoberts, 2010). The Carnian GSSP is just above the base of a normal-polarity magnetic magnetozone (S2n in the local scale of Broglio Loriga et al., 1999; UT1n in the synthesis scale of Hounslow and Muttoni, 2010; or MA5n in the nomenclature of Maron et al., 2019), and lies just above an interpreted maximum flooding surface within Sequence Lad 3 of Hardenbol et al. (1998) or TLa3 of Haq (2018).

The ratified placement of the base-Carnian at the appearance of *Daxatina* ammonoids, rather than the *T. aon* ammonoid, implies that the Carnian now begins in the middle of the classical "uppermost Ladinian" *Frankites regoledanus* ammonoid zone.

#### 25.1.4.1.2 Carnian substages and wet intermezzo

Mojsisovics et al. (1895) subdivided the Carnian into three substages (Cordevolian, Julian, and Tuvalian) corresponding to his three ammonoid zones. Cordevolian (his *T. aon* Zone, from the St. Cassian Beds, was named after the Cordevol people who lived in this area of northern Italy. Julian (*Trachyceras aonoides* Zone) was based on the Raibl Formation of the Julian Alps in southern Austria. The Tuvalian (*Tropites subbullatus* Zone) was named after the Tuval mountains, the Roman term for the region between Berchtesgaden and Hallein near Salzburg, Austria. Mojsisovics trio of ammonoid zones was later split into additional zones; but his main divisions can be correlated among regions.

## Base of the Carnian Stage of the Triassic System in the Prati di Stuores/ Stuores Wiesen Section, near San Cassiano, Italy

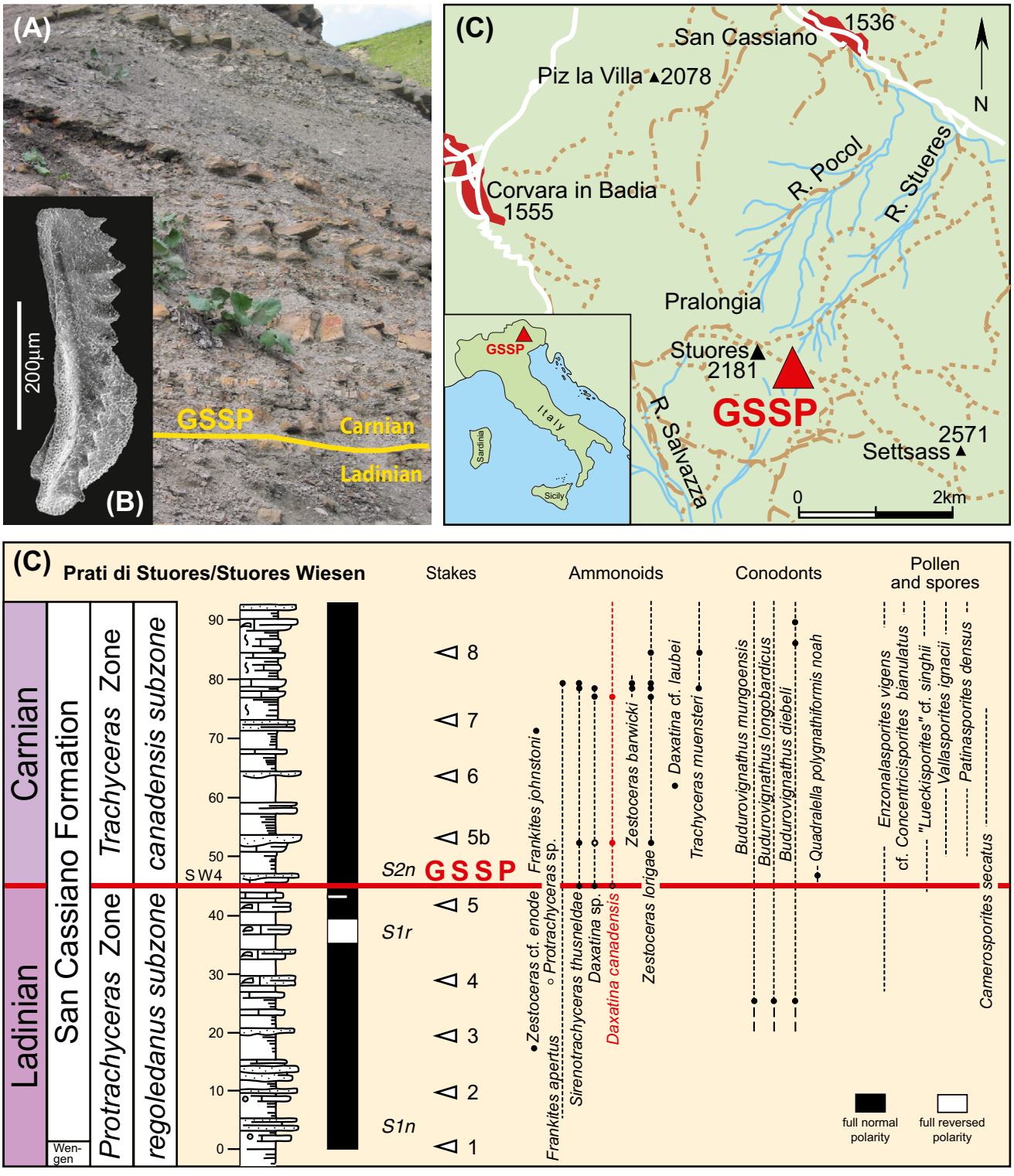


**FIGURE 25.4** GSSP for the base of the Upper Triassic (base of Carnian Stage) at the Prati di Stuores (Stuores Wiesen) section, Dolomites region of north Italy. The GSSP level coincides with the lowest occurrence of the cosmopolitan ammonoid *Daxatina* (base of *Daxatina canadensis* Subzone, lowest subzone of *Trachyceras* Zone), and is near the lowest occurrence of conodont *Quadrelella polygnathiformis* (inset "B," formerly assigned to the *Paragondolella* genus). Photographs of outcrop and conodont provided by Manuel Rigo. *GSSP*, Global Boundary Stratotype Section and Point.

Stratigraphers often combine Mojsisovics's Cordevolian and Julian into a single Julian Substage, with the Julian/Tuvalian (Lower/Upper Carnian) boundary traditionally assigned as the first occurrence of *Tropites* ammonoids (base of the *T. subbullatus* ammonoid zone of Tethys and *Tropites dilleri* Zone of Canada). Across this substage boundary, the change in ammonoid assemblages is more significant than at the bases of either the Carnian or the Norian stage (Tozer, 1984), the conodont diversity may have been reduced to two genera (Mazza et al., 2010), and there were major changes in radiolarians and other faunal groups (Kozur and Bachmann, 2010).

A dramatic event in the latest Julian that immediately preceded this Julian/Tuvalian boundary is considered to be "the most distinctive climate change within the Triassic" (Preto et al., 2010). This global disruption of the Earth's land-ocean-biological system has various regional names, for example, "Reingraben turnover" (Schlager and Schöllnberger, 1974), "Raibl Event," "Carnian Pluvial Episode" (Simms and Ruffel, 1989; Dal Corso et al., 2018a, 2018b), "Middle Carnian Wet Intermezzo" (Kozur and Bachmann, 2010), or "Carnian Humid Episode" (Ruffell et al., 2016). The distinct fossil assemblages within this "wet intermezzo" interval provide an important means of calibration among terrestrial settings (conchostracans, pollen, ostracod, and tetrapod biostratigraphy) from the southwest United States to Germanic Basin and into marine settings (ammonoid, conodont, ostracod, and bivalve biostratigraphy) (Roghi et al., 2010; Kozur and Weems, 2010). There is growing evidence that this mid-Carnian episode was marked by sudden warming and associated increased rainfall in many continental regions, the widespread termination of tropical carbonate platforms and a brief major negative excursion in $\delta^{13}C_{org}$ (e.g., Simms and Ruffel, 1989; Ogg, 2015; Dal Corso et al., 2012, 2018a, 2018b). For example, the mid-Carnian episode was initially recognized within Germanic Basin by an influx of fluvial to brackish-water sands (Stuttgart Formation or Schilfsandstein) and within the Alpine region by the sudden termination of prograding reefs by an influx of terrigenous clastics (Raibl Formation). Black shale facies developed in restricted basins (e.g., Hornung and Brandner, 2005). The trigger for the onset of this "Carnian Pluvial Episode" could be a combination of paleogeographic and paleoceanographic factors (e.g., Kozur and Bachmann, 2010), including the formation of the Wrangellia large igneous province (Dal Corso et al., 2012).

### *25.1.4.2 Norian*

#### 25.1.4.2.1 History, revised definition, and boundary stratotype candidates

Norian derives its name from the Roman province of Noria, south of the Danube and including the area of Hallstatt, Austria (Mojsisovics, 1869). The stratigraphic extent of strata assigned as "Norian" had a contorted history (reviewed in Tozer, 1984).

Ammonoid successions in Nevada and British Columbia led to a proposal that the base of the Norian is assigned to the base of the *Stikinoceras kerri* ammonoid zone, which is overlying the *Klamathites macrolobatus* Zone (Silberling and Tozer, 1968). This level is approximately coeval with a Tethyan placement between the *Anatropites* and *Guembelites jandianus* ammonoid zones (Krystyn, 1980; Orchard et al., 2000; Jenks et al., 2015). Examinations of conodont lineages have indicated that the first appearance of *Metapolygnathus echinatus* (reclassified as *Metapolygnathus parvus* by Orchard, 2014) is at approximately the beginning of the *S. kerri* ammonoid zone and coincides with a major faunal turnover (Orchard, 2010, 2014) and is approximately coincident with the FAD of the widespread *Halobia austriaca* bivalve. Therefore the *Meta. parvus* conodont level has become favored for assigning the base of the Norian (Mazza et al., 2018; Orchard, 2019).

There are two candidates for the Norian GSSP based on the FAD of *Meta. parvus* conodont: (1) The candidate of Pizzo Mondello in Sicily (Muttoni et al., 2001a; Nicora et al., 2007; Mazza et al., 2012; Balini et al., 2012) has a detailed magnetostratigraphy in which the proposed GSSP level (FAD of *Meta. parvus*) coincides with the uppermost part of normal-polarity magnetozone (magnetozone "PM4n" in local terminology of Muttoni et al., 2001a, 2001b), is just above a positive shift in $\delta^{13}C_{carb}$ and, relative to the magnetostratigraphic scale, is about 0.6 Myr below the lowest occurrence of *Halobia austriaca* (Mazza et al., 2018). (2) The proposed GSSP level at Black Bear Ridge on Williston Lake of northeast British Columbia (Orchard et al., 2001; Orchard, 2007b) is below the local occurrence of the bivalve *Halobia austriaca* (McRoberts, 2007) and coincides with geochemical excursions "implying anoxia and a temperature maximum during the *Meta. parvus* Zone (Orchard, 2019). Unfortunately, the Black Bear Ridge section did not yield a useful magnetostratigraphy (Muttoni et al., 2001b); whereas the magnetostratigraphy at Pizzo Mondello can be correlated to the cyclo-magnetostratigraphic reference scale from the Newark Basin (e.g., Kent et al., 2017: Maron et al., 2019). Therefore in this chapter, the calibration by Mazza et al. (2018; Fig. 5) of c. 85% up in normal-polarity zone PM4n (equivalent to uppermost E7n of Newark Basin) is used for the implied age model for the Carnian–Norian boundary.

#### 25.1.4.2.2 Norian substages

The Norian is traditionally subdivided into three substages, following Mojsisovics et al. (1895). The boundary between the lower Norian (or "Lacian," after the Roman name for the Salzkammergut region of the northern Austrian Alps) and

middle Norian (or "Alaunian," named for the Alauns, who lived in the Hallein region of Austria during Roman times) is the base of the Tethyan *Cyrtopleurites bicrenatus* ammonoid zone. The base of the upper Norian (or "Sevatian," after the Celtic tribe who lived between the Inn and Enns rivers of Austria) is generally assigned as the base of the North American *Gnomohalorites cordilleranus* ammonoid zone or the Tethyan *Sagenites quinquepunctatus* ammonoid zone; however, there has not been a consistent usage of this Sevatian Substage and some include the underlying *Halorites macer* ammonoid zone within it (e.g., Kozur, 1999).

### 25.1.4.3 Rhaetian

The Rhaetian was the first Triassic stage to be established, when von Gümbel (1861) applied the term to strata containing the pteriid bivalve *Rhaetavicula contorta*, such as the Kössen Beds of Austria. This distinctive bivalve is found in shallow-marine facies from the western Tethys and across northwestern Europe. His "Rhätische Gebilde" name was derived from either the Rhätische Alpen or the Roman province of Rhaetium. For a while, it appeared that the Rhaetian interval would be incorporated into the Jurassic (and perhaps renamed as a "Bavarian Stage) or incorporated into the Norian Stage (reviewed in Lucas, 2010a). For example, the Rhaetian was eliminated in some Triassic time scales (e.g., Zapfe, 1974; Palmer, 1983; Tozer, 1984, 1990). In 1991 the Subcommission on Triassic Stratigraphy decided to retain the Rhaetian as an independent stage. Many options were considered for the primary biostratigraphic marker for the lower boundary.

In 2010 the Norian–Rhaetian boundary working group decided that a GSSP level should coincide with lowest occurrence of the conodont *Misikella posthernsteini* (Krystyn, 2010). This conodont is a phylogenetic descendent of *Misikella hernsteini* but is very rare at the beginning of its range. However, even though this morphogenesis is seen worldwide, it appears that the distinctions between the component taxa are not standardized (e.g., discussions in Rigo et al., 2016; Lucas, 2016; Orchard, 2016). Therefore secondary markers should also be employed to assign the base of the Rhaetian (Krystyn, 2010) including the possible: (1) lowest occurrence of conodont *Epigondolella mosheri* (morphotype B sensu Orchard), (2) lowest occurrence of ammonoid *Paracochloceras suessi* and the closely allied genus *Cochloceras* and other taxa, (3) disappearance of ammonoid genus *Metasibirites*, (4) lowest occurrence of radiolarian *Proparvicingula moniliformis* and other species (Carter and Orchard, 2007), (5) disappearance of *Monitis* bivalves, except for continuation by dwarf *Monotis* species in parts of the Tethys (McRoberts et al., 2008), and especially a (6) magnetostratigraphy which would allow a correlation to the cyclo–magnetic reference scale from the Newark Basin.

In the candidate GSSP section at Steinbergkogel near Hallstatt in Austria (Krystyn et al., 2007c, 2007d), the interpreted base of *Mi. posthernsteini* is just above a change from a major normal-polarity magnetozone upward to a reversed-polarity-dominated magnetozone (Gallet et al., 2007; Muttoni et al., 2010; Hounslow and Muttoni, 2010; Hüsing et al., 2011). In contrast, at the candidate section of Pignola-Abriola in Sicily, the interpreted base of the *Mi. posthernsteini* conodont is very high within a reversed-polarity-dominated magnetozone (Maron et al, 2015; Rigo et al., 2016). It appears that the finer features of both of these reversed-dominated magnetozones can be reliably correlated between Austria and Sicily; therefore the proposed correlation of these Rhaetian magnetostratigraphies to the astronomical-cycle-scaled magnetic polarity reference pattern of the Newark Basin implies nearly a 4-million-year offset of the interpreted bases of *Mi. posthernsteini* between those two candidate GSSPs (Maron et al., 2015; Rigo et al., 2016). To explain this discrepancy, Maron et al. (2015) proposed that the interpreted earliest form of *Mi. posthernsteini* at the Austria GSSP candidate is an initial transitional form (sensu lato) at c. 209.5 Ma, whereas the interpreted lowest *Mi. posthernsteini* at the Sicily GSSP is the developed form (sensu stricto) with an estimated age of 205.7 Ma. The proponents of the Pignola-Abriola section consider that the higher level (and the implied shorter-duration Rhaetian) to be more consistent with the traditional recognition of the base of the Rhaetian in other regions, and note that the proposed GSSP level is near a negative isotope excursion in organic-carbon (Rigo et al., 2016). A negative excursion in $\delta^{13}C_{org}$ at the same cyclo-magnetostratigraphic level is observed in terrestrial deposits in Sichuan, China (Li et al., 2017a, 2017b). However, in the Austrian GSSP candidate, the two conodont morphotypes are only separated by one bed (Galbrun et al., 2020).

Both options for the Rhaetian GSSP depending on the eventual morphotype for *Mi. posthernsteini* for the Rhaetian GSSP—the sensu latu (s.l.; Austria candidate) and sensu stricto (s.str.; Italian candidate) are shown on the figures in this chapter; but the Italian "short Rhaetian" is used for the Phanerozoic synthesis.

## 25.2 Triassic stratigraphy

Ammonoids dominate the historical zonation of the Triassic, but conodonts have become the major tool for global correlation. Thin-shelled bivalves (e.g., *Daonella*, *Halobia*) provide important regional markers. During much of the Triassic, the sedimentary record across the Pangea Supercontinent was dominated by terrestrial deposits, therefore widespread conchostracan, tetrapod, and plant remains are important for global correlation.

Other biostratigraphic, magnetostratigraphic, chemostratigraphic, and other events are typically calibrated to

these standard ammonoid or conodont zones. Extensive compilations and intercorrelation of Triassic stratigraphy of European basins were coordinated by Hardenbol et al. (1998), and a suite of detailed Triassic stratigraphic scales are in *The Triassic Timescale* (Lucas, 2010a).

## 25.2.1 Marine biostratigraphy

### *25.2.1.1 Ammonoids*

The ammonoid successions of the Alps and Canada have historically served as global primary standards for the Triassic (reviews in Tozer, 1967, 1984; Balini et al., 2010). Ammonoids were nearly extinguished at the end of the Permian, with termination of three of the four major Permian clades. However, the rare surviving ammonoids diversified much faster than other marine groups following this catastrophe (Brayard et al., 2009a; Marshall and Jacobs, 2009). The entire Triassic ceratitid group of Ammonoidea is usually considered to have been derived from the morphologically simple *Ophiceras* genus survivor. This rapid surge in diversity was interrupted by major waves of extinction at the end of the Smithian Substage (mid-Olenekian), base of Anisian and end of Julian Substage (mid-Carnian) (e.g., Brayard et al., 2009a, 2009b; Jenks et al., 2015). Peak diversity was attained in middle Norian. A decline in diversity through the latest Triassic culminated in apparently only a single genus, *Psiloceras*, surviving the end-Triassic mass extinctions and rapidly evolving to conquer the Jurassic seas.

Despite their historical importance in subdividing the Triassic, there is not yet a standardized ammonoid zonation (or nomenclature) for the alpine regions. For example, Mietto and Manfrin (1995) proposed a generalized standard for the Middle Triassic of the Tethyan realm that utilized first appearances of widespread genera to define zones and major species to define subzones. But this zonal scheme was immediately rejected by some alpine workers (e.g., critiques by Brack and Rieber, 1996; Vörös et al., 1996). Contributing to this situation is the lack of consensus definitions of species and genera, historical confusions with taxonomy and relative chronostratigraphic placement of taxa, distinct latitudinal and endemic assemblages, use of assemblage or association zones, omission by many authors to provide clarity in their definition of zonal boundaries, and a current reduction in the number of active ammonoid specialists (Balini et al., 2010).

A selection of Triassic zonations and their main index ammonoids are figured in Balini et al. (2010) and in Jenks et al. (2015). The ammonoid zonal columns in the charts in this chapter are generalized versions for the Tethyan and for a blend of the West Canadian Sedimentary Basin and Canadian Arctic realms and are derived mainly from Jenks et al. (2015) and from advice from M. Orchard, respectively.

### *25.2.1.2 Conodonts*

Conodonts are phosphatic feeding apparatuses of an enigmatic pelagic swimmer. The conodont taxa are based on variability of these jaw-like elements, and these evolving features enable widespread correlation of Triassic strata. After surviving the end-Permian mass extinctions and explosively diversifying in the early Olenekian (Orchard, 2007a), the conodonts tragically vanished shortly before the end of the Triassic. Conodonts are generally more widespread than ammonites both in paleogeography and in different marine facies and are approaching a well-defined taxonomy and biostratigraphy (e.g., Anisian through Carnian synthesis by Chen et al., 2016; Carnian through Rhaetian synthesis by Rigo et al., 2018; discussions between Orchard, 2016, and Lucas, 2016). However, there remains a lack of standardization of taxonomic groupings among conodont specialists which implies that publications commonly place species-level taxa under different genera.

Compilations of the calibrations among conodont zones and ammonoids have been proposed for several realms, including Canada (e.g., Orchard and Tozer, 1997; Orchard, 2010, 2014, 2018; Golding, 2019; Golding et al., 2014, 2017), Tethys region (e.g., Krystyn et al., 2002; Kozur, 2003; Rigo et al., 2018), China (Tong et al., 2019), and European basins (Vrielynck, 1998). The generalized columns in the charts in this chapter are composites for the Tethyan (Kozur, 2003; with Carnian through Rhaetian of Moix et al., 2007, as shown in Rigo et al., 2018), for eastern Tethys (Rigo et al., 2018), for China (Tong et al., 2019, with selected enhancements by Haishui Jiang, pers. commun.) and for the Western Canadian Sedimentary Basin or "Arctic/Panthalassa" (contributed by Michael Orchard and Martyn Golding for inclusion in a future synthesis chart by Robert Fensome and Manuel Bringué at the Geological Survey of Canada). Names of genera were standardized to the taxonomy preferred by Michael Orchard.

### *25.2.1.3 Bivalves*

The end-Permian mass extinctions terminated the dominance by the communities of brachiopods, crinoids (and other pelmatozoan echinoderms), and bryozoans that had been typical of Paleozoic marine seabeds. Bivalve and gastropod mollusk communities are typical of Early Triassic shelves, with a later increase in the importance of scleractinian corals. Among the Triassic bivalves, a succession of pelagic forms of thin-shelled "flat clams" (pectinacean pteriid bivalves) was largely restricted to deeper water settings and tend to occur in high densities on certain bedding planes (Hallam, 1981). The distinctive thin-shelled bivalve genera (*Claria*, *Enteropleura*, *Daonella*, *Halobia*, *Monotis*, etc.), which have no modern counterparts, are valuable for global Triassic correlations because

their species have both widespread distributions and a mean duration of only 1–2 Myr. Their Jurassic and Cretaceous relatives (*Bositra*, *Buchia*, inoceramids) occupied the same settings. The first comprehensive summary of the ranges of these Triassic pelagic bivalves relative to ammonoid zones in different biogeographic provinces was by McRoberts (2010), who defined 30 discrete zones and regional variants.

#### 25.2.1.4 Radiolarians

The sand-sized opaline skeletons of radiolarians are typically found in Triassic deep-marine facies. After the end-Permian, the most severe extinction event for radiolarians, diversity slowly increased through the Early Triassic, then surged in the Anisian to reach a maximum in early Carnian. Diversity declined through the Late Triassic until the end-Triassic mass extinctions again decimated the radiolarian genera (O'Dogherty et al., 2010).

Radiolarian datums and zonations have been compiled for different regions, including alpine exposures (e.g., De Wever, 1982, 1998; Kozur and Mostler, 1994; Kozur, 2003), Japan (e.g., Sugiyama, 1997), and western North America (e.g., Blome, 1984; Carter, 1993; Carter and Orchard, 2007). A correlation among these regional zonations and a summary for the ranges of the main 281 genera (including schematic images) relative to Triassic substages are compiled by O'Dogherty et al. (2010).

#### 25.2.1.5 Other microfossils

Except for radiolarians, marine microfossil biostratigraphy has not yet been developed as a widespread correlation tool within the Triassic. In contrast to Permian and Jurassic syntheses, the benthic foraminifer stratigraphy of the Triassic has not been compiled on a global scale. Regional scales include a stratigraphic summary of larger benthic foraminifera of the Tethyan realm (Peybernes, 1998) and zonations proposed for the Caucasus (e.g., Vuks, 2000, 2007).

Calcareous nannofossils are only known from Carnian and younger strata, and the first "real coccoliths" appear in the Norian (von Salis, 1998; Bown, 1998).

Records of dinoflagellates are rare, and the oldest representative of this group may be middle Triassic (Hochuli, 1998). However, the latest Triassic species, *Rhaetogonyaulax rhaetica*, is an important means for correlating Rhaetian strata.

#### 25.2.1.6 Reefs

Although not biostratigraphy, per se, there are broad trends with global shallow-water carbonate systems during the Triassic. The metazoan communities that built Permian reefs were completely destroyed in the end-Permian mass extinction, and a "reef gap" ensued that spanned much of the Early Triassic. Simultaneously, there was an Early Triassic "chert gap" following the termination of the extensive Permian chert accumulations (Beauchamp and Baud, 2002). The accompanying extinction of many benthic grazers probably contributed to the distinctive microbial-dominated carbonates (stromatolites, wavy-laminated micrites, oolites) that are characteristic of the earliest Triassic (Flügel, 2002; Chen and Benton, 2012; Chen et al., 2019). Elevated carbon dioxide levels and/or a pulse of carbonate saturation following $CO_2$-induced dissolution in an ocean that lacked deep-water carbonate buffering may have contributed to this latest Permian and earliest Triassic interval of microbial and oolitic limestones (e.g., Payne et al., 2007, 2009; Xie et al., 2010). This Early Triassic "reef gap" was mainly caused by a lack of reef-building biota, rather than a crisis in carbonate production/accumulation (Preto et al., 2010). Microbial-sponge and *Tubiphytes* reef communities with a modest contribution from the oldest crown-type scleractinian corals are characteristic of the middle and late Anisian (Kiessling, 2010). Growth rates for some late Anisian through Ladinian reefs were phenomenal, with radioisotopic dates suggesting up to 500 m/Myr for some platforms in the Dolomites of northern Italy (e.g., Brack et al., 2007; Meyers, 2008). The Ladinian-earliest Carnian peak of these microbial-sponge reefs was terminated by the events associated with the mid-Carnian pluvial event (wet intermezzo) (e.g., Stefani et al., 2010). Scleractinian corals contributed to the second phase of reef expansion, which peaked in the Late Norian (Kiessling, 2010). A rapid sea-level fall near the time of the Norian/Rhaetian boundary contributed to the end-Norian Cessation of the spectacular Dolomia Principale/Hauptdolomit platforms of the Alps and other regions (e.g., Berra et al., 2010). The end-Rhaetian wave of extinctions led to a reef crisis that mirrored the end-Permian episode, and reefs were again rare through much of the Early and Middle Jurassic (Kiessling, 2010).

#### 25.2.1.7 Marine reptiles

Beginning in the late Early Triassic, the seas became inhabited by large marine reptiles. Ichthyopterygia ("fish flippers"; or Ichthyosaurs) with their dolphin-like morphology and Sauropterygia (lizard flippers) that retained a more crocodile-like form rapidly diversified during the late Early Triassic (e.g., Motani, 2010). The adaptation of the ichthyosaurs to the open seas, perhaps including a warm-blooded anatomy, enabled their expansion in the Middle and Late Triassic as coastal habitats for other marine reptiles declined (Motani, 2010; Renesto and Dalla Vecchio, 2018). Most of the Sauropterygia clade vanished during the Late Triassic prior to the end-Triassic mass extinction of other marine fauna. The open-ocean long-necked plesiosaurs of the Sauropterygia clade and the parvipelvian group of ichthyosaurs appeared during the Late Triassic and underwent radiation during the Jurassic (Renesto and Dalla Vecchio, 2018).

### 25.2.2 Terrestrial biostratigraphy

The terrestrial successions of tetrapods (amphibians, reptiles, earliest mammals), plants (spores/pollen, macroflora), and lacustrine organisms (ostracods, and especially conchostracans) are broadly intercorrelated in different regions of Pangea. The calibration of the evolving terrestrial ecosystems to marine-based Triassic stages and substages is fairly well established for the Lower Triassic via a distinctive cycle-scaled magnetostratigraphy in the Germanic Basin, but ties are much less certain and controversial through the Middle and Upper Triassic. An unambiguous correlation of the cycle-scaled magnetostratigraphy of the Carnian–Norian lacustrine-rich strata of the Newark group from the rift valleys of easternmost North America to the magnetostratigraphy of Tethyan marine zones would enable a precise Late Triassic time scale. The interregional calibration of the pollen-tetrapod-conchostracan occurrences within those Newark beds is a work in progress (e.g., Kozur and Weems, 2010; Irmis et al., 2010; Lucas, 2010c, 2010d).

Other nonmarine biostratigraphy, including charophyte cysts (gyrogonites or calcified spores of charophyte green algae), macrofossil plant assemblages, ostracods, bivalves, and fishes, can be useful on a regional scale, but have not yet been developed for use in global correlations (e.g., reviews by Lucas, 2010c, 2018c).

#### *25.2.2.1 Tetrapods and dinosaurs*

The Mesozoic is popularly known as the "Age of Dinosaurs," but these famed reptiles did not diverge from other tetrapods until the mid-Triassic. The suite of proposed global zones for tetrapod stratigraphy for Pangea is largely based on widespread occurrences of select semiaquatic tetrapods (both reptiles and amphibians) whose thick skulls, body armor, or other resistant body parts were commonly preserved in the sedimentary record. The Pangean configuration enabled many of these forms to spread across most of the world's land area, therefore the lowest occurrences of distinctive widespread genera enable subdivision of the Triassic into eight "land-vertebrate faunachrons" (LVFs) (Lucas, 1998, 1999, 2010d, and references therein). These "LVFs" have an intercontinental correlation potential that is approximately equivalent to standard Triassic stages; although the placement relative to marine-based substages has not yet been firmly established for all LVFs (e.g., Irmis et al., 2010; Lucas, 2018a, 2018b). When skeletal material is not available, distinctive footprints of tetrapods are a secondary, but less precise, method of correlation (Klein and Lucas, 2010).

The predominant terrestrial or semiaquatic forms in the Early Triassic were therapsids, a major lineage of synapsids (fused arch) that are considered to be "mammal-like reptiles" (e.g., Fraser, 2006). Three groups of therapsids survived the end-Permian mass extinction—cynodonts (dog-toothed), dicynodonts ("two dog-toothed," with two tusks in its upper jaw), and large-skulled therocephalian (beast head) carnivores. The therapsids diminished in importance through the Triassic, but true mammals, of which the oldest record is a mouse-sized *Adelobasileus* of Late Triassic (e.g., Lucas, 2008), are interpreted to be derived from this group. The type-area for the Early Triassic LVFs is the Karoo Basin in South Africa. The Lootsbergian LVF begins in latest Permian with the first appearance of *Lystrosaurus*, a squat, dog-sized, dicynodont herbivore that may have been semiaquatic. The extinction of the *Dicynodon* dicynodont is approximately at the end of the Permian (Lucas, 2009). The lowest occurrence of the robustly built *Cynognathus* cynodont defines the base of the Nonesian LVF, which is approximately equivalent to the marine Olenekian Stage.

The Middle Triassic LVFs (Perokvan and Berdyankian) are derived from the lowest occurrences of massive temnospondyl amphibians (*Eocyclotosaurus* and *Mastodonsaurus giganteus*, respectively) in the Ural foreland basin in Russia.

Diapsid (two arches) reptiles had diverged into different major orders during Early Triassic, and its Archosauria (ruling reptiles) group (dinosaurs, pterosaurs, crocodiles, etc.) would dominate the terrestrial and aerial ecosystems of the Jurassic through Cretaceous. The first occurrences of types of crocodile-like phytosaurs and of large armored herbivore aetosaurs, which resembled elongate armadillos with stout claws, define most of the Late Triassic LVFs. The fossil-rich deposits of the Chinle basin of southwest United States are the main reference sections for four Late Triassic LVFs.

The Otischalkian and Adamanian LVFs of Carnian are defined by FADs of phytosaurs *Parasuchus* (=*Paleorhinus*) and *Rutiodon*, respectively. The beginning of the Revueltian LVF that begins with the aetosaur *Typothorax coccinarium* is estimated to begin near the base of the Norian by Lucas (2018b), but he also places that base at c. 220 Ma, which corresponds to lower-middle Norian and is used on the charts in this chapter. However, Ramezani et al. (2009) place the Adamanian–Revueltian faunal turnover between 219 and 213 Ma based on an array of radiometric ages from the Chinle Formation of southwest United States. The Apachean LVF spans approximately the Late Norian through Rhaetian and begins with by FAD of the phytosaur *Redondasaurus* (e.g., Lucas, 2010d, 2018a, 2018b, 2018c). The Jurassic begins with the FAD of the crocodylomorph *Protosuchus* that defines the base of the Wassonian LVF.

Within this tetrapod-LVF framework, the main groups of dinosaurs seem to have radiated during the late-Middle Triassic (e.g., Heckert and Lucas, 1999; Fraser, 2006). The major dinosaur lineages (Sauropodomorpha, Theropoda, and Ornithischia divisions) became established during the Carnian (Nesbitt et al., 2009; Lucas, 2010a, 2010b, 2010c, 2010d; Benton et al., 2014). But these dinosaurs did not

become the dominant land reptiles until the end-Triassic mass extinctions removed their competition from other terrestrial reptiles.

#### 25.2.2.2 Conchostracans (now renamed as Spinicaudata)

Brackish-to-freshwater crustaceans of clam shrimp that were formerly known as conchostracans have a chitinous bivalve carapace of two lateral valves that are typically 2−40 mm in length. However, the group that was called "conchostracans" is now considered to be paraphyletic, therefore this group within the Class Branchiopida have been renamed Spinicaudata (Olesen, 2009, as cited in Geyer and Kelber, 2018). This clade once also lived in the sea during the Paleozoic and early Triassic, then became restricted to non-marine environments.

Their tiny drought-resistant eggs were easily dispersed by wind and water, and rapidly hatched upon exposure to suitable environments. These characteristics and their brief life cycle of only 1−3 weeks enabled conchostracans to be widespread in lakes, shallow seas and temporary pools throughout Pangaea. Their distinctive carapaces were preserved in lacustrine, shallow sea, salt flat, and floodplain deposits. Even through conchostracans are present in pre-Permian through modern sediments, their potential for biostratigraphy and interregional correlation has only been fully developed in Triassic strata (e.g., Kozur and Weems, 2010, and references therein). The application of conchostracan biostratigraphy for other time intervals awaits careful studies of taxonomy, recognition of distinctive taxa, and calibration to other biostratigraphic scales.

Approximately 30 conchostracans zones and regional variants have been defined within the Triassic. These zones have been recognized and intercorrelated within the Germanic Basin, through the southwest United States, in the Newark Supergroup of easternmost North America and within other regions (summarized in Kozur and Weems, 2010, 2011; see also Kozur and Bachmann, 2008). Correlations to marine-based Triassic substages are partially constrained by levels containing ostracods and palynology markers, distinctive facies shifts (e.g., the mid-Carnian "Pluvial Event") and cycle-scaled magnetic magnetozones. The framework established by Kozur and coworkers in the Germanic and Newark basins has been enhanced and modified for Carnian−Norian (Weems and Lucas, 2015; Geyer and Kelber, 2018; Franz et al., 2018) and for the late Permian through Early Triassic (Scholze et al., 2016; Schneider and Scholze, 2018). In particular, the occurrence of *Euestheria gutta* beginning at the base of the Triassic has enabled examination of the response and recovery of terrestrial environments to the catastrophic end-Permian climatic events in basins and terrestrial-marine transitional settings from Germany to southwestern and northern China (e.g., Chu et al., 2019; Zhu et al., 2019; Scholze et al., 2019). The zonal detail of conchostracans is also important for the calibration of the tetrapod LVFs to marine substages (e.g., Weems and Lucas, 2015) and aids in projecting magnetostratigraphy and radioisotopic ages between terrestrial and marine strata.

#### 25.2.2.3 Plants, pollen, and spores

Spores and pollen are important for correlation of marine and terrestrial strata. However, most taxa have relatively long ranges, and changes in assemblages may indicate local climatic-ecosystem shifts rather than a useful temporal marker. Major compilations of Triassic palynology and plant ecosystem evolution are by Wing and Sues (1992), Warrington (2002), Traverse (2007), Yu et al., 2015; Nowak et al., 2018; and Kustatscher et al., 2018. Palynoflora zonations for Triassic strata have been compiled for the Alpine and Germanic regions (e.g., Visscher and Brügman, 1981; Visscher et al., 1994; Hochuli, 1998; Herngreen, 2005; Kürschner and Herngreen, 2010), Australia (Helby et al., 1987), southwest United States (Litwin et al., 1991; Cornet, 1993), Newark basins of eastern United States (e.g., Cornet, 1977; Cornet and Olsen, 1985), and Arctic (Van Veen et al., 1998). However, only the Late Triassic and early Jurassic have a detailed interregional compilation among different continents (Cirilli, 2010; Kustatscher et al., 2018).

Regional diversity of palynomorphs declined at the time of the end-Permian mass extinctions (Kürschner and Herngreen, 2010). Latest Permian plant ecosystems may have undergone a short-lived explosion in abundance in lycopods that interrupted the dominance by gymnosperms to create a c. 10-kyr "spore-spike" within the major negative C-13 isotope decline, but the plant communities rapidly recovered before the main catastrophic marine extinction (Hochuli et al., 2010). Widespread marine clastics of lower Triassic (Induan to lower Olenekian) record a uniquely cosmopolitan "acritarch spike" assemblage of lycopsid spores, small acanthomorph acritarchs, and *Lunatisporites* coniferalean pollen (e.g., Balme and Foster, 1996). Diversity of both pollen and spores peaked in the Germanic Basin during Ladinian−Carnian (Kürschner and Herngreen, 2010; Kustatscher et al., 2018). Globally during this time, there is a rapid diversification of Circumpolloid genera. This broad episode is followed, at least in the Tethyan realm, by a gradual change in palynofloral assemblages without abrupt changes from Carnian into earliest Hettangian (e.g., Cirilli, 2010).

Even though the palynology shifts are generally gradual and mainly important at regional scales, the trends can help identify major hiatuses and correlations in terrestrial records. For example, the strata slightly below flood basalts in the Newark rift basins in the eastern North America display a relatively sharp transition from diverse assemblages of monsaccate and bisaccate pollen to an overlying assemblage

containing 60%–90% *Corollina meyeriana* spores, and this level was considered as a regional marker for the Triassic/Jurassic boundary (e.g., Cornet, 1977; Cornet and Olsen, 1985; Fowell and Olsen, 1993, 1995). However, similar palynological changes are recorded near the base of the typical Rhaetian of Europe (e.g., Schuurman, 1979; Orbell, 1983; Van Veen, 1995), therefore some palynologists have interpreted this level to be a major hiatus that includes most of the Rhaetian stage (e.g., Cirilli et al., 2009), as was initially also suggested by the conchostracan assemblages (Kozur and Weems, 2005, 2010). This interpretation of the absence of the uppermost Norian and most of the Rhaetian between the radioisotopic-dated flood basalts and the underlying cycle-scaled magnetozones of the Newark Supergroup lacustrine strata contributed to a pair of Late Triassic age models in GTS2012 (Ogg, 2012); but it now seems from later magnetostratigraphic correlations to marine deposits and to levels dated by radioisotopes in a reference borehole on the Colorado Plateau that there is no significant hiatus in the uppermost Rhaetian of the Newark Basin (Kent et al., 2017, 2018).

## 25.2.3 Physical stratigraphy

### *25.2.3.1 Magnetostratigraphy*

The compilation of the magnetic polarity time scale for the Triassic is better developed than for the Jurassic or for any of the Paleozoic systems. A concentrated effort by paleomagnetists working closely with biostratigraphers and cyclostratigraphers during the 1990s and first decade of the 21st century has revealed approximately 50 main magnetozones and twice as many lesser polarity subzones (Hounslow and Muttoni, 2010). The composite polarity scale from marine strata has been calibrated to ammonoid and conodont datums in different regions. A parallel polarity scale from terrestrial settings has been partly correlated to conchostracan zones and scaled with cycle-stratigraphy. Magnetic reversals are globally synchronous; therefore the placement of biostratigraphic datums relative to distinctive polarity patterns has been used to determine diachroneity or local distortions in relative timing of markers and a polarity boundary may potentially be used as the primary marker for at least one Triassic GSSP (e.g., GSSP for Anisian by Hounslow et al., 2007). Within Triassic substages, the average of about four major and five minor polarity intervals commonly display a characteristic pattern. However, the sheer abundance of magnetic polarity chrons and lack of broad fingerprints in the patterns at the stage-level implies that utilization of Triassic magnetostratigraphy for interregional or interfacies correlations requires adequate biostratigraphic constraints.

A total of the 133 validated magnetozones in the Triassic have a mean reversal rate of 2.6/Myr, which is similar to the average Cenozoic rate of geomagnetic reversals (Hounslow and Muttoni, 2010). The apparent reversal rate of the Early and Middle Triassic (4/Myr) is twice the average rate within the Late Triassic.

Each magnetostratigraphy study employed a different system for labeling the observed magnetozones. The verification of these studies by demonstrating reproducibility within the biostratigraphic constraints among different regions enables a nomenclature for the main and minor polarity chrons. In the milestone synthesis by Hounslow and Muttoni (2010), the subjective groupings into main magnetozones are systematically numbered upward within each Triassic series (e.g., MT7 is the seventh "main" polarity episode in the Middle Triassic, although it may contain several brief polarity subchrons, with a normal-polarity-dominated "MT7n" portion followed by a reversed-polarity-dominated "MT7r" portion). An alternative would be to label each magnetozone according to its placement relative to Triassic substages (e.g., Illy-N2; for the second cluster of normal-polarity in the Illyrian Substage of Anisian; which is the same as "MT7n," thereby enabling a user to know the approximate geologic-age relationship (e.g., scales in Ogg et al., 2008). This "stage-abbreviation-then-number" system is the same nomenclature philosophy as used for Phanerozoic sequences (e.g., Hardenbol et al., 1998; Haq, 2018). A third option used by Maron et al. (2019) was to select a single detailed magneto-biostratigraphic reference section (e.g., Seceda in Italy for lower Ladinian) and use its polarity zones ("SC1n," "SC2r," etc.) and their relative thicknesses as the nomenclature and scaling for the global polarity pattern. It was not convenient to show all three systems in the summary figures in this chapter; therefore a hybrid set was used that partly depended upon a subjective decision on the relative documentation of the polarity zones. In any case, there is a caveat that portions of these composite polarity patterns are not well calibrated to boundaries of ammonoid (or conodont) zones and the scaling of the patterns within zones is probably distorted by variable sedimentation rates in the reference sections.

The Triassic magnetic polarity reference scales derived from biostratigraphic-dated marine successions (e.g., composite syntheses by Hounslow and Muttoni, 2010, and Maron et al., 2019) and for astronomically scaled terrestrial basins (e.g., Early Triassic by Szurlies, 2007; Late Triassic by Kent and Olsen, 1999) have been verified by extensive conodont-dated magnetostratigraphy in European and Chinese sections (e.g., Muttoni et al., 2014; Maron et al., 2015, 2019; Lehrmann et al., 2015) including cycle-scaling of significant intervals (e.g., Li et al, 2016, 2017a, 2018; Zhang et al., 2015). The comparison between the magnetostratigraphies of marine sections and of cycle-scaled terrestrial sections appears to have resolved some of the uncertainties about the age models for the Late Triassic and for the Early Triassic. For example, the "long Rhaetian-short Tuvalian" option that was preferred for the GTS2012 scale (Ogg, 2012; Ogg et al., 2014) is consistent with those later

compilations; although that Rhaetian appears to correspond to the "*sensu lato*" interpretation of the marker conodont taxon rather than the shorter *sensu stricto* version adapted for the composite Phanerozoic scale (Maron et al., 2015).

The following summary is mainly from Hounslow and Muttoni (2010) and Maron et al. (2019), and only a selection of their main reference sections for biomagnetic calibrations and conclusions are given here. In addition to placing the generalized patterns onto the relevant biostratigraphic scales, they have standardized the stratigraphy of the different regional sections onto a common Tethyan ammonoid zone or substage scale.

#### 25.2.3.1.1 Early Triassic magnetic polarity scales

The Induan stage has two pairs and the Olenekian has seven pairs of polarity chrons that are correlated to Boreal ammonoid and conodont satums in the Arctic (e.g., Ogg and Steiner, 1991; Hounslow et al., 2008a, 2008b) and to conodont ranges in several Tethyan sections in China (e.g., Steiner et al., 1989; Heller et al., 1995; Glen et al., 2009; Li et al., 2016), Iran, and Italy. The Permian–Triassic boundary is near the base of a relatively long normal-magnetozone ("LT1n" or "Gries-N1"; Steiner, 2006). This feature can be identified in the composite magnetostratigraphy from terrestrial deposits within the Germanic Basin (e.g., Nawrocki, 1997; Szurlies, 2004, 2007; Scholze et al., 2016), implying that the base-Triassic is approximately at the transition from the Zechstein evaporite-dominated strata to the Buntsandstein Formation.

The correlation of the marine-based magnetic polarity scale to this Germanic Basin polarity pattern is well established. There is a distinctive dominance of reversed-polarity in the upper Induan and lowermost Olenekian followed by predominantly normal polarity in upper Lower Triassic in both scales, which enables a one-to-one correlation of the individual cycle-scaled Buntsandstein magnetic polarity chrons to those in the marine composite (e.g., Szurlies, 2007; Hounslow and Muttoni, 2010). The same change in polarity dominance and other features are tentatively used to assign geologic stages/substages to terrestrial deposits in the Karoo Basin, southwestern United States, and Russia (Hounslow and Muttoni, 2010; Fig. 4). Therefore the proposed astronomical cyclicity can be projected via these biomagnetostratigraphic correlations to estimate the time spans for Lower Triassic stages and substages (Li et al., 2016).

#### 25.2.3.1.2 Middle Triassic magnetic polarity scales

The seven main polarity pairs of the Anisian display dominance by normal polarity in the lower substages (Aegean, Bithynian) followed by a relative dominance by reversed-polarity through the lowermost Ladinian. This pattern is derived from sections containing Boreal ammonoid zones in Spitsbergen (arctic Norway; Hounslow et al., 2008a, 2008b) and from those with conodont ranges in China (e.g., Lehrmann et al., 2006, 2015), Albania (e.g., Muttoni et al., 1996b), Romania (e.g., Gradinaru et al., 2007), Austria (Muttoni et al., 1996a), and other regions. The distinctive switch in dominance of polarity is the first-order constraint on projecting ages onto terrestrial facies in the Germanic Basin (e.g., Nawrocki and Szulc, 2000; Szurlies, 2007) and the Catalan and Iberian basins of Spain (e.g., Dinarès-Turell et al., 2005), and to England and China (Hounslow and Muttoni, 2010; Fig. 4).

The main reference sections for the eight main polarity pairs of the Ladinian are in the alpine region of Italy and Austria (Seceda, Mayerling, Stuores sections; e.g., Gallet et al., 1998; Broglio Loriga et al., 1999; Muttoni et al., 2004a; Maron et al., 2019).

#### 25.2.3.1.3 Late Triassic magnetic polarity scales

The alpine Mayerling and Stuores sections, plus the Wayao cyclo-magnetostratigraphic section in Guizhou province of South China (Zhang et al., 2015) and the Bolücektasi Tepe in Turkey (Gallet et al., 1992) are the main reference sections for the Julian Substage (lower Carnian). There had been no adequate biostratigraphic controls on magnetostratigraphic studies that might span the upper Carnian (Tuvalian Substage); therefore Hounslow and Muttoni (2010) assigned a "holding" nomenclature of "UT5–UT12." This interval in boreholes through nonmarine strata in the Germanic Basin is dominated by normal polarity above a lowermost Tuvalian reversed-polarity zone (Zhang et al., 2020).

The uppermost Carnian through Norian pattern is mainly derived from the GSSP candidate for the base-Norian at Pizzo Mondello in Sicily (Muttoni et al., 2001, 2004b) and the Silickà Brezovà section of Turkey (Channell et al., 2003). The uppermost Norian to lowermost Rhaetian is calibrated to conodont datums in Austria (Scheiblkogel, Gallet et al., 1998; and the Austrian candidate for the Rhaetian GSSP at Steinbergkogel; Krystyn et al., 2007c, 2007d; Hüsing et al., 2011) and the Italian candidate for the Rhaetian GSSP at Pignola-Abriola (Rigo et al., 2016). A pair of thick overlapping sections in the southern Alps (Brumano and Italcementi Quarry; Muttoni et al., 2010) spans the middle Rhaetian through lowermost Hettangian, although minor faults complicate the stratigraphy.

In general, the magnetozones of the lower Norian (Lacian and Alaunian substages) are dominated by reversed-polarity; whereas the upper Norian (Sevalian) has approximately equal proportions of normal and reversed-polarity. The uppermost Norian to lowermost Rhaetian (depending upon eventual placement of the Rhaetian GSSP) is mainly reversed-polarity; followed by a prevalence of normal polarity that continues into the Hettangian.

During the Late Triassic, a series of rift valleys along the western margin of the future Central Atlantic

accumulated very thick successions of lacustrine deposits that recorded climatic responses to Milankovitch orbital cycles. Drilling of these Newark Basin strata has yielded a complete 30-Myr cycle-scaled pattern of the magnetic reversal history during the Late Triassic (Kent et al., 1995). A few meters above the brief reversed-polarity E23r zone is a palynological turnover event, and a few centimeters higher the lacustrine deposits are overlain by the Orange Mountain basalts, part of the onset of a regional Central Atlantic Magmatic Province (CAMP) dated at approximately 201.5 Ma (e.g., Mundil et al., 2010). Therefore Kent and Olsen (1999; and web page update of 2002) assigned an age of 202 Ma to the top of E23 and tuned the cyclic stratigraphy using the 405-kyr eccentricity cycle and a 1.75-Myr modulating cycle to project the ages of the Late Triassic polarity pattern. Based on palynology (e.g., Cornet, 1977), the base of the Norian had been tentatively assigned to Newark magnetozone E13 at the base of the Passiac Formation (Olsen et al., 1996), but projected to a much lower level (E8r) by correlation to the proposed Norian GSSP at Pizzo Mondello (e.g., option 2 of Muttoni et al., 2004b; Kent et al., 2017). Radioisotopic age control on lower Norian magnetozones in a borehole on the Colorado Plateau supports the cyclostratigraphic age model for the Newark polarity pattern (Kent et al., 2018).

There are many published versions of how this cycle-scaled Newark polarity pattern might correlate to the upper Carnian, Norian and Rhaetian magnetostratigraphy derived from marine sections and composites (e.g., options 1 and 2 of Muttoni et al., 2004b; Ogg, 2004; Ogg et al., 2008; options A, B, and C of Hounslow and Muttoni, 2010; Gallet et al., 2007; Muttoni et al., 2010; Ogg, 2012; Ogg et al., 2016; Maron et al, 2019). Radioisotopic age control and/or cyclostratigraphic scaling of the polarity zones in Norian–Rhaetian marine reference sections is not yet available to provide unambiguous constraints. Once there is an established correlation of the terrestrial to the marine polarity patterns, then the extensive cycle-scaled Newark suite will provide a precise duration and timing for most of the events in the Late Triassic.

### *25.2.3.2 Chemical stratigraphy*

In addition to the major disruptions of climate accompanying the end-Permian and end-Triassic mass extinctions, there are at least two major climatic events indicated by simultaneous excursions in oxygen (temperature) and carbon isotopes (e.g., compilations and reviews by Tanner, 2010a; Preto et al., 2010; Muttoni et al., 2014; Trotter et al., 2015), which are summarized within the geochemical stratigraphy chapters of this book. The anomalous "lethal" tropical temperatures of the Early Triassic (Sun et al., 2012) include an abrupt drop in ammonoid and conodont diversity that was coincident a negative excursion in $\delta^{13}C_{carb}$ near the end of the Smithian Substage. A sudden warming and humid event in the middle of the Carnian stage is considered to be "the most distinctive climate change within the Triassic" (Preto et al., 2010) and disrupted the global land-ocean-biological system (summarized above with the Carnian substages). The current hypotheses for the triggers for these environmental perturbations may have focused on volcanic activity—eruptive phases from the Siberian Traps and the emplacement of the Wrangellia large igneous province, respectively.

#### 25.2.3.2.1 Carbon-isotope trends and major excursions

The $\delta^{13}C$ curve of Fig. 25.1 is a merger of generalized trends from several publications, including a compilation of Early Triassic to earliest Ladinian from Sun et al. (2012) and a synthesis of Late Ladinian through Rhaetian from Muttoni et al. (2014). Five major carbon-isotope excursions are currently important for global correlations among marine and terrestrial settings. In contrast to the common coincidence of widespread anoxic events with negative carbon-excursions during the Devonian and the Jurassic-Cretaceous, there are not yet any identified widespread black-shale episodes associated with these events, although there are indications that low-oxygen deep-sea waters did impinge onto the continental shelves.

1. End-Permian—The main set of end-Permian marine mass extinctions occurs abruptly within a broader major negative excursion in carbon isotopes in both marine carbonates and organic-carbon. High-resolution studies indicate that the stepwise downward trend in negative carbon isotopes was interrupted by a minor positive-isotope excursion that approximately coincided with this main marine extinction level, followed by a pronounced minimum $^{13}C$-values immediately above the basal Triassic (e.g., Korte and Kozur, 2010; Hermann et al., 2010; Luo et al., 2011). Cramer and Jarvis (2020, Ch. 11: Carbon isotope stratigraphy; this book) called the minimum peak the "EGE" for Early-Griesbachian Event. This pronounced trend toward negative carbon-isotope values may have been caused by a combination of decreased marine productivity and influx of light carbon from volcanic, soil-carbon or methane sources (e.g., Holser and Magaritz, 1987; Baud et al., 1989, 1996; Erwin et al., 2002; Korte et al., 2010; Wignall, 2015; Grasby et al., 2016a, 2016b; Chen et al., 2016).
2. Early Triassic—Two positive peaks in carbon-13 within the lower Triassic have been suggested as secondary markers for the bases of the Olenekian (Smithian Substage) and of the Spathian Substage. Therefore Cramer and Jarvis (2020, Ch. 11: Carbon isotope stratigraphy; this book) suggest an abbreviated terminology of DSBE and SSpBE for these two positive excursions. An abrupt drop in ammonoid and conodont diversity is associated with

the onset of the positive carbon-13 excursion at the base of the Spathian Substage (Galfetti et al., 2007a; Algeo et al., 2019a). One hypothesis for the origin of the intervening relatively high-amplitude negative carbon-isotope excursions during the Dienerian through early Spathian is that there were multiple pulses of carbon release during phases of eruption and intrusion of the Siberian Trap flood basalts (e.g., Payne and Kump, 2007; Wignall, 2015; Grasby et al., 2016a, 2016b).

3. Earliest Anisian—The last of these early Triassic positive carbon-isotope excursions is a gradual rise that spans the Olenekian–Anisian boundary. This "Early Anisian Event" or EAnE in the suggested terminology of Cramer and Jarvis (2020, Ch. 11: Carbon isotope stratigraphy; this book) will also be a secondary marker for the yet-to-be-formalized base-Anisian GSSP (Chen et al., 2020).
4. Middle Carnian Event—Carbon isotopes remain relatively constant within a c. 2 per-mil band for c. 30 Myr from middle Anisian to middle Norian, except for a brief set of pronounced negative-excursions that coincide with the middle Carnian "Pluvial Episode" (e.g., Dal Corso et al., 2012, 2018a,b). This excursion may have been caused by the eruption of the Wrangellia large igneous province, which was later accreted to become part of the Alaska-Canada coast.
5. Norian–Rhaetian boundary—A brief positive $\delta^{13}C_{org}$ peak reported from in organic-carbon components at the Norian–Rhaetian boundary (Sephton et al., 2002b; Rigo et al., 2016) has been tentatively attributed to widespread oceanic stagnation coincident with extinction of deep-water invertebrate fauna, but this feature requires verification in additional sections.
6. End-Triassic—The Late Rhaetian (end-Triassic) mass extinctions coincide with a negative carbon-isotope excursion, which, like the end-Permian Event, may be linked to widespread volcanism, oceanic productivity collapse, and a release of methane (e.g., Pálfy et al., 2001; Ward et al., 2001; Hesselbo et al., 2002; Ruhl et al., 2009; Zaffani et al., 2018). However, the interpretation of these carbon-isotope records may be distorted by facies variations in some sections (Zaffani et al., 2018).

#### 25.2.3.2.2 Oxygen isotopes and temperature excursions and trends

The Triassic $\delta^{18}O$ curve from conodont apatite of Fig. 25.1 is a synthesis of several studies, especially for the Early Triassic by Sun et al. (2012) and Middle and Late Triassic trends from Trotter et al. (2015). These imply that tropical temperature during much of the Early Triassic may have exceeded levels that were lethal to larger land-dwelling vertebrates, which may partly explain the dearth of their skeletal remains from these latitudes until the Middle Triassic (Sun et al., 2012; Wignall, 2015).

The $\delta^{18}O$ curve of Fig. 25.1 from Grossman and Joachimski (2020, Ch. 10: Oxygen isotope stratigraphy; this book) implies a general warming trend from Middle Triassic to mid-Norian, followed by a cooling trend to the end of the Triassic. The resolution of this generalized curve-fit to conodont-apatite data has apparently smoothed over the brief global warm and humid episode in the mid-Carnian (e.g., Preto et al., 2010; Dal Corso et al., 2018a).

#### 25.2.3.2.3 Sulfur-isotope trends and excursions

The marine record of sulfur isotopes ($\delta^{34}S$; Paytan et al., 2020, Ch. 9: Sulfur isotope stratigraphy; this book) display low values of c. 12‰ prior to the end-Permian mass extinction, followed by a brief excursion to approximately 25‰–30‰ near the end-Permian, with potentially a continuation into a broad peak near the Induan–Olenekian boundary (e.g., Kampschulte and Strauss, 2004; Newton et al., 2004; Horacek et al., 2010a, 2010b; Luo et al., 2010; Song et al., 2013; Bernasconi et al., 2017). One interpretation for the rate and magnitude of these excursions is that sequestered hydrogen-sulfide in a latest Permian anoxic ocean was released by oceanic overturning (e.g., review in Paytan et al., 2020, Ch. 9: Sulfur isotope stratigraphy; this book) and that the oceanic sulfate reservoir was anomalously low, perhaps less than 15% of modern size (Luo et al., 2010). Sulfur-isotope stratigraphy within the rest of the Triassic is currently at a low-precision reconnaissance status.

#### 25.2.3.2.4 Strontium and osmium-isotope trends and excursions

The curve of marine $^{87}Sr/^{86}Sr$ through the latest Permian through Triassic (Fig. 25.1) begins with a slow increase from the major trough (0.7068) near the end of the Middle Permian, which suddenly undergoes a sharp increase in the rate of rise at the Permian–Triassic boundary to peak (0.7081) near the base of the Middle Triassic (e.g., review in McArthur et al., 2020, Ch. 7: Strontium isotope stratigraphy; this book). The rapid rise in $^{87}Sr/^{86}Sr$ through the Early Triassic may be a response to increased continental weathering during the anomalous warm temperatures of the Early Triassic (e.g., Martin and Macdougall, 1995; Sedlacek et al., 2014). A relatively rapid decline a minimum (0.7076) at the end of the Middle Triassic is followed by a gradual rise through the Norian to a second peak (c. 0.7079) in latest Triassic followed by a continuous decline through the Rhaetian and Early Jurassic to another major low (to c. 0.7071) in latest Pliensbachian (e.g., Koepnick et al., 1990; Korte et al., 2003; Cohen and Coe, 2007).

Osmium-isotope stratigraphy has not yet been systematically compiled for the Triassic (Peucker-Ehrenbrink and Ravizza, 2020, Ch. 8: Osmium isotope stratigraphy; this

book). Analysis of black shales of latest Anisian from Svalbard yielded initial $^{187}Os/^{188}Os$ ratio of $0.83 \pm 0.03$, which is one of the highest recorded ratios for global seawater between the earliest Cambrian and the Late Early Jurassic (Xu et al., 2009). This peak remains to be verified and delimited in additional sections. In general, the trends in Osmium mirrors those of the Strontium curve, including a gradual decline through the Rhaetian from an initial $^{187}Os/^{188}Os$ ratio from a Late Norian peak of 0.75 that was interrupted by a brief excursion to high (radiogenic) ratios upon eruption of the CAMP at the end of the Triassic (e.g., Cohen and Coe, 2007; Peucker-Ehrenbrink and Ravizza, 2020, Ch. 8: Osmium isotope stratigraphy; this book).

### 25.2.3.3 Cycle stratigraphy

Numerous cyclostratigraphy analyses have been applied to continental and marine deposits of Triassic age. Huang (2018) compiled over 30 of these Triassic studies to select seven major ones that both encompassed a relatively long time span without major stratigraphic breaks and published the original datasets in a form applicable to a standardized retuning to the 405-kyr long-eccentricity cycle. The merger of these seven cyclostratigraphic datasets enabled an initial estimate of a full astronomical-tuned time scale for the entire Triassic. Those selected studies were the Lower to Middle Triassic carbonates of South China (Li et al., 2016, 2018), Middle to Upper Triassic radiolarian-rich pelagic sediments accreted to Japan (Ikeda et al., 2014; Ikeda et al., 2017), Carnian carbonates of South China (Zhang et al., 2015), and Upper Triassic Lacustrine Sediments of the Newark Basin (Olsen and Kent, 1999; Kent et al., 2017). This suite demonstrates the potential for a full astronomical-tuned Triassic time scale, but this goal is currently hindered by uncertainties in merging the magnetic polarity scales, radiolarian zones, and conodont datums into a global composite.

In continental settings, the monsoon-dominated climate of the Pangea megacontinent was sensitive to Milankovitch orbital-climate cycles, especially to the precession-eccentricity components. Extended and quasi-continuous deposits of continental facies having both excellent magnetostratigraphy and unambiguous cycles are present in central Europe (Lower Triassic) and eastern North America (Upper Triassic). In theory, these successions should be the Rosetta stone to project cycle−scaled durations onto marine sequences for a precise relative time scale, similar to what has been developed for the Cenozoic. In practice, as noted previously, there is a lack of a unique pattern match for correlation of these extended intervals of cycle-scaled magnetostratigraphies with marine-based composite polarity patterns. The interpretations and controversies concerning these Triassic cyclic deposits are critically examined by Tanner (2010b).

Variations in clastic input and the extent of lacustrine influences in the Buntsandstein basins of central Europe during the Early Triassic provide a detailed regional stratigraphy that is applicable to surface exposures and downhole logs (e.g., reviews in Röhling, 1991; Bachmann and Kozur, 2004; Szurlies, 2004; Menning et al., 2005; Feist-Burkhardt et al., 2008). The cycles, spanning about 10−20 m with sandstones fining upward into more clay-rich sediments, are generally interpreted as oscillations between more arid and more humid conditions. Constraints from terrestrial biostratigraphy (conchostracan, pollen-spores) combined with radioisotope ages on the span of the Early Triassic indicate that the depositional sequences appear to coincide with the 100-kyr short-eccentricity cycle (e.g., Bachmann and Kozur, 2004; Menning et al., 2005). However, the expected 405-kyr long-eccentricity has not been unambiguously resolved. The magnetostratigraphy from the Buntsandstein, especially within the lower portion, which has relatively longer duration polarity zones and biostratigraphic constraints, is fairly well correlated to other Early Triassic reference sections (Szurlies, 2007; Hounslow and Muttoni, 2010). Even though a monotonic 100-kyr periodicity is not expected for short-eccentricity and there is a possibility of "missing beats" at possible exposure horizons within this Buntsandstein succession, the projected cycle-scaling of the marine zonation and associated Early Triassic substages via this magnetostratigraphy is a close fit to radioisotopic ages and most of the polarity pattern correlates with the independent cyclo-magnetostratigraphy from Lower Triassic and Anisian Limestones of South China (Li et al., 2016, 2018).

Interbedded marls and limestones of shallow-marine origin spanning the Permian−Triassic boundary interval in the Austrian Alps display cycles with ratios matching Milankovitch periodicities and have been interpreted to imply that the latest Permian extinction and negative carbon-isotope spike spanned less than 30 kyr (Rampino et al., 2000, 2002), which agrees with radioisotopic constraints at the Triassic GSSP at Meishan, China (Burgess et al., 2014).

The Latemar massif in the Italian Dolomites was an atoll-like feature with a core of flat-lying Anisian and Ladinian platform carbonates. Oscillations in sea level were created over 500 thin depositional cycles (Goldhammer et al., 1987). Stacking patterns and spectral analysis of the sea-level oscillations had been interpreted as representing precession modulated by short-term (100 kyr) eccentricity, therefore yielding an implication that the Latemar deposit spans approximately 10 Myr (Goldhammer et al., 1990; Hinnov and Goldhammer, 1991). In contrast, U−Pb ages from coeval tuff-bearing basinal deposits appear to constrain the Latemar platform to span only 2−4 Myr (e.g., Brack et al., 1996, 1997; Mundil et al., 1996; Hardie and Hinnov, 1997; and extended review in Tanner, 2010a). A possible solution to

this disparity is that an extremely rapid rate of platform construction (c. 500 m/Myr or greater) enabled recording of sub-Milankovitch sea-level oscillations with misleading similarity in ratios to precession-eccentricity (e.g., Kent et al., 2004, 2006; Hinnov, 2006; Meyers, 2008). This ambiguity in cyclostratigraphic interpretation demonstrates that any cycle-stratigraphic analysis based only on a single section requires verification from other independent basins and facies. Studies of similar oscillating Lofer facies within upper Triassic platform carbonates of the Austrian Alps played an important role in developing fundamental concepts of cyclostratigraphy (e.g., Fischer, 1964), but the reality of regular cyclicity in these deposits has also been debated (e.g., Satterley, 1996, versus Schwarzacher, 2005, and Cozzi et al., 2005; reviewed in Tanner, 2010b).

Radiolarian-rich pelagic chert successions from Japan spanning the Middle Triassic are characterized by ribbon bedding. These chert-clay couplets have been interpreted as productivity fluctuations induced by 20-kyr precession cycles, and the longer term trends in bed thickness correspond to 100- and 405-kyr eccentricity cycles (Ikeda et al., 2010, 2017). These cyclostratigraphic interpretations, the tentative correlation of radiolarian taxa to geologic stages, a potential long-term modulation of c. 3.6 Myr, and the continuity of the bedded-chert sections await further verification.

During the late-Middle Triassic through Early Jurassic, a set of rift basins formed as Pangea underwent an initial phase of breakup. The thick Newark Group of lacustrine sediments from these tropical basins are characterized by oscillations between semistagnant deep lakes and arid playas as the intensity of monsoonal rains responded to Earth's precession modulated by short- (c. 100 kyr) and long-term (c. 400 kyr) eccentricity cycles. Spectral analysis of sediment facies successions in a series of deep-drilling cores enabled compilation of a cycle-scaled stratigraphic record, including a detailed polarity pattern that is unprecedented in its 30-Myr temporal span (e.g., Kent et al., 1995; Olsen et al., 1996; Kent and Olsen, 1999). As discussed previously, the comparison of the cycle-scaled terrestrial polarity signature to the un-scaled marine magnetostratigraphy does not always provide a unique match. However, uppermost Triassic lacustrine deposits with alternating red-to-green coloration at St. Audrie's Bay have yielded both a magnetostratigraphy (Hounslow et al., 2004) and an interpreted 3.7 Myr cyclostratigraphy (Kemp and Coe, 2007) that have a polarity scaling resembling the upper Newark interval of polarity zones E19n–E16n. Cyclostratigraphy of a composite Rhaetian succession in Austria indicates that this stage (using the Austrian GSSP candidate) has a minimum duration of 6.7 Myr (Galbrun et al., 2020).

Details and discussion of these and other Triassic cyclostratigraphic studies are given in Huang (2018).

### 25.2.3.4 Sequence stratigraphy

Triassic sea-level Trends and sequences of different relative magnitudes have been compiled for Boreal basins (e.g., Embry, 1988; Mørk et al., 1989; Skjold et al., 1998), the classic Germanic Trias (e.g., Aigner and Bachmann, 1992; Geluk and Röhling, 1997), the Dolomites and Italian Alps regions (e.g., De Zanche et al., 1993; Gaetani et al., 1998; Gianolla et al., 1998, Gianolla and Jacquin, 1998), and other regions. Some of these sea-level trends appear to correlate on an interbasin to global scale (e.g., Haq et al., 1988; Haq, 2018; Hallam, 1992; Embry, 1997; Gianolla and Jacquin, 1998). The significant disparity in some proposed major global features for the Triassic (e.g., Hardenbol et al., 1998, compared to Simmons et al., 2007) was difficult to resolve, because the supporting details of reference sections and biostratigraphic control are generally not adequately published.

The major sequences in Figs. 25.1 and 25.5–25.7 are from a Triassic synthesis by Haq (2018) that enhanced a previous compilation and systematic numbering system by Jacquin and Vail (1998). In this compilation the main first-order Triassic sea-level trend is dominated by a single cycle—a progressive transgression that began in the early Anisian, peaks near the Carnian–Norian boundary, followed by a very gradual regression through the middle Rhaetian that turns into a faster regression in the latest Rhaetian through early Hettangian. A lesser transgression–regression cycle began in the latest Permian with a minor peak in latest Induan. Superimposed on these main cycles are several second-order facies cycles with major sequence boundaries at the Induan–Olenekian boundary, Anisian–Ladinian boundary, mid-Carnian (Julian-Tuvalian boundary), latest Carnian, and latest Norian (or the proposed Norian–Rhaetian boundary candidate in Austria). In contrast, Simmons et al. (2007) published a general Triassic scale with seven main sequences (*Tr10* to *Tr80*). See also review in Simmons et al. (2020, Ch. 13: Phanerozoic eustasy, this book). These proposed Triassic suites of sequences and sea-level trend await published documentation of the different compilations and a community consensus on the regional versus global components.

### 25.2.3.5 Other major stratigraphic events

#### 25.2.3.5.1 Large igneous provinces

The Triassic is delimited by two major volcanic provinces: the Siberian Traps at the base and the CAMP at the top.

1. End-Permian—The Siberian Traps exposed mainly on the Siberian craton was one of the most voluminous volcanic eruption provinces of the Phanerozoic, with an estimated volume greater than 2 million cubic kilometers of basalt flows and volcaniclastic rocks (e.g., reviews by Reichow et al., 2004; Ernst, 2014; Wignall, 2015; in Ernst et al., 2020; and at the Large Igneous Provinces Commission website). The volcanic province on the Siberian craton is

generally subdivided into four distinct geographic regions: Noril'sk, Putorana, Nizhnaya Tunguska, and Maimecha-Kotuy. The main pulses of the voluminous Siberian Trap flood basalts are approximately coeval with the latest Permian mass extinctions, and the waning stages of this volcanic activity continued into the earliest Triassic (e.g., Renne et al., 1995; Erwin et al., 2002, and references therein; Reichow et al., 2009; Burgess and Bowring, 2015; Burgess et al., 2014, 2017; Wang et al., 2018).

2. Middle Carnian—The Wrangellia terrane, which is accreted to British Columbia and Alaska, contains a major episode of tholeiitic flood volcanism in submarine and subaerial environments. Radiometric dating (c. 227 and 232 Ma) and the overlying fossiliferous strata indicate an eruption during Carnian. The original volcanic volume is estimated as 1 million cubic kilometers (e.g., Greene et al., 2008, 2010, 2011).
3. End-Triassic—The CAMP has ages clustering at c. 201 Ma just prior to Triassic–Jurassic boundary and is considered to have been a major causal factor in the end-Triassic extinctions (e.g., Marzoli et al., 1999; Jourdan et al., 2009a; Schoene et al., 2010; Blackburn et al., 2013; Ernst, 2014). The total extrusive volume may have been even greater than the Siberian Traps.

#### 25.2.3.5.2 Major bolide impacts

The 100-km diameter Manicouagan impact structure of Quebec has melt rock directly dated by modern U/Pb methods (214.56 ± 0.05 Ma; Ramezani et al., 2005; Hodych and Dunning, 1992, as reevaluated by Jourdan et al., 2009b). This impact event and associated environmental catastrophe may have contributed to the large-scale turnover of continental tetrapods during mid-Norian, during which dinosaurs attained dominance over competing families (e.g., Benton, 1986, 1993; Lucas, 2010d). However, no record of this impact or major environmental catastrophe has yet been discovered within the extensive lacustrine deposits of the Newark Group of northeastern North America.

The only other significant impact that is assigned to the Triassic is the Saint Martin crater with a c. 40 km diameter in Manitoba, Canada, has a vague estimated mid-Triassic age of 220 ± 32 Ma (Earth Impact Database, 2018, and references therein).

## 25.3 Triassic time scale

### 25.3.1 Overview

After the publication of GTS2004 the Triassic was the focus of extensive sampling and application of ultra-high-resolution methods by different geochronology laboratories. Triassic and uppermost Permian strata enabled testing enhanced techniques for single-zircon dating, provided sets for intercalibration of U–Pb and Ar–Ar methods and the standardization of procedures among laboratories. These new age sets had replaced or called into question nearly all of the Triassic radiogenic isotope ages published before 2004 (reviewed by Mundil et al., 2010). The initiation and termination of the Triassic Period and many of its GSSP-defined stages have been constrained by a remarkably extensive suite of high-precision radioisotopic dates (Appendix 2, this volume), implying a span from 251.9 to 201.4 Ma (50 Myr). The radioisotopic details and stratigraphic placement of these dates are compiled in Appendix 2, and only those dates that constrain stage boundaries will be highlighted below.

The merger of astronomical cycles with magnetostratigraphy is the framework for scaling the majority of the Triassic. The cyclo-magnetostratigraphy is tied to the subset of high-precision radiometric U–Pb dates obtained by ID-TIMS methods. The ages for many of the biozone zones and some of the geochemical curves are derived either from direct correlations to the astronomical scaling in reference sections or from their relative position within magnetic polarity chrons. The age models for all other biostratigraphic datums and geochemical curves are from their estimated placement relative to these primary biostratigraphic or magnetostratigraphic scales. Therefore this composite cyclo–magnetic–biostratigraphic age model that has been developed by different international teams is similar to what has been accomplished for the cyclo–magnetic scaling of the Cenozoic Era.

The precision of the direct radiometric age control on the cyclostratigraphic or magnetic polarity scales is generally less than 0.1 Myr, and the placement of biozones within cyclostratigraphic reference sections is usually to an accuracy of one short-eccentricity cycle of a similar 0.1 Myr duration. As with all other age models for intervals within the Paleozoic–Mesozoic, some caveats include that the published placement of biostratigraphic datums within the main reference sections may not represent global first occurrences and may be influenced by uncertain taxonomic assignments (especially for some conodonts), that some of the cyclo–magnetic–biostratigraphic scales have not yet been verified from independent basins, and that the assignment of some regional biostratigraphic zones is not well calibrated to the primary age scales. Some of these less-certain scalings are indicated by dashed or dotted lines in the synthesis charts (Figs. 25.5–25.7).

### 25.3.2 Early Triassic through Anisian age model

For the Early Triassic through early Anisian, the magnetic polarity pattern that was calibrated to short-eccentricity (100-kyr) changes in monsoon intensity recorded by clastic cycles in the Germanic Basin (e.g., Szurlies, 2007) has been duplicated in the cyclo-magnetostratigraphy of conodont-bearing carbonate deposits on the margins of the paleogeographic Yangtze Platform of South China (Li

et al., 2016, 2018). This cycle-magnetic compilation of South China includes the GSSPs for the Induan (base-Triassic) at Meishan (Zhejiang province), the candidate for the Olenekian GSSP at West Pingdingshan near Chaohu (Anhui province), and a candidate for the Anisian GSSP candidate at Guandao (Guizhou province). The astronomical tuning is tied to the base-Triassic **Induan** GSSP at Meishan, which has an interpolated age of **251.902 ± 0.024 Ma** based on close-spaced U–Pb ID-TIMS dates (Burgess et al., 2014). *[Note that an external uncertainty of c. 0.29 Myr should be included when comparing this version of EARTHTIME-standardized dates to previous versions, as explained in Burgess* et al. (2014)].

The cyclo-bio-magnetostratigraphic reference section at West Pingdingshan near Chaohu in South China is a candidate for the **Olenekian** GSSP. According to the astronomical tuning, the Induan/Olenekian boundary level is 2.0 Myr later than the base-Triassic therefore has an age of **249.9 Ma** (Li et al, 2016). This 2.0-Myr span is independently verified by the 1.9 ± 0.1 Myr duration for the Induan stage derived from cyclo-biostratigraphy of conodont zones in the Montney Formation of British Columbia (Shen et al., 2017; Moslow et al., 2018; Henderson et al, 2018; Shen, 2018).

If the Griesbachian–Dienerian substage boundary is assigned as the base of the conodont *S. kummeli* Zone in these astronomically tuned sections of South China, then the base of **Dienerian** has a projected age of **250.5 Ma** (Li et al., 2016). The 1.4-Myr duration of the Griesbachian Substage is also consistent with a U–Pb date of 251.50 ± 0.6 Ma from the lower-middle Griesbachian at Meishan (Burgess et al., 2014). A reported date of 251.22 ± 0.2 Ma on a volcanic ash from lower Smithian (Galfetti et al., 2007b) was based on pre-EARTHTIME standards, and therefore is anomalously old and should be reanalyzed (Burgess et al., 2014).

There is ID-TIMS radiometric dating of the volcanic-ash beds in the Olenekian–Anisian boundary interval at the GSSP candidate at Wantou (Guangxi province) section (Ovtcharova et al., 2015) and at the Guandao section (Guizhou province) (Lehrmann et al., 2015). These dates, when coupled with the composite cyclostratigraphy for Early Triassic through Anisian (Li et al., 2016), indicate that the lowest occurrence of the conodont *Ch. timorensis s.str.* as the preferred marker for the base of **Anisian** at approximately **246.7 Ma** (Chen et al., 2020). U–Pb-dated volcanic-ash beds bracketing this base-Anisian marker at Wantou by Ovtcharova et al. (2015) had been interpreted by them to imply a slightly older age (c. 247.3 Ma) for a slightly different conodont marker for the base-Anisian, but they caution that there are inconsistencies in the progression of interpreted dates from the zircon populations in successive layers and the statistical derivation of a mean date from each ash bed was influenced by the decisions of which individual zircons within the distribution of ID-TIMS dates should be included. Therefore the cyclostratigraphic age of 246.7 Ma relative to the base-Triassic control date is used here.

If the Smithian–Spathian substage boundary is placed at the lowest occurrence of conodont *Novispathodus pingdingshanensis* in these sections, then the base of the **Spathian** has a projected age from the astronomical tuning of **248.1 Ma** (Li et al., 2016).

The magnetostratigraphy and interpreted 405-kyr eccentricity-driven cycles at the conodont-rich Guandao section span the Anisian through lowest Ladinian (Lehrmann et al., 2015; Li et al., 2018). This cyclo-magnetostratigraphy age model was applied to estimate the ages for the bases of Anisian substages according to their Tethyan ammonoid-based correlations to magnetic polarity zones (e.g., Hounslow and Muttoni, 2010). The corresponding cyclo-magneto-ammonoid age model projects the base of **Bithynian** at **245.0 Ma** (base of *Kocaella* ammonoid zone), the base of **Pelsonian** at **244.2 Ma** (base of *B. balatonicus* ammonoid zone), and the base of **Illyrian** at **243.3 Ma** (base of *Paraceratities trinodosus* ammonoid zone).

In some cases, these ammonoid-defined substages are different from their conodont-based placements relative to polarity zones in South China (e.g., Lehrmann et al., 2015), for example, the basal substage of Aegean includes 5 ammonoid zones (Jenks et al., 2015), but its conodont-based duration at Guandao would have been only 0.3 Myr, compared to a c. 1.7-Myr duration based on ammonoid correlation to the

**FIGURE 25.5** Selected marine and terrestrial biostratigraphic zonations of the Late Triassic. ("*Age*" is the term for the time equivalent of the rock-record *stage*. *Note that the Ma-age scale is more compact than in* Figs. 25.6 or 25.7). Marine-facies magnetostratigraphy zones are labeled in Rhaetian after Gallet et al. (2007), in Norian after Hounslow and Muttoni (2010), in Carnian–Norian boundary interval after Muttoni et al. (2004b), in Carnian after Zhang et al. (2020) and in Ladinian–Carnian boundary interval after Maron et al. (2019). Those of late Carnian through Rhaetian are shown with one option for the calibrations to the astronomical-scaled polarity chrons of the Newark Basin (Kent et al., 2017). [Note that the durations of Newark Basin polarity zones E1 through E6, which are within noncyclic fluvial sediments, were projected by Kent and Olsen (1999) based on the average accumulation rate for the overlying polarity zones E9 through E14 preserved in lacustrine sediments, and E1 through E4 are uncertain.] Tethyan and Arctic/Panthalassan ammonoid zones are modified from Jenks et al. (2015) and Orchard and Tozer (1997). Tethyan conodont zones are modified from Moix et al. (2007), Kozur (2003) and Rigo et al. (2018) with genera standardized by Michael Orchard, and Tethyan bivalve zones are from McRoberts (2010). Arctic/Panthalassan conodont zones are from Michael Orchard and Martyn Golding (see text). Spinicaudatun (Conchostracan) zones of the Germanic Basin are modified from Kozur and Weems (2010), Weems and Lucas (2015), Geyer and Kelber (2018), and Franz et al. (2018). Land vertebrate zones and markers are from Lucas (2010d, 2018). Main sea-level trends are from Haq (2018). Additional Triassic (and all Phanerozoic) zonations, biostratigraphic markers, geochemical trends, sea-level curves, and details on calibrations are compiled in the internal datasets within the *TimeScale Creator* visualization system (free at www.tscreator.org).

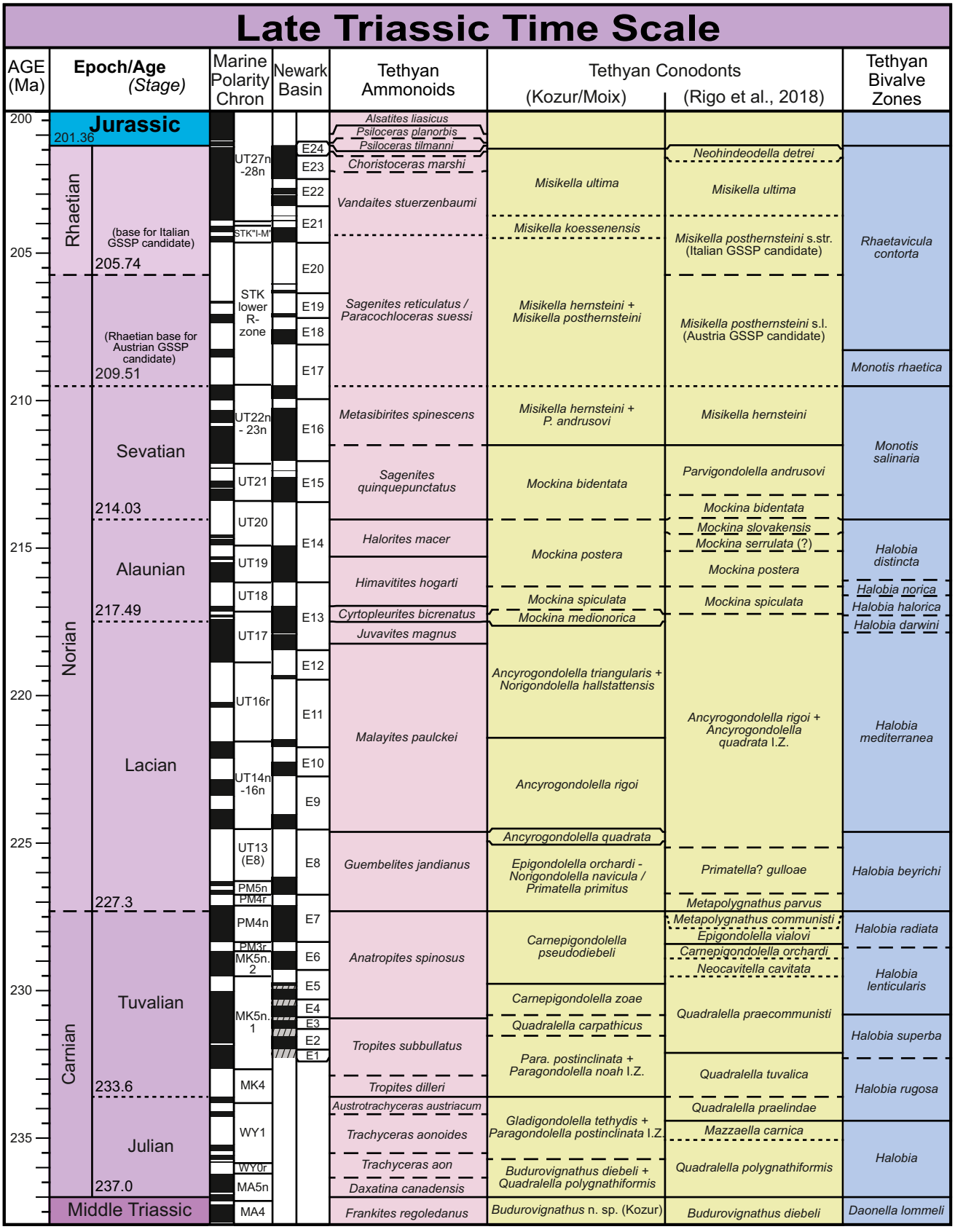


FIGURE 25.5 (Continued).

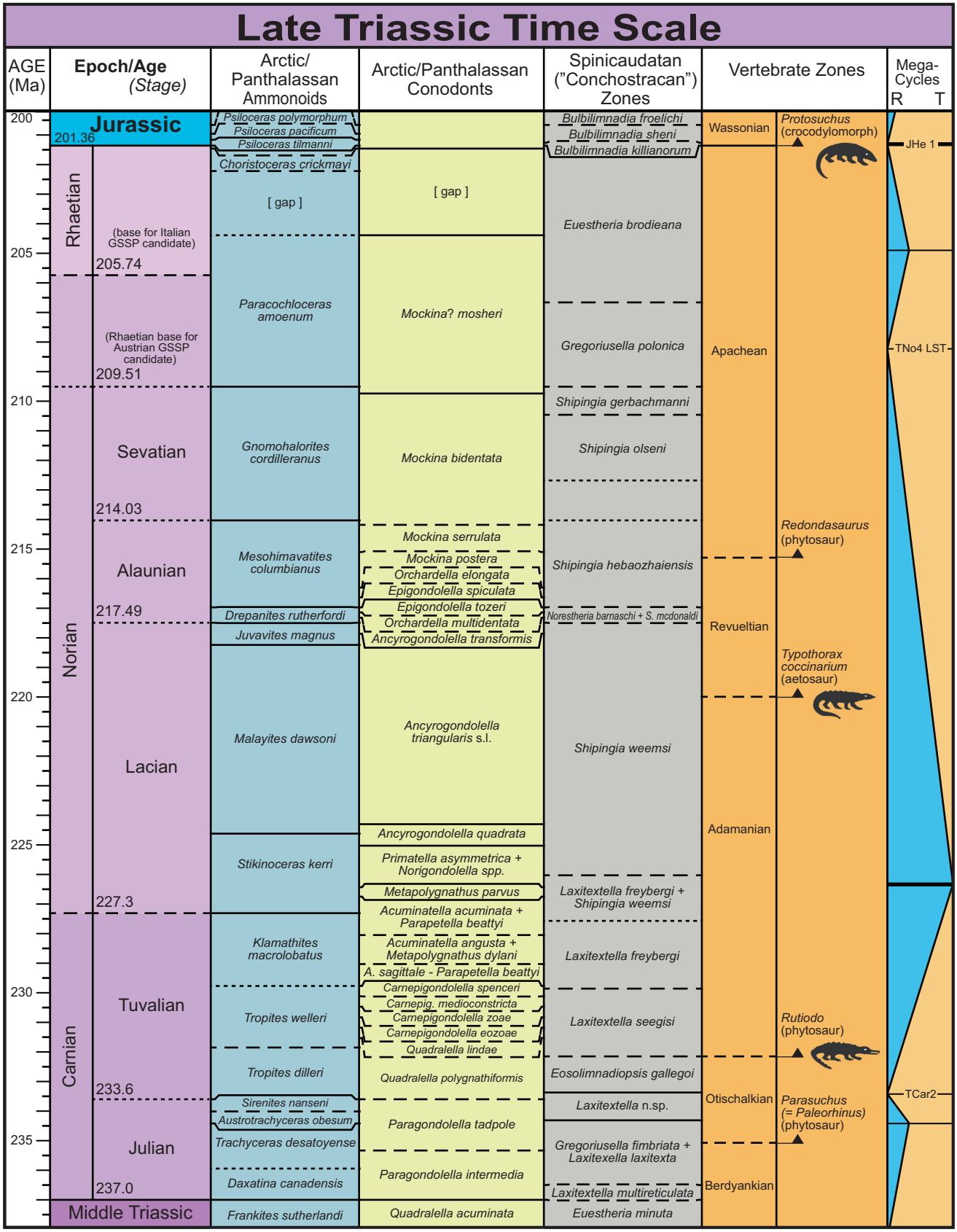


FIGURE 25.5 (Continued)

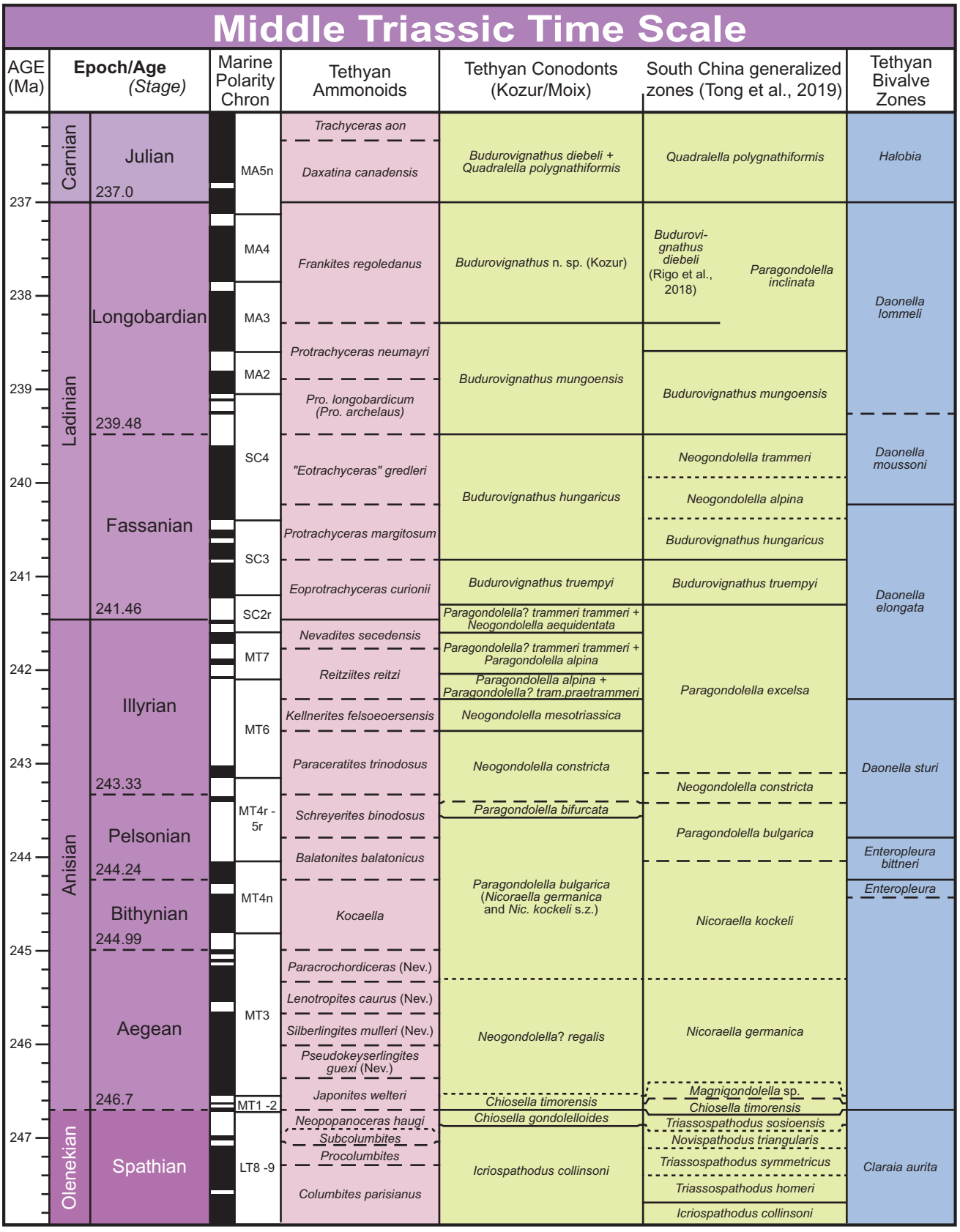


**FIGURE 25.6** (Continued)

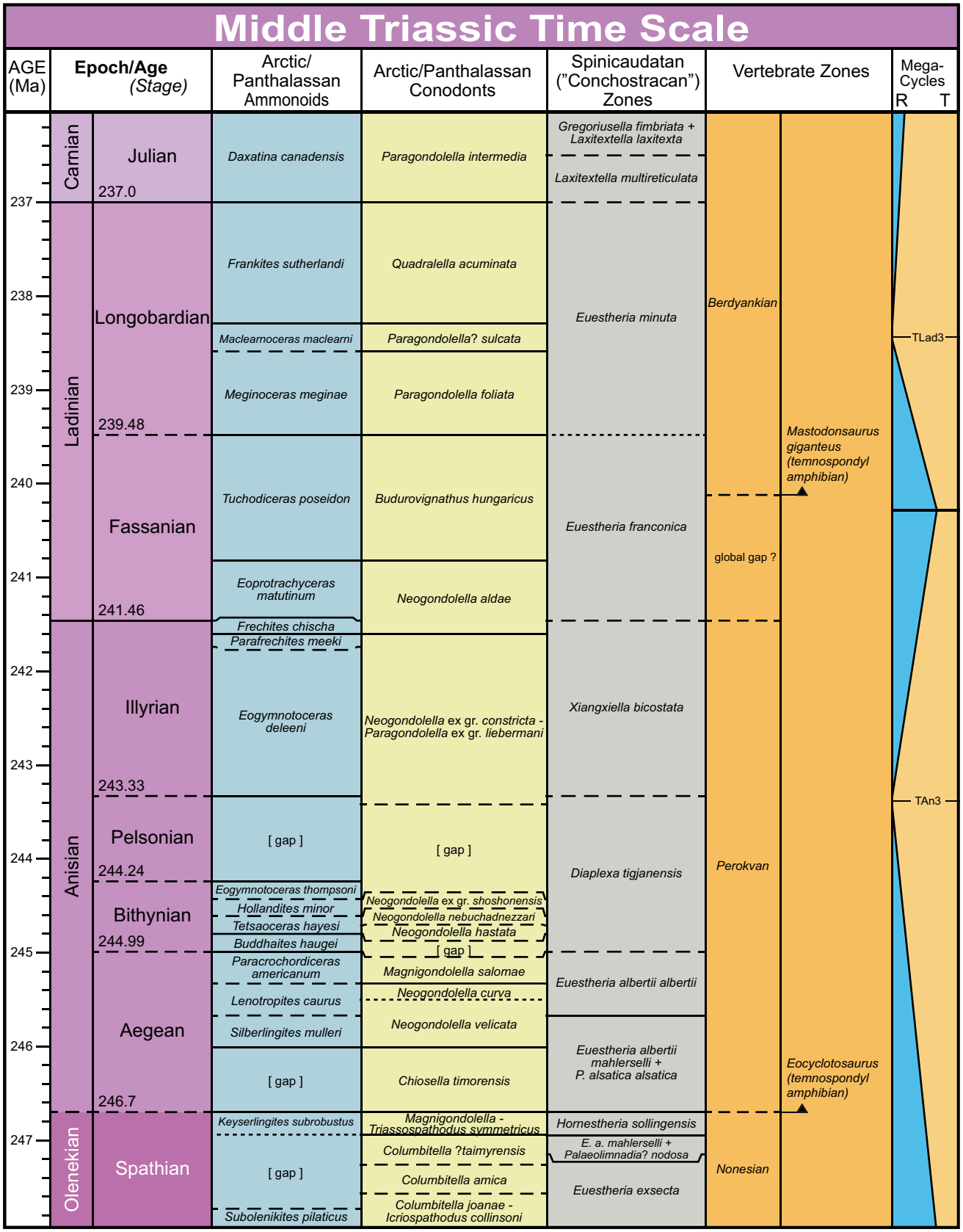


FIGURE 25.6 (Continued)

reference magnetic polarity pattern elsewhere (Hounslow and Muttoni, 2010). Therefore because the bases of Anisian substages have been traditionally assigned with ammonoid zones, these versions for the substages are dashed in the GTS2020 charts.

The ages for all other biozones, sea-level sequences, geochemical trends, and other events are derived from their published calibrations to the astronomical-tuned age model for Early Triassic through Anisian conodont zones of South China or to their calibration to the magnetic polarity zones. For example, the age model for ammonoid zones of the Arctic is according to magnetostratigraphy studies (e.g., Ogg and Steiner, 1991; Hounslow et al., 2008a, 2008b; Hounslow and Muttoni, 2010) as correlated to the Chaohu and Guandao cyclo-magnetostratigraphic scales.

### 25.3.3 Ladinian through Carnian age model

The Seceda reference section of northern Italy provides an array of high-precision U–Pb radiometric dates, magnetostratigraphy, and partial cyclostratigraphy to constrain the ages and durations of Ladinian ammonoid zones and magnetic polarity zones (Wotzlaw et al., 2018; Maron et al., 2019). These beds can be directly correlated to the GSSP for the Ladinian at nearby Bagolino. The dating of the bracketing tuff beds (tabulated in Appendix 2) when combined with the cyclostratigraphy enable a precise dating of Anisian–**Ladinian** boundary as **241.464 ± 0.28 Ma**, plus constraints on the ages of the ammonoid zones and "SC" magnetic polarity zones of latest Anisian through middle Ladinian (Wotzlaw et al., 2018; Maron et al., 2019). The Fassanian–**Longobardian** substage boundary (base of *P. longobardicum* ammonoid zone) of the Ladinian is at approximate **239.5 Ma**.

The Ladinian–**Carnian** stage boundary is dated at its GSSP at Prati di Stuores of northern Italy one ammonoid zone above a level dated as 237.77 ± 0.14 Ma; therefore is considered to have an approximate age of **237 Ma** (Mietto et al., 2012). The GSSP section and nearby Mayerling section have a detailed magnetostratigraphy and ammonoid zonation, and the chart for GTS2020 uses the "MA" age model from Maron et al. (2019).

The placement of the **Carnian** GSSP at Prati di Stuores in the Southern Alps of Italy is one ammonoid subzone above a level dated at 237.77 ± 0.14 Ma therefore is considered to have an approximate age of **237 Ma** (Mietto et al., 2012). Maron et al. (2019) suggest that sediment accumulation rates might indicate a more precise estimate of 236.8 Ma; but until there are additional dated levels or cyclostratigraphy, we retained the rounded age of c. **237 Ma** as used in GTS2012.

The Early Carnian has a partial cyclostratigraphic scaling of magnetic zones with approximate conodont zones derived from duplicate sections in the Guizhou province of South China (Zhang et al., 2015). The magnetostratigraphy has been verified in boreholes in the Germanic Basin up to the "Carnian Pluvial Episode" of latest Julian (Zhang et al., 2020). The "Carnian Pluvial Event" spans c. 1 Myr (Kozur and Bachmann, 2008; Roghi et al., 2010), therefore the Julian-**Tuvalian** substage boundary has a projected age relative to the base-Carnian of approximately **233.6 Ma**; but with a high uncertainty.

A radiometric date of 230.91 ± 0.33 Ma (Furin et al., 2006) on a partial magnetostratigraphic section at Pignola in the Lagonegro Basin of Italy (Maron et al., 2017) constrains the Tuvalian magnetostratigraphic scale from those Germanic Basin boreholes (Zhang et al, 2020). The latest Carnian portion of that Germanic Basin magnetostratigraphy overlaps with the conodont-dated magnetic polarity pattern from the candidate for the Carnian–Norian GSSP at Pizzo Mondello in Sicily, Italy (Muttoni et al., 2004a, 2004b; Kent et al., 2017). That Pizzo Modello "PM" magnetostratigraphy has been correlated to the lowest portion of the extraordinary cyclo-magnetostratigraphy from the lacustrine deposits in the Newark Basin that is anchored to a radiometric date of 201.57 Ma on the overlying Orange Mountain Basalt (Kent et al., 2017; Maron et al., 2019). Unfortunately, the middle-upper Carnian set of Newark polarity zones are in a fluvial facies and do not have direct cyclostratigraphic scaling; therefore the age model for the Late Carnian (Tuvalian Substage) is mainly based on the relative accumulation rates for the thick magnetostratigraphic sections in the Germanic Basin as constrained by the single radiometric date from Pignola, Italy. These Germanic Basin strata have only terrestrial conchostracan biostratigraphy; therefore the age model for the marine biozones in the Tuvalian Substage is dotted in these GTS2020 charts. The age model for the Tuvalian substage is probably the least-well-constrained interval within the entire Triassic.

### 25.3.4 Norian through Rhaetian age model

The age model for the entire Norian through Rhaetian is based on the magnetostratigraphic correlation of marine sec-

**FIGURE 25.6** Selected marine and terrestrial biostratigraphic zonations of the Middle Triassic. ("*Age*" is the term for the time equivalent of the rock-record *stage*. *Note that the Ma-age scale is more expanded than in* Fig. 25.5*)*. Marine-facies magnetostratigraphy zones are labeled in Ladinian after Maron et al. (2019) and in the latest Spathian and Anisian after Hounslow and Muttoni (2010). Sources for Tethyan ammonoid, conodont and bivalve zones, Arctic/Panthalassan ammonoid and conodont zones, land vertebrate zones, and major sea-level trends are the same as in Fig. 25.5. South China conodont zones are from Tong et al. (2018). Spinicaudatun (Conchostracan) zones of the Germanic Basin are from Kozur and Weems (2010).

tions to the astronomical-tuned magnetic polarity pattern from the boreholes in the lacustrine strata of the Newark Basin of eastern North America (e.g., Hounslow and Muttoni, 2010; Muttoni et al., 2014; Maron et al., 2015, 2019; Kent et al., 2017). The astronomical tuning of the Newark magnetic polarity time scale has been partially verified by correlation to U–Pb detrital-zircon dates that constrain the magnetostratigraphy from boreholes into the Chinle Formation of southwestern United States (Kent et al., 2018).

The proposed placement of the Carnian–Norian boundary is the lowest occurrence of conodont *Meta. parvus*. In the detailed conodont lineage study of the PM GSSP candidate, this conodont begins at a level 5/6ths up in polarity zone "PM4n" (Mazza et al., 2018), which is equivalent to chron E7n of this astronomical-tuned Newark polarity scale. Therefore the base-**Norian**, based on this working definition and Kent et al. (2017) chron ages, has a projected age of **227.3 Ma**.

This age assignment is partly supported by the U–Pb CA-TIMS radioisotopic dates of 223.81 ± 0.78 Ma and 224.52 ± 0.22 Ma reported from volcanic tuffs in British Columbia that bracket the lower/middle Norian substage boundary, as placed by adjacent conodont assemblages as used in North America (Diakow et al., 2010, abstract; and Mike Orchard, pers. commun., Sept 2015). Unfortunately, when this GTS2020 chapter was being prepared, these and other Triassic ages from Canada still had not yet been officially published.

However, the Carnian–Norian boundary is not yet formalized, and other ages have been promoted that may be partly dependent upon the implicit working definitions. For example, a base-Norian age estimate of c. 220 Ma has been proposed that is partly based on terrestrial correlations and implied potential problems with the Newark cycle–based age model (e.g., Lucas, 2018a, 2018b; Lucas et al., 2012). In GTS2012, two different options for a Norian–Rhaetian age Model were presented of "long Norian" and "short Norian" end members with potential different correlations of the Newark magnetic scale to the magnetostratigraphic records assembled (by Hounslow and Muttoni, 2010) from sedimentary sections that had marine biostratigraphy (Ogg et al., 2012, 2014). The construction of a Norian time scale is also difficult because many portions of the Newark magnetic polarity pattern lack an adequate "fingerprint" to correlate with compilations of magnetostratigraphy of marine-zoned strata (e.g., two options of Muttoni et al., 2004b, and in Ogg et al., 2008; three options discussed in detail within Hounslow and Muttoni, 2010). However, based on the apparent correlations to the candidate for the Norian GSSP at Pizzo Mondello, the c. 231 Ma date from mid-Tuvalian strata in Sicily and the supporting correlations with the Chinle Magnetostratigraphy with detrital-zircon dating, then only a variation of the "long Norian" option is proposed in this GTS2020.

Using the suggested minimal set of a few magnetostratigraphic correlations shown in Fig. 25.5, then the base of the **Alaunian** Substage (base of Tethyan *C. bicrenatus* ammonoid zone) has a projected age of **217.5 Ma** and the base of the **Sevatian** Substage (if using the base of Tethyan *S. quinquepunctatus* ammonoid zone) is **214.0 Ma**. Visually, there are several other potential magnetostratigraphic correlations within individual biozones or pairs of biozones, but we tried to preserve the approximate scaling of polarity zones as compiled by Hounslow and Muttoni (2010). Obviously, the entire Norian age model for marine biostratigraphy needs to be enhanced and verified with astronomical tuning and radiometric dating of magnetostratigraphic sections having well-defined marine biostratigraphy.

The Norian–Rhaetian boundary will be assigned in a GSSP at a level corresponding to the lowest occurrence of the conodont marker *Mi. posthernsteini*. However, there are different concepts of when that taxon can be differentiated on the *Misikella* morphology lineage (Rigo et al., 2016; Orchard, 2016). There are two main candidate GSSP sections, each having magnetostratigraphy that can be correlated to the astronomically tuned Newark magnetic polarity reference time scale (Maron et al., 2015): (1) Steinbergkogel in Austria that uses a broader *Mi. posthernsteini* sensu lato (Austria; Krystyn et al., 2007c, 2007d; Hüsing et al., 2011) with an implied age of 209.5 Ma and (2) Pignola-Abriola in Sicily that uses a *Mi. posthernsteini* sensu stricto (Maron et al, 2015; Rigo et al., 2016) with an implied age of 205.7 Ma. Both options are shown in Fig. 25.5, but the *Mi. posthernsteini* s.str. (**205.7 Ma**) is used as the base-**Rhaetian** for the summary scales in this GTS2020. The younger option for the base of the Rhaetian is near the extinction of the bivalve *Monotis*, and this level has been dated in Peru as between 205.7 ± 0.15 and 205.3 ± 0.14 Ma (Wotzlaw et al., 2014).

The **Triassic–Jurassic boundary** dated by Schoene et al. (2010) was revised by them (in Wotzlaw et al., 2014) using updated EARTHTIME tracers. This changed the interpolated boundary age from 201.31 ± 0.18 Ma (used in GTS2012) to a slightly older **201.36 ± 0.17 Ma**.

### 25.3.5 Estimated uncertainties and future enhancements of Triassic age model

The few high-precision radioisotopic dates with well-constrained biostratigraphic ages and astronomical tuning of stratigraphic zonations that constrain the Triassic time scale

**FIGURE 25.7** Selected marine and terrestrial biostratigraphic zonations of the Early Triassic. ("*Age*" is the term for the time equivalent of the rock-record *stage*. *Note that the Ma-age scale is more expanded than in* Figs. 25.5 or 25.6). Marine-facies magnetostratigraphy zones are labeled after Hounslow and Muttoni (2010). Sources for Tethyan ammonoid, conodont and bivalve zones, South China conodont zones, Arctic/Panthalassan ammonoid and conodont zones, land vertebrate zones, and major sea-level trends are the same as in Figs. 25.5 and 25.6. Spinicaudatun (Conchostracan) zones of the Germanic Basin are from Kozur and Weems (2010), Scholze et al. (2016), and Schneider and Scholze (2018).

See Ammonoid ages with minor corrections (Spathian) in added files "GTS2020 Fig 25.7a_Low_Trias_left_Spathian-corrected_14Feb2021" and "Fig. 27.7b"

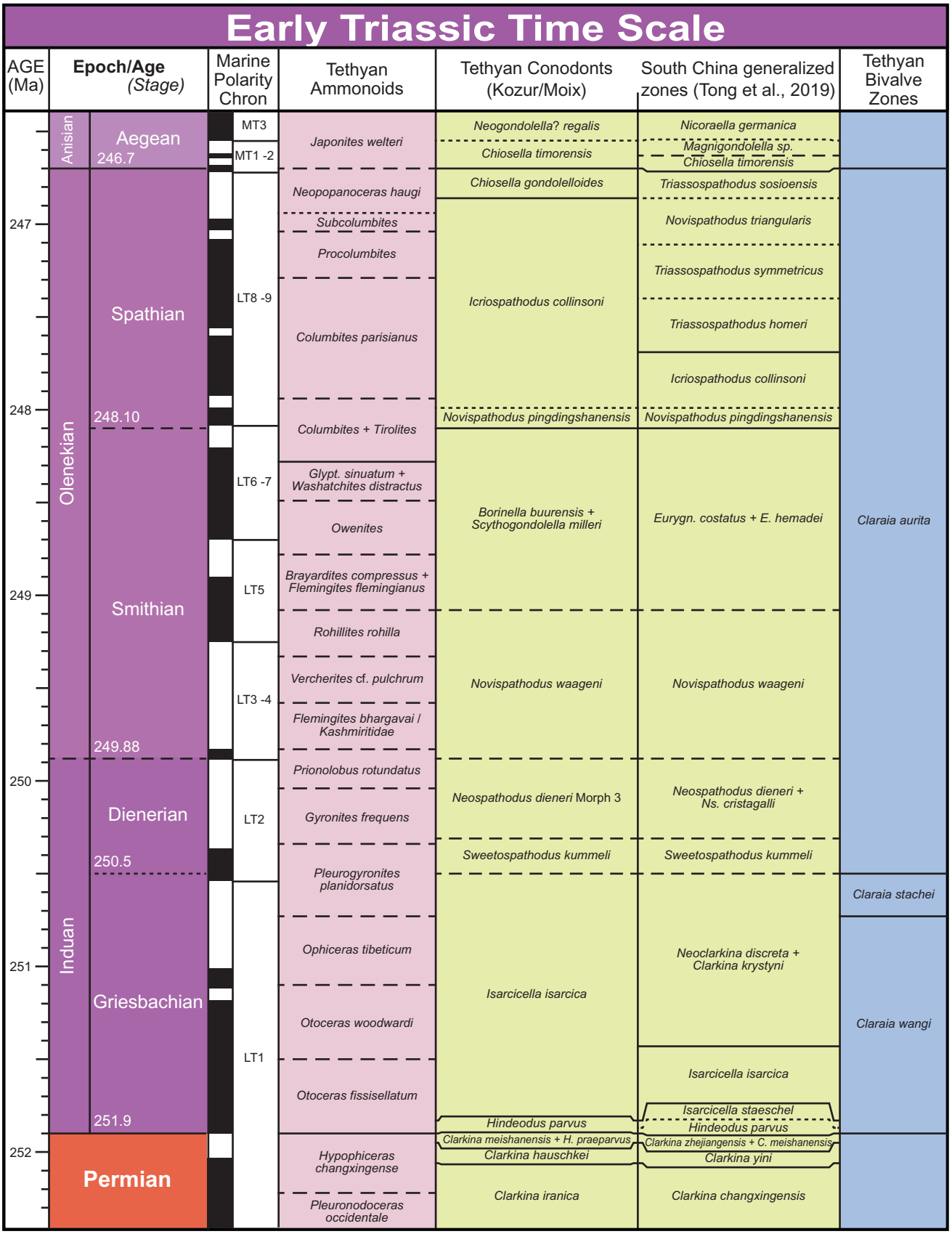


FIGURE 25.7 (Continued).

See Ammonoid ages with minor corrections (Spathian) in added files "GTS2020 Fig 25.7a_Low_Trias_left_Spathian-corrected_14Feb2021" and "Fig. 27.7b"



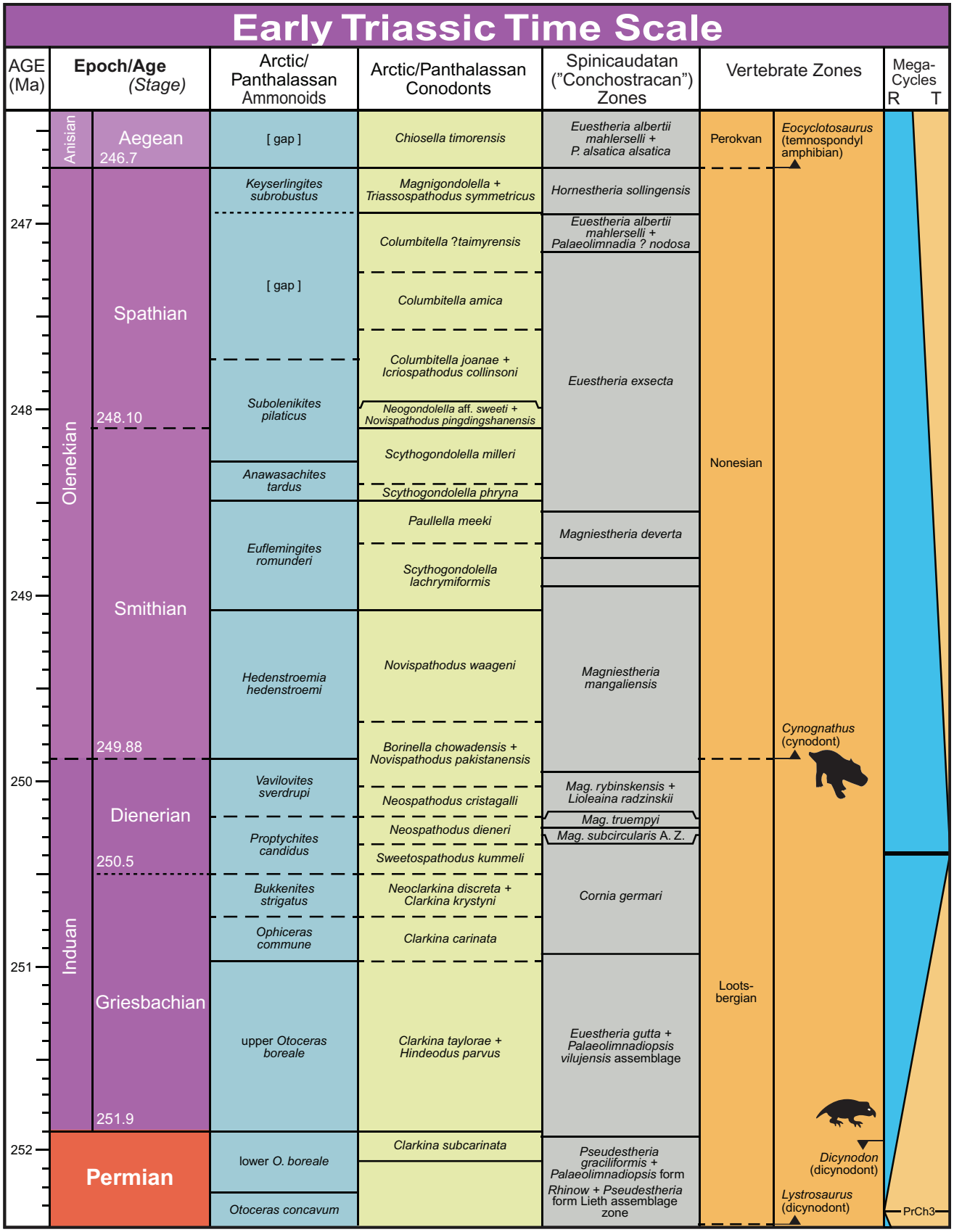


FIGURE 25.7 (Continued).

**TABLE 25.1** Derivation of the Triassic Age Model of GTS2020 and comparison to selected previous publications.

| | GTS2004 | | Concise GTS08 alternate | | Mundil et al. (2010) | | GTS2012—Option 1 (long Carnian) | | GTS2012—Option 2 (long Norian–Rhaet) | | GTS2016 | | **GTS2020** | | | Derivation of GTS2020 Age Model and estimated uncertainty |
|---|---|---|---|---|---|---|---|---|---|---|---|---|---|---|---|---|
| Stage | Base | Duration | Base | Duration | Base | Duration | Base | Duration | Base | Duration | Base | Duration | Base | Uncertainty | Duration | |
| Jurassic (Hettangian) | 200 | | 201 | | 202 | | 201.3 | | 201.3 | | 201 | | **201.4** | 0.2 | | Age interpolated from bounding radioisotopic dates in Peru with a similar ammonoid marker as GSSP is 201.36 ± 0.17 Ma. |
| **Rhaetian** | 204 | 4.0 | 205 | 3.6 | x | | 205.4 | 4.1 | 209.5 | 8.2 | 205.8/ 209.6 | 4.4 | **205.7**/ 209.5 | 0.1 | 4.3 | Basal placement is awaiting GSSP decision. Basal age according to magnetostratigraphy correlations of GSSP candidates to Newark Basin astronomical-tuned magnetic polarity time scale. Uncertainty for that correlation is c. 0.1 Myr (1 short-eccentricity cycle). |
| **Norian** | 217 | 12.9 | 229 | 24.3 | <230 | | 221.0 | 15.7 | 228.4 | 18.9 | 229 | 22.7 | **227.3** | 0.1 | 21.6 | Basal placement is also awaiting GSSP decision. Basal age according to magnetostratigraphy correlation of GSSP candidate to Newark Basin astronomical-tuned magnetic polarity time scale. Uncertainty for that correlation is ± 0.1 Myr (1 short-eccentricity cycle). |
| **Carnian** | 229 | 12.2 | 237 | 8.0 | <236 | | 237.0 | 16.0 | 237.0 | 8.7 | 237 | 8.5 | **237** | 0.5 | 9.7 | Age estimated from radioisotopic date of 237.77 ± 0.14 Ma that is one ammonoid subzone below base. Uncertainty = c. 0.5 Myr. |
| **Ladinian** | 237 | 8.3 | 241 | 3.7 | 242 | | 241.5 | 4.5 | 241.5 | 4.5 | 242 | 4.5 | **241.5** | 0.3 | 4.5 | Age interpolated from bounding radioisotopic dates correlated to the nearby GSSP section is 241.464 ± 0.28 Ma. |
| **Anisian** | 246 | 8.9 | 247 | 6.9 | 247 | 5.2 | 247.1 | 5.6 | 247.1 | 5.6 | 247 | 5.3 | **246.7** | 0.2 | 5.2 | Basal placement is awaiting GSSP decision. Basal age derived from cycles at South China GSSP candidates relative to base-Triassic, plus U–Pb dates at potential GSSP. Uncertainty estimated as ± 0.2 Myr (1/2 long-eccentricity cycle). |
| **Olenekian** | 250 | 3.6 | 251 | 3.6 | 251 | 4.1 | 250.0 | 2.9 | 250.0 | 2.9 | 250 | 3.0 | **249.9** | 0.2 | 3.2 | Basal placement is awaiting GSSP decision. Basal age derived from cycles at South China GSSP candidate relative to base-Triassic. Uncertainty estimated as ± 0.2 Myr (1/2 long-eccentricity cycle). |
| **Induan** | 251 | 1.5 | 253 | 1.5 | 252 | 1.0 | 252.2 | 2.2 | 252.2 | 2.2 | 252 | 2.1 | **251.9** | 0.3 | 2 | Age from bounding radioisotopic dates at GSSP is 251.902 ± 0.024 Ma. Total uncertainty is 0.3 Myr. |
| Permian (Changhsingian) | | | | | | | | | | | | | | | | |

Ages for bases are in Ma; durations and uncertainties are in Myr. GSSP, Global Boundary Stratotype Section and Point. Radioisotopic dates on stage boundaries do not include the estimated 0.3 Myr external uncertainty as explained in Burgess et al., (2014).

typically have a published uncertainty less than 0.2 Myr. However, an external uncertainty of c. 0.3 Myr should be included if comparing these Triassic EARTHTIME-standardized dates to other dating methods, as explained in Burgess et al. (2014). These dates anchor the cyclostratigraphic scaling for much of the Early and the Late Triassic and for the GSSPs and current GSSP candidates (Table 25.1). There is probably an additional c. 0.2-Myr uncertainty in the assignment of any event within a 405-kyr long-eccentricity cycle. Therefore most of the age assignments for Triassic stage boundaries have a relatively low uncertainty (Table 25.1) when compared to other Paleozoic–Mesozoic stages. However, the uncertainties are greater for the base of the Carnian and for many of the biozone boundaries within the individual stages which have age models that required additional extrapolation from the nearest radioisotopic dates or from the estimated calibrations to other reference scales.

The main future enhancements to the age model for the Triassic stages will be the decisions on GSSP definition for the Olenekian, Anisian, Norian, and Rhaetian. Other essential developments will be the verification of the cyclescaling and interregional correlation of the magnetostratigraphy of each stage, and obtaining an astronomical tuning for the zonations within the Ladinian and Carnian stages. It is anticipated that the integration of magnetostratigraphy, astronomical cycles coupled with periodic major changes in sea level, and distinctive stable isotopic excursions will enable a more reliable interregional correlation of biostratigraphic datums for both marine (Tethyan through Boreal realms) and terrestrials settings.

## 25.4 Summary

During the past decade, Triassic workers have defined most of the stages (Fig. 25.8), greatly enhanced the intercorrelation of biostratigraphic zones, enabled compilation of a nearly complete magnetic polarity pattern calibrated to marine biostratigraphic datums, discovered excursions in stable isotopes (especially major carbon-isotope and oxygen-isotope

**GSSPs of the Triassic Stages, with location and primary correlation criteria**

| Stage | GSSP Location | Latitude, Longitude | Boundary Level | Correlation Events | Reference |
|---|---|---|---|---|---|
| *Rhaetian* | *Candidates are Pizzo Mondello, Sicily, Italy, and Steinbergkogel, Austria* | | | *Near FADs of conodont* Misikella posthernsteini *s.s. or* Misikella posthernsteini *s.l.* | |
| *Norian* | *Candidates are Black Bear Ridge in British Columbia (Canada) and Pizzo Mondello, Sicily, Italy* | | | *FAD of conodont* Metapolygnathus parvus. *Near base of* Stikinoceras kerri *ammonoid zone and FAD of bivalve* Halobia austriaca | |
| **Carnian** | Section at Prati di Stuores, Dolomites, Italy | 46°31'37"N 11°55'49"E | GSSP is base of marly limestone bed SW4, 45 m from base of San Cassiano Formation | FAD of ammonoid *Daxatina canadensis,* conodont *Quadralella polygnathiformis* and *Halobia* bivalves | Episodes **35**/3, 2012 |
| **Ladinian** | Bagolino, Province of Brescia, Northern Italy | 45°49'09.5"N 10°28'15.5"E | base of a 15 – 20 cm thick limestone bed overlying a distinctive groove ("Chiesense groove") of limestone nodules in a shaly matrix, located about 5 m above the base of the Buchenstein Beds | Ammonoid, FAD of *Eoprotrachyceras curionii* | Episodes **28**/4, 2005 |
| *Anisian* | *Candidates are Desli Caira (Romania), Kçira (Albania), Wantou (Guangxi Province, S. China) and Guandao (Guizhou Province, S. China)* | | | *FAD of conodont* Chiosella timorensis *or base of magnetic normal- polarity chronozone MT1n* | |
| *Olenekian* | *Candidates are Chaohu, China and Mud (Muth) village, Spiti Valley, India* | | | *FAD of conodont* Novispathodus waageni, *near base of* Flemingites *ammonoid genera* | |
| **Induan** | Meishan, Zhejiang Province, China | 31°4'47.28"N 119°42'20.90"E | base of Bed 27c in the Meishan Section | Conodont, FAD of *Hindeodus parvus* | Episodes **24**/2, 2001 |

* according to Google Earth

**FIGURE 25.8** Ratified GSSPs and potential primary markers under consideration for defining the Triassic stages *(status as of January 2020)*. Details of each GSSP are available at http://www.stratigraphy.org, https://timescalefoundation.org/gssp/, and in the *Episodes* publications. *GSSP*, Global Boundary Stratotype Section and Point.

excursions within the lower Triassic), and achieved or rejected cycle-stratigraphic scaling of several intervals. A generalized synthesis of selected Triassic stratigraphic scales is compiled in Figs. 25.5–25.7; and additional geochemical trends are summarized in the geochemical chapters of this book.

Extensive radioisotopic dating using advanced techniques and the astronomical tuning of reference sections in China and Italy (including GSSPs or candidate GSSPs) have replaced much of the radioisotopic-date dataset and extrapolations that were used in GTS2012. The combination of these methods has established a well-constrained age model for the stages and many of the biozones within the Lower and Middle Triassic (Induan GSSP, Olenekian and Anisian candidates, Ladinian and Carnian GSSPs) and for the top of the Triassic (base of Hettangian Stage). There are lingering major uncertainties on the age model and durations for biozones within the yet-to-be-defined Upper Triassic stages of Norian and Rhaetian. Establishing a robust Late Triassic time scale for these zones and other events requires both definitive radioisotopic dates and cyclostratigraphy on marine sections that have standard biostratigraphy. Further advances in formalizing GSSPs, zonal schemes, interregional correlations, and eventual consensus on the best numerical age model interpolations will be found in the *Albertiana* newsletters of the Subcommission on Triassic Stratigraphy.

## Acknowledgments

The compilation of the Triassic chronostratigraphy and understanding the disputes on correlations and the age models was also greatly aided over the years by discussions with several colleagues, of which a few are, in alphabetical order: Marco Balini, Charles Henderson (who also reviewed this chapter), Chunju Huang, Mark Hounslow, the late Heinz Kozur (including an intensive 3-day working session at his home), Leopold Krystyn, Spencer Lucas, Manfred Menning, Paul Olsen, Lawrence Tanner, and Hongfu Yin. Mingsong Li and Yang "Wendy" Zhang provided their important cycle-scaling of Early Triassic, Anisian, and Carnian stratigraphy. None of them entirely agree with the selected taxonomic nomenclature for zones used in the figures or with the age models, but all agree that further international efforts will soon resolve all of the disputed calibrations. This work was partly supported by three NSFC grants (41821001, 41830323, 41930322). James Ogg's participation was partly enabled by distinguished visiting professorships at Chengdu University of Technology (Chengdu) and at the China University of Geoscience (Wuhan), China. Additional and alternative zonal schemes are available through the *TimeScale Creator* visualization datapacks (https://timescalecreator.org).

## Bibliography

Aigner, T., and Bachmann, G.H., 1992, Sequence-stratigraphic framework of the German Triassic. *Sedimentary Geology*, **80**: 115–135.

Algeo, T., Brayard, A., and Richoz, S. (eds), 2019a. The Smithian-Spathian boundary: a critical juncture in the early Triassic recovery of marine ecosystems. *Earth-Science Reviews,* **Special volume, 195**: 212 pp.

Algeo, T., Brayard, A., and Richoz, S., 2019b, The Smithian-Spathian boundary: a critical juncture in the Early Triassic recovery of marine ecosystems. *Earth-Science Reviews*, **195**: 1–6. https://doi.org/10.1016/j.earscirev.2019.102877.

Assereto, R., 1974, Aegean and Bithynian: proposal for two new Anisian substages. *Schriftenreihe der Erdwissenschaftlichen Kommissionen, Österreichische Akademie der Wissenschaften*, **2**: 23–39.

Bachmann, G.H., and Kozur, H.W., 2004, The Germanic Triassic: correlations with the international scale, numerical ages and Milankovitch cyclicity. *Hallesches Jahrbuch fur Geowissenschaften*, **B26**: 17–62.

Balini, M., Drystyn, L., and Torti, V., 1998, In search of the Ladinian/Carnian boundary: perspectives from Spiti (Tethys Himalaya). *Albertiana*, **21**: 26–32.

Balini, M., Krystyn, L., Nicora, A., and Torti, V., 2001, The Ladinian-Carnian boundary succession in Spiti (Tethys Himalaya) and its bearing to the definition of the GSSP for the Carnian stage (Upper Triassic). *Journal of Asian Earth Sciences*, **19** (3A), 3–4.

Balini, M., Lucas, S.G., Jenks, J.F., and Spielmann, J.A., 2010, Triassic ammonoid biostratigraphy: an overview. In: Lucas, S.G. (ed), The Triassic Timescale, *The Geological Society of London Special Publications*, **334**: 221–262.

Balini, M., Krystyn, L., Levera, M., and Tripodo, A., 2012, Late Carnian-early Norian ammonoids from the GSSP candidate section Pizzo Mondello (Sicani Mountains, Sicily). *Rivista Italiana di Paleontologia e Stratigrafia*, **118**: 47–84.

Balme, B.E., and Foster, C.B., 1996, Triassic, explanatory notes on Biostratigraphic charts. *In* Young, G.C., and Laurie, J.R. (eds), *Australian Phanerozoic Timescales.* Oxford: Oxford University Press, Chart 7.

Baud, A., 2001, The new GSSP, base of the Triassic: some consequences. *Albertiana*, **26**: 4–6.

Baud, A., 2014, The global marine Permian-Triassic boundary: over a century of adventures and controversies (1880-2001). *Albertiana*, **42**: 1–21 Available at: <https://albertiana-sts.org/>.

Baud, A., and Beauchamp, B., 2001, Proposals for the redefinition of the Griesbachian Substage and for the base of the Triassic in the Arctic regions. *In* Yan, J., and Peng, Y. (eds), *Proceedings of the International Symposium on the Global Stratotype of the Permian-Triassic boundary and the Paleozoic-Mesozoic Events*. Changxing: University of Geosciences Press, 26–28.

Baud, A., Magaritz, M., and Holser, W.T., 1989, Permian-Triassic of the Tethys: carbon isotope studies. *Sonderdruck aus Geologische Rundschau*, **78**: 649–677.

Baud, A., Atudorei, V., and Sharp, Z., 1996, Late Permian and early Triassic evolution of the northern Indian margin: carbon isotope and sequence stratigraphy. *Geodinamica Acta*, **9**: 57–77.

Benton, M.J., 1986, The Late Triassic tetrapod extinction events. *In* Padian, K. (ed), *The Beginning of the Age of Dinosaurs. Faunal Change Across the Triassic-Jurassic Boundary*. Cambridge: Cambridge University Press, 303–320.

Benton, M.J., 1993, Late Triassic extinctions and the origin of the dinosaurs. *Science*, **260**: 769–770.

Benton, M.J., Zhang, Q.Y., Hu, S.X., Chen, Z.Q., Wen, W., Liu, J., et al., 2013, Exceptional vertebrate biotas from the Triassic of China, and the expansion of marine ecosystems after the Permo-Triassic mass extinction. *Earth-Science Reviews*, **125**: 199–243. https://doi.org/10.1016/j.earscirev.2013.05.014.

Benton, M.J., Forth, J., and Langer, M.C., 2014, Models for the rise of the dinosaurs. *Current Biology*, **24**: R87–R95 <https://doi.org/10.1016/j.cub.2013.11.063>.

Bernasconi, S.M., Meier, I., Wohlwend, S., Brack, P., Hochuli, P.A., Bläsi, H., et al., 2017, An evaporite-based high-resolution sulfur isotope record of Late Permian and Triassic seawater sulfate. *Geochimica et Cosmochimica Acta*, **204**: 331–349.

Berra, F., Jadoul, F., and Anelli, A., 2010, Environmental control on the end of the Dolomia Principale/Hauptdolomit depositional system in the central Alps: coupling sea-level and climatic changes. In: Kustatscher, E., Preto, N., Wignall, P. (eds), Triassic climates, *Palaeogeography, Palaeoclimatology, Palaeoecology*, **290**: 138–150.

Beauchamp, B., and Baud, A., 2002, Growth and demise of Permian biogenic chert along northwest Pangea: evidence for end-Permain collapse of thermohaline circulation. *Palaeogeography, Palaeoclimatology, Palaeoecology*, **184**: 37–63.

Bittner, A., 1892, Was ist norisch? *Jahrbuch Geologischen Reichsanstalt*, **42**: 387–396.

Blackburn, T.J., Olsen, P.E., Browning, S.A., McLean, N.M., Kent, D.V., Puffer, J., et al., 2013, Zircon U-Pb geochronology links the End-Triassic extinction with the Central Atlantic Magmatic Province. *Science*, **340**: 941–945. https://doi.org/10.1126/science.1234204.

Blome, C.D., 1984, Upper Triassic Radiolaria and radiolarian zonation from western North America. *Bulletins of American Paleontology*, **85**: 88 pp.

Bown, P.R. (ed), 1998. Calcareous nanofossils biostratigraphy. Chapman and Hall. London, 314 pp.

Bowring, S.A., Erwin, D.H., Jin, Y.G., Martin, M.W., Davidek, K., and Wang, W., 1998, U/Pb zircon geochronology and tempo of the end-Permian mass extinction. *Science*, **280**: 1039–1045.

Brack, P., 2010, The "golden spike" for the Ladinian is set!. *Albertiana*, **38**: 8–10.

Brack, P., and Rieber, H., 1994, The Anisian/Ladinian boundary: retrospective and new constraints. *Albertiana*, **13**: 25–36.

Brack, P., and Rieber, H., 1996, The new 'High-resolution Middle Triassic ammonoid standard scale' proposed by Triassic researchers from Padova—a discussion of the Anisian/Ladinian boundary interval. *Albertiana*, **17**: 42–50.

Brack, P., Rieber, H., and Mundil, R., 1995, The Anisian/Ladinian boundary interval at Bagolino (Southern Alps, Italy): I. Summary and new results on ammonoid horizons and radiometric dating. *Albertiana*, **15**: 45–56.

Brack, P., Mundil, R., Oberli, F., Meier, M., and Rieber, H., 1996, Biostratigraphic and radiometric age data question the Milankovitch characteristics of the Latemar cycles (Southern Alps, Italy). *Geology*, **24**: 371–375.

Brack, P., Mundil, R., Oberli, F., Meier, M., and Rieber, H., 1997, Biostratigraphic and radiometric age data question the Milankovitch characteristics of the Latemar cycles (Southern Alps, Italy) – reply. *Geology*, **25**: 471–472.

Brack, P., Rieber, H., Nicora, A., and Mundil, R., 2005, The Global Boundary Stratotype Section and Point (GSSP) of the Ladinian Stage (Middle Triassic) at Bagolino (Southern Alps, Northern Italy) and its implications for the Triassic time scale. *Episodes*, **28** (4), 233–244.

Brack, P., Rieber, H., Mundil, R., Blendinger, W., and Maurer, F., 2007, Geometry and chronology of growth and drowning of Middle Triassic carbonate platforms (Cernera and Bivera/Clapsavon) in the Southern Alps (northern Italy). *Swiss Journal of Geosciences*, **10**: 327–347.

Brayard, A., Escarguel, G., Bucher, H., and Brühwiler, 2009a, Smithian and Spathian (Early Triassic) ammonoid assemblages from terranes: paleoceanographic and paleogeographic implications. In: Metcalfe, I., and Isozaki, Y. (eds), End-Permian mass extinction: events & processes, age & timescale, causative mechanism(s) & recovery, *Journal of Asian Earth Sciences*, **36**(6): 420–433.

Brayard, A., Escarguel, G., Bucher, H., Monnet, C., Brühwiler, Goudemand, N., et al., 2009b, Good genes and good luck: ammonoid diversity and the end-Permian mass extinction. *Science*, **325**: 1118–1121.

Broglio Loriga, C., and Cassinis, G., 1992, The Permo–Triassic boundary in the Southern Alps (Italy) and in adjacent Periadriatic regions. *In* Sweet, W.C., Yang, Z., Dickins, J.M., and Yin, H. (eds), *Permo–Triassic Events in the Eastern Tethys. Stratigraphy, Classification, and Relations With the Western Tethys*. Cambridge: Cambridge University Press, 78–97.

Broglio Loriga, C., Cirilli, S., De Zanche, V., di Bari, D., Gianolla, P., Laghi, G.R., et al., 1998, A GSSP candidate for the Ladinian-Carnian boundary: the Prati di Stuores/Stuores Wiesen section (Dolomites, Italy). *Albertiana*, **21**: 2–18.

Broglio Loriga, C., Cirilli, S., De Zanche, V., di Bari, D., Gianolla, P., Laghi, G.R., et al., 1999, The Prati di Stuores/Stuores Wiesen section (Dolomites, Italy): a candidate Global Stratotype Section and Point for the base of the Carnian stage. *Rivista Italiana di Paleontologia e Stratigrafia*, **105**: 37–78.

Brühwiler, T., Hochuli, P., Mundil, R., Schatz, W., and Brack, P., 2007, Bio- and chronostratigraphy of the Middle Triassic Reifling Formation of the westernmost Northern Calcareous Alps. *Swiss Journal of Geosciences*, **100**: 443–455.

Burgess, S.D., and Bowring, S.A., 2015, High-precision geochronology confirms voluminous magmatism before, during, and after Earth's most severe extinction. *Science Advances*, **1** (7), article # e1500470: 14 pp. http://dx.doi.org/10.1126/sciadv.1500470.

Burgess, S.D., Bowring, S., and Shen, Z.Q., 2014, High-precision timeline for Earth's most severe extinction. *Proceedings of the National Academy of Sciences of the United States of America*, **111**: 3316–3321.

Burgess, S.D., Muirhead, J.D., and Bowring, S.A., 2017, Initial pulse of Siberian Traps sills as the trigger of the end-Permian mass extinction. *Nature Communications*, **8**: 164–169. https://doi.org/10.1038/s41467-017-00083-9.

Carter, E.S., 1993, Biochronology and paleontology of uppermost Triassic (Rhaetian) radiolarians, Queen Charlotte Islands, British Columbia, Canada. *Mémoires Géologie (Lausanne)*, **11**: 175 pp.

Carter, E.S., and Orchard, M.J., 2007, Radiolarian–conodont–ammonoid intercalibration around the Norian-Rhaetian Boundary and implications for trans-Panthalassan correlation. *Albertiana*, **36**: 149–163.

Cao, C.Q., Love, G.D., Hays, L.E., Wang, W., Shen, S.Z., and Summons, 2009, Biogeochemical evidence for euxinic oceans and ecological disturbance presaging the end-Permian mass extinction. *Earth and Planetary Science Letters*, **281**: 188–201.

Channell, J.E.T., Kozur, H.W., Sievers, T., Mocl, R., Aubrecht, R., and Sykora, M., 2003, Carnian–Norian biomagnetostratigraphy at Silickà Brezovà (Slovakia): correlation to other Tethyan sections and to the Newark Basin. *Palaeogeography, Palaeoclimatology, Palaecology*, **191**: 65–109.

Chen, Z.Q., and Benton, M.J., 2012, The timing and pattern of biotic recovery following the end-Permian mass extinction. *Nature Geoscience*, **5** (6), 375–383. https://doi.org/10.1038/NGEO1475.

Chen, Y.L., Krystyn, L., Orchard, M.J., Lai, X.L., and Richoz, S., 2016, A review of the evolution, biostratigraphy, provincialism and diversity of Middle and early Late Triassic conodonts. *Papers in Palaeontology*, **2** (2), 235–263. http://dx.doi.org/10.1002/spp2.1038 [and data at Dryad Digital Repository, < https://doi.org/10.5061/dryad.34r55 > .

Chen, Z.Q., Zhao, L.S., Wang, X.D., Luo, M., and Guo, Z., 2018, Great Paleozoic-Mesozoic biotic turnings and paleontological education in China: A tribute to the achievements of Professor Zunyi Yang. *Journal of Earth Science*, **29**: 721–732. https://doi.org/10.1007/s12583-018-0797-1.

Chen, Z.Q., Tu, C.Y., Pei, Y., Ogg, J., Fang, Y.H., Wu, S.Q., et al., 2019, Biosedimentological features of major microbe-metazoan transitions (MMTs) from Precambrian to Cenozoic. *Earth-Science Reviews*, **189**: 21–50. https://doi.org/10.1016/j.earscirev.2019.01.015.

Chen, Y., Jiang, H.S., Ogg, J.G., Zhang, Y., Gong, Y.F., and Yan, C.B., 2020, Early-Middle Triassic boundary interval: integrated chemo-bio-magneto-stratigraphy of potential GSSPs for the base of the Anisian Stage in South China. *Earth and Planetary Science Letters*, **530**, article #115863: 13 pp. https://doi.org/10.1016/j.epsl.2019.115863.

Chen, Z.Q., Algeo, T.J., and Bottjer, D.J., 2014, Global review of the Permian–Triassic mass extinction and subsequent recovery: part I. *Earth-Science Reviews*, **137**: 1–5.

Chen, Z.Q., Yang, H., Luo, M., Benton, J.J., Kaiho, K., Zhao, L., et al., 2015, Complete biotic and sedimentary records of the Permian–Triassic transition from Meishan section, South China: ecologically assessing mass extinction and its aftermath. *Earth-Science Reviews*, **149**: 67–107. http://dx.doi.org/10.1016/j.earscirev.2014.10.005.

Chinese Triassic Working Group, 2007, Final report of the GSSP candidate for the I/O boundary at West Pingdingshan Section in Chaohu, Southeastern China. *Albertiana*, **36**: 10–21.

Chu, D.L., Tong, J.N., Benton, M.J., Yu, J.X., and Huang, Y.F., 2019, Mixed continental-marine biotas following the Permian-Triassic mass extinction in South and North China. *Palaeogeography, Palaeoclimatology, Palaeoecology*, **519**: 95–107.

Cirilli, S., 2010, Upper Triassic–lowermost Jurassic palynology and palynostratigraphy: a review. In: Lucas, S.G. (eds), *The Triassic Timescale*. The Geological Society of London Special Publications, **334**: 285–314.

Cirilli, S., Marzoli, A., Tanner, L., Bertrand, H., Buratti, N., Jourdan, F., et al., 2009, Latest Triassic onset of the Central Atlantic Magmatic Province (CAMP) volcanism in the Fundy Basin (Nova Scotia): new stratigraphic constraints. *Earth and Planetary Science Letters*, **286**: 514–525.

Cohen, A.S., and Coe, A.L., 2007, The impact of the Central Atlantic Magmatic Province on climate and on the Sr- and Os-isotope evolution of seawater. *Palaeogeography, Palaeoclimatology, Palaeoecology*, **244**: 374–390.

Cornet, B., 1977, The Palynology and Age of the Newark Supergroup. *Ph. D. thesis*. Pennsylvania State University, College Park, PA, 505 pp.

Cornet, B., 1993, Applications and limitations of palynology in age, climatic, and paleoenvironmental analyzes of Triassic sequences in North America. In: Lucas, S.G., Morales, M. (eds), The Nonmarine Triassic, *New Mexico Museum of Natural History & Science Bulletin*, **3**: 75–93.

Cornet, B., and Olsen, P.E., 1985, A summary of the biostratigraphy of the Newark Supergroup of Eastern North America with comments on early Mesozoic provinciality. *In* Weber, R. (ed), III Congreso Latinoamericano de Paleontologia Mexico, Simposio Sobre Floras del Triasico Tardio, su Fitogeograpfia y Paleoecologia, Memoria. Mexico: Universidad Nacional Autónoma de México, 67–81.

Cozzi, A., Hinnov, L.A., and Hardie, L.A., 2005, Orbitally forced Lofer cycles in the Dachstein Limestone of the Julian Alps (northeastern Italy). *Geology*, **33**: 789–792.

Cramer, B.D., and Jarvis, I., 2020, Chapter 11 - Carbon isotope stratigraphy. *In* Gradstein, F.M., Ogg, J.G., Schmitz, M.D., and Ogg, G.M. (eds), *The Geologic Time Scale 2020*. **Vol. 1** (this book). Elsevier, Boston, MA.

Dal Corso, J., Mietto, P., Newton, R.J., Pancost, R.D., Preto, N., Roghi, G., et al., 2012, Discovery of a major negative $\delta^{13}C$ spike in the Carnian (Late Triassic) linked to the eruption of Wrangellia flood basalts. *Geology*, **40** (1), 79–82. https://doi.org/10.1130/G32473.1.

Dal Corso, J., Benton, M.J., Bernardi, M., Franz, M., Gianolla, P., Hohn, S., et al., 2018a, First workshop on the Carnian Pluvial Episode (Late Triassic): a report. *Albertiana*, **44**: 49–57.

Dal Corso, J., Gianolla, P., Rigo, M., Franceschi, M., Roghi, G., Mietto, P., et al., 2018b, Multiple negative carbon-isotope excursions during the Carnian Pluvial Episode (Late Triassic). *Earth-Science Reviews*, **185**: 732–750. https://doi.org/10.1016/j.earscirev.2018.07.004.

De Wever, P., 1982, Radiolaires du Trias et du Lias de la Téthys: systématique, stratigraphy. *Societé Géologique du Nord, Lille*, **7**: 599 pp.

De Wever, P., 1998, Radiolarians. Column for Triassic chart of Mesozoic and Cenozoic sequence chronostratigraphic framework of European basins, by Hardenbol, J., Thierry, J., Farley, M.B., Jacquin, Th., de Graciansky, P.-C., and Vail, P.R. (coordinators). *In* de Graciansky, P.-C., Hardenbol, J., Jacquin, T., and Vail, P.R. (eds), *Mesozoic-Cenozoic Sequence Stratigraphy of European Basins*. SEPM Special Publication, p. 60 Chart 8.

De Zanche, V., Gianolla, P., Mietto, P., Siorpaes, C., and Vail, P.R., 1993, Triassic sequence stratigraphy in the Dolomites. *Memorie di Scienze Geologiche*, **45**: 1–27.

Deenen, M.H.L., 2010, A new chronology for the late Triassic to early Jurassic. PhD thesis, Utrecht University, Faculty of Geosciences, Department of Earth Sciences. *Geologica Ultraiectina*, **323**.

Deenen, M.H.L., Langereis, C.G., Krijgsman, W., El Hachimi, H., and El Hassane, C., 2010a, Paleomagnetic research in the Argana basin, Morocco: Trans-Atlantic correlation of CAMP volcanism and implications for the late Triassic geomagnetic polarity time scale. In: Deenen, M.H.L. (ed), A new chronology for the late Triassic to early Jurassic, *Geologica Ultraiectina*, **323**: 43–64.

Deenen, M.H.L., Ruhl, M., Bonis, N.R., Krijgsman, W., Kuerschner, W.M., Reitsma, M., et al., 2010b, A new chronology for the end-Triassic mass extinction. *Earth and Planetary Science Letters*, **291**: 113–125.

Diakow, L., Orchard, M.J., and Friedman, R., 2010, Absolute ages for the Norian Stage: a contribution from southern British Columbia, Canada. *21st Canadian Paleontological Conference. University of British Columbia, 19–20 Aug 2011, Abstracts and additional details sent by M.J. Orchard to J. Ogg, July 2011 and Sept 2015*.

Diener, C., 1912, The Trials of the Himalayas. *Memoirs of the Geological Survey of India*, **36** (3), 159 pp.

Dinarès-Turell, J., Diez, J.D., Rey, D., and Arnal, I., 2005, 'Buntsandstein' magnetostratigraphy and biostratigraphic reappraisal from eastern Iberia: Early and Middle Triassic stage boundary definitions through correlation to Tethyan sections. *Palaeogeography, Palaeoclimatology, Palaeoecology*, **229**: 158–177.

Dunning, G.R., and Hodych, J.P., 1990, U/Pb zircon and baddeleyite ages for the Palisades and Gettysburg sills of the northeastern

United States: implications for the age of the Triassic/Jurassic boundary. *Geology*, **18**: 795–798.

Earth Impact Database, 2018, *Maintained by the Planetary and Space Science Centre*. University of New Brunswick. Available at: www.passc.net/EarthImpactDatabase/.

Embry, A.F., 1988, Triassic sea-level changes: evidence from the Canadian Arctic Archipelago. In: Wilgus, C. (ed), *Sea level changes—an integrated approach*. SEPM Special Publication, **42**: 249–259.

Embry, A.F., 1997, Global sequence boundaries of the Triassic and their identification in the Western Canada Sedimentary Basin. *Bulletin of Canadian Petroleum Geology*, **45**: 415–533.

Enos, P., Lehrmann, D.J., Wei, J.Y., Yu, Y.Y., Xiao, J.F., Chaikin, et al., 2006, Triassic Evolution of the Yangtze Platform in Guizhou Province, People's Republic of China. *Geological Society of America Special Paper*, **417**: 1–105. https://doi.org/10.1130/SPE417.

Ernst, R.E., 2014, *Large Igneous Provinces*. Cambridge University Press 653 pp.

Ernst, R.E., Dickson, A.J., and Bekker, A. (eds), 2020. *Large Igneous Provinces: A Driver of Global Environmental and Biotic Changes*. AGU Geophysical Monograph. **255** (in press).

Erwin, D.H., 1993, *The Great Paleozoic Crisis: Life and Death in the Permian*. New York: Columbia University Press 327 pp.

Erwin, D.H., 2006, *Extinction: How Life on Earth Nearly Ended 250 Million Years Ago*. Princeton, NJ: Princeton University Press 320 pp.

Erwin, D.H., Bowring, S.A., and Yugan, J., 2002, End-Permian mass extinctions: a review. In: Koeberl, C., MacLeod, K.G. (eds), Catastrophic events and mass extinctions: impacts and beyond, *Geological Society of America Special Paper*, **356**: 363–383.

Feist-Burkhardt, S., Götz, A.E., Szulc, J., Borkhataria, R., Geluk, M., Haas, J., et al., 2008, Triassic. *In* McCann, T. (ed), *The Geology of Central Europe. Vol. 2: Mesozoic and Cenozoic*. London: The Geological Society, 749–821.

Fischer, A.G., 1964, The Lofer cyclothems of the Alpine Triassic. In: Merriam, D.F. (ed), Symposium on Cyclic Sedimentation, *Kansas Geological Survey Bulletin*, **169**: 107–149.

Flügel, E., 2002, Triassic reef patterns. In: Kiessling, W., Flügel, E., Golonka, J. (eds), Phanerozoic Reef Patterns. *SEPM Special Publication*, **72**: 691–733.

Fowell, S.J., and Olsen, P.E., 1993, Time calibration of Triassic/Jurassic microfloral turnover, eastern North America. *Tectonophysics*, **222**: 361–369.

Fowell, S.J., and Olsen, P.E., 1995, Time calibration of Triassic/Jurassic microfloral turnover, eastern North America—reply. *Tectonophysics*, **245**: 96–99.

Franz, M., Bachmann, G.H., Barnasch, J., Heunisch, C., and Röhling, H.-G., 2018, Der Keuper in der Stratigraphischen Tabelle von Deutschland 2016 – kontinuierliche Sedimentation in der norddeutschen Beckenfazies (Variante B)/The Keuper Group in the Stratigraphic Table of Germany 2016 – continuous sedimentation in the North German Basin (variant B). *Zeitschrift der Deutschen Gesellschaft für Geowissenschaften (German Journal of Geology)*, **169** (2), 203–224. https://doi.org/10.1127/zdgg/2018/0114.

Fraser, N.D., 2006, *Dawn of the Dinosaurs: Life in the Triassic*. Bloomington, IN: Indiana University Press 310 pp.

Furin, S., Preto, N., Rigo, M., Roghi, G., Gianolla, P., Crowley, J.L., et al., 2006, High-precision U-Pb zircon age from the Triassic of Italy: implications for the Triassic time scale and the Carnian origin of calcareous nannoplankton and dinosaurs. *Geology*, **34**: 1009–1012.

Gaetani, M., 1993, Anisian/Ladinian boundary field workshop, Southern Alps—Balaton Highlands, 27 June–4 July 1993. *Albertiana*, **12**: 5–9.

Gaetani, M., Gnaccolini, M., Jadoul, Fl., and Garzanti, E., 1998, Multiorder sequence stratigraphy in the Triassic system of the western Southern Alps. In: de Graciansky, P.-C., Hardenbol, J., Jacquin, T., Vail, P.R. (Eds.), Mesozoic-Cenozoic Sequence Stratigraphy of European Basins, *SEPM Special Publication*, **60**: 701–717.

Galbrun, B., Boulila, S., Krystyn, L., Richoz, S., Gardin, S., Bartolini, A., and Maslo, M., 2020, "Short" or "long" Rhaetian? Astronomical calibration of Austrian key sections. *Global and Planetary Change*, **192**, article #103253: 20 pp. https://doi.org/10.1016/j.gloplacha.2020.103253.

Galfetti, T., Hochuli, P.A., Brayard, A., Bucher, H., Weissert, H., and Vigran, J.O., 2007a, The Smithian/Spathian boundary event: a global climatic change in the wake of the end-Permian biotic crisis. Evidence from palynology, ammonoids and stable isotopes. *Geology*, **35**: 291–294.

Galfetti, T., Bucher, H., Ovtcharova, M., Schaltegger, U., Brayard, A., Brühwiler, T., et al., 2007b, Timing of the Early Triassic carbon cycle perturbations inferred from new U-Pb ages and ammonoid biochronozones. *Earth and Planetary Science Letters*, **258**: 593–604.

Galfetti, T., Bucher, H., Brayard, A., Hochuli, P.A., Weissert, H., Guodun, K., et al., 2007c, Late Early Triassic climate change: insights from carbonate carbon isotopes, sedimentary evolution and ammonoid paleobiogeography. *Palaeogeography, Palaeoclimatology, Palaeoecology*, **243**: 394–411.

Galfetti, T., Bucher, H., Martini, R., Hochuli, P.A., Weissert, H., Crasquin-Soleua, S., et al., 2008, Evolution of Early Triassic outer platform paleoenvironments in the Nanpanjiang Basin (South China) and their significance for the biotic recovery. *Sedimentary Geology*, **204**: 36–60.

Gallet, Y., Besse, J., Krystyn, L., Marcoux, J., and Théveniaut, H., 1992, Magnetostratigraphy of the late Triassic Bolücektasi Tepe section (southwestern Turkey): implications for changes in magnetic reversal frequency. *Physics of the Earth and Planetary Interiors*, **73**: 85–108.

Gallet, Y., Krystyn, L., and Besse, J., 1998, Upper Anisian to Lower Carnian magnetostratigraphy from the Northern Calcareous Alps (Austria). *Journal of Geophysical Research*, **103**: 605–621.

Gallet, Y., Krystyn, L., Marcoux, J., and Besse, J., 2007, New constraints on the End-Triassic (Upper Norian–Rhaetian) magnetostratigraphy. *Earth and Planetary Science Letters*, **255**: 458–470.

Gehrels, G.E., Saleeby, J.B., and Berg, H.C., 1987, Geology of Annette, Gravina, and Duke islands, southeastern Alaska. *Canadian Journal of Earth Sciences*, **24**: 866–881.

Geluk, M.C., and Röhling, H.-G., 1997, High-resolution sequence stratigraphy of the Lower Triassic 'Buntsandstein' in the Netherlands and northwestern Germany. *Geologie en Mijnbouw*, **76**: 227–246.

Geyer, G., and Kelber, K.-P., 2018, Spinicaudata ("Conchostraca", Crustacea) from the Middle Keuper (Upper Triassic) of the southern Germanic Basin, with a review of Carnian–Norian taxa and suggested biozones. *Paläontologische Zeitschrift (PalZ)*, **92**: 1–34.

Gianolla, P., and Jacquin, T., 1998, Triassic sequence stratigraphic framework of western European basins. In: de Graciansky, P.-C., Hardenbol, J., Jacquin, Th., Vail, P.R. (eds), Mesozoic-Cenozoic Sequence Stratigraphy of European Basins, *SEPM Special Publication*, **60**: 643–650.

Gianolla, P., De Zanche, V., and Mietto, P., 1998, Triassic sequence stratigraphy in the Southern Alps (northern Italy): definition of sequences and basin evolution. In: de Graciansky, P.-C., Hardenbol, J., Jacquin, Th., Vail, P.R. (eds.), Mesozoic-Cenozoic Sequence Stratigraphy of European Basins, *SEPM Special Publication*, **60**: 719–747.

Glen, J.M.G., Nomade, S., Lyons, J.J., Metcalfe, I., Mundil, R., and Renne, J.R., 2009, Magnetostratigraphic correlations of Permian–Triassic marine-to-terrestrial sections from China. In: Metcalfe, I., Isozaki, Y. (eds), End-Permian mass extinction: events & processes, age & time-scale, causative mechanism(s) & recovery, *Journal of Asian Earth Sciences*, **36**(6): 520–540.

Goldhammer, R.K., Dunn, P.A., and Hardie, L.A., 1987, High frequency glacio-eustatic oscillations with Milankovitch characteristics recorded in northern Italy. *American Journal of Science*, **287**: 853–892.

Goldhammer, R.K., Dunn, P.A., and Hardie, L.A., 1990, Depositional cycles, composite sea level changes, cycle stacking patterns, and the hierarchy of stratigraphic forcing: examples from the Alpine Triassic platform carbonates. *Geological Society of America Bulletin*, **102** (535), 562.

Golding, M.L., 2019, Evaluating tectonic models for the formation of the North American Cordillera using multivariate statistical analysis of Late Triassic conodont faunas. *Palaeobiodiversity Palaeoenvironments*. https://doi.org/10.1007/s12549-019-00393-4.

Golding, M.L., Orchard, M.J., and Zonneveld, J.-P., 2014, A summary of new conodont biostratigraphy and correlation of the Anisian (Middle Triassic) strata in British Columbia, Canada. *Albertiana*, **42**: 33–40.

Golding, M.L., Orchard, M.J., and Zagorevski, A., 2017, Conodonts from the Stikine Terrane in northern British Columbia and southern Yukon. *Geological Survey of Canada, Open File*, **8278**: 23 pp.

Goudemand, N., Orchard, M., Bucher, H., Brayard, A., Brühwiler, T., Galfetti, T., et al., 2008, Smithian-Spathian boundary: the biggest crisis in Triassic conodont history. *Geological Society of America Abstracts With Programs*, **40** (6), 505.

Goudemand, N., Romano, C., Leu, M., Bucher, H., Trotter, J.A., and Williams, I.S., 2019, Dynamic interplay between climate and marine biodiversity upheavals during the Early Triassic Smithian-Spathian biotic crisis. *Earth-Science Reviews*, **195**: 169–178. https://doi.org/10.1016/j.earscirev.2019.01.013.

Gradinaru, E., Orchard, M.J., Nicora, A., Gallet, Y., Besse, J., Krystyn, L., et al., 2007, The Global Boundary Stratotype Section and Point (GSSP) for the base of the Anisian Stage: Desli Caira Hill, North Dobrogea, Romania. *Albertiana*, **36**: 54–71.

Grasby, S.E., Beauchamp, B., and Knies, J., 2016a, Early Triassic productivity crises delayed recovery from world's worst mass extinction. *Geology*, **44** (9), 779–782. https://doi.org/10.1130/abs/2016am-279493.

Grasby, S.E., Beauchamp, B., Bond, D.P., Wignall, P.B., and Sanei, H., 2016b, Mercury anomalies associated with three extinction events (Capitanian crisis, latest Permian extinction and the Smithian/Spathian extinction) in NW Pangea. *Geological Magazine*, **153**: 285–297. https://doi.org/10.1017/S0016756815000436.

Greene, A., Scoates, J., and Weis, D., 2008, The Accreted Wrangellia Oceanic Plateau in Alaska, Yukon, and British Columbia. *Internet Article From Large Igneous Provinces Commission, Large Igneous Province of the Month*: December 2008. Available at: <www.largeigneousprovinces.org/>

Greene, A.R., Scoates, J.S., Weis, D., Katvala, E.C., Israel, S., and Nixon, G.T., 2010, The architecture of oceanic plateaus revealed by the volcanic stratigraphy of the accreted Wrangellia oceanic plateau. *Geosphere*, **6**: 47–73.

Greene, A., Scoates, J., and Weis, D., 2011, *The Accreted Wrangellia Oceanic Plateau in Alaska, Yukon, and British Columbia*. Available at: <www.eos.ubc.ca/research/wrangellia> [Last update was 2010 when viewed Feb., 2011].

Griesbach, C.L., 1880, Paleontological notes on the Lower Trias on the Himalayas. *Records of the Geological Survey of India*, **13** (2), 94–113.

Grossman, E.L., and Joachimski, M.M., 2020, Chapter 10 - Oxygen isotope stratigraphy. *In* Gradstein, F.M., Ogg, J.G., Schmitz, M.D., and Ogg, G.M. (eds), *The Geologic Time Scale 2020*. **Vol. 1** (this book). Elsevier, Boston, MA.

Hallam, A., 1981, The end-Triassic bivalve extinction event. *Palaeogeography, Palaeoclimatology, Palaeoecology*, **35**: 1–44.

Hallam, A., 1992, *Phanerozoic Sea-Level Changes*. New York: Columbia University Press 266 pp.

Hallam, A., and Wignall, P.B., 1999, Mass extinctions and sea-level changes. *Earth-Science Reviews*, **48**: 217–250.

Haq, B.U., 2018, Triassic eustatic variations reexamined. *GSA Today*, **28**: 4–9 https://doi.org/10.1130/GSATG381A.1; with supplement online at <www.geosociety.org/datarepository/2018/>.

Haq, B.U., and Al-Qahtani, A.M., 2005, Phanerozoic cycles of sea-level change on the Arabian Platform. *GeoArabia*, **10** (2), 127–160.

Haq, B.U., Hardenbol, J., and Vail, P.R., 1988, Mesozoic and Cenozoic chronostratigraphy and eustatic cycles. In: Wilgus, C.K., Hastings, B.S., Kendall, G.St.C., Posamentier, H.W., Ross, C.A., van Wagoner, J.C. (eds), Sea-Level Changes: An Integrated Approach, *SEPM Special Publication*, **42**: 71–108.

Hardenbol, J., Thierry, J., Farley, M.B., Jacquin, Th., de Graciansky, P.-C., Vail, P.R., et al., 1998, Mesozoic and Cenozoic sequence chronostratigraphic framework of European basins. In: de Graciansky, P.-C., Hardenbol, J., Jacquin, Th., and Vail, P.R. (eds), Mesozoic-Cenozoic Sequence Stratigraphy of European Basins, *SEPM Special Publication*, **60**: 3–13, 763–781.

Hardie, L.A., and Hinnov, L.A., 1997, Biostratigraphic and radiometric age data question the Milankovitch characteristics of the Latemar cycles (Southern Alps, Italy) – comment. *Geology*, **25**: 470–471.

Hayes, J.M., Strauss, H., and Kaufman, 1999, The abundance of $^{13}C$ in marine organic matter and isotopic fractionation in the global biogeochemical cycle of carbon during the past 800 Ma. *Chemical Geology*, **161**: 103–125.

Heckert, A.B., and Lucas, S.G., 1999, Global correlation and chronology of Triassic theropods (Archosauria: Dinosauria). *Albertiana*, **23**: 22–35.

Heckert, A.B., Lucas, S.G., Dickinson, W.R., and Mortensen, J.K., 2009, New ID-TIMS U-Pb ages for Chinle Group strata (Upper Triassic) in New Mexico and Arizona, correlation to the Newark Supergroup, and implications for the "long Norian". *Geological Society of America Abstracts With Programs*, **41** (7), 123.

Helby, R., Morgan, R., and Partridge, A.D., 1987, A palynological zonation of the Australian Mesozoic. In Jell, P.A. (ed), Studies in Australian Mesozoic Palynology, *Memoir Association Australaisian Paleontologists*, **4**: 1–94.

Heller, F., Haihong, C., Dobson, J., and Haag, M., 1995, Permian-Triassic magnetostratigraphy – new results from south China. *Physics of the Earth and Planetary Interiors*, **89**: 281–295.

Henderson, C., and Baud, A., 1997, Correlation of the Permian- Triassic boundary in Arctic Canada and comparaison with Meishan, China.

*In* Naiwen, W., and Remane, J. (eds), *Stratigraphy, 11, Proceedings of the 30th IGC*. Beijing: VSP, 143–152.

Henderson, C.M., Golding, M.L., and Orchard, M.J., 2018, Conodont sequence biostratigraphy of the Lower Triassic Montney Formation. In: Euzen, T., Moslow, T.F., Caplan, M. (eds.), The Montney Play: Deposition to Development, *Bulletin of Canadian Petroleum Geology*, Special Volume, **66**: 7–22.

Henderson, C.M., and Shen, S.-Z., 2020, Chapter 24 - The Permian Period. *In* Gradstein, F.M., Ogg, J.G., Schmitz, M.D., and Ogg, G.M. (eds), *The Geologic Time Scale 2020*. **Vol. 2** (this book). Elsevier, Boston, MA.

Hermann, E., Hochuli, P.A., Bucher, H., Vigran, J.O., Weissert, H., and Bernasconi, S.M., 2010, A close-up view of the Permian–Triassic boundary based on expanded organic carbon isotope records from Norway (Trøndelag and Finnmark Platform). *Global and Planetary Change*, **74**: 156–167.

Herngreen, G.F.W., 2005, Triassic sporomorphs of NW Europe: taxonomy, morphology and ranges of marker species with remarks on botanical relationship and ecology and comparison with ranges in the Alpine Triassic. *Kenniscentrum Biogeology, Nederlands Instituut voor Toegepaste Geowetenschappen TNO, Utrecht, TNO report, NITG 04-176-C*.

Hesselbo, S.P., Robinson, S.A., Surlyk, F., and Piasecki, S., 2002, Terrestrial and marine extinctions at the Triassic-Jurassic boundary synchronized with major carbon-cycle perturbation: a link to initiation of massive volcanism? *Geology*, **30**: 251–254.

Hinnov, L.A., 2006, Discussion of "Magnetostratigraphic confirmation of a much faster tempo for sea-level change for the Middle Triassic Latemar platform carbonates" by D.V. Kent, G. Muttoni and P. Brack [Earth Planet. Sci. Lett. 228 (2004), 369–377]. *Earth and Planetary Science Letters*, **243**: 841–846.

Hinnov, L.A., and Goldhammer, R.K., 1991, Spectral analysis of the Middle Triassic Latemar Limestone. *Journal of Sedimentary Research*, **61**: 1173–1193.

Hochuli, P., 1998. Dinoflagellate cysts and Spore pollen. Columns for Triassic chart of Mesozoic and Cenozoic sequence chronostratigraphic framework of European basins, by Hardenbol, J., Thierry, J., Farley, M.B., Jacquin, Th., de Graciansky, P.-C., and Vail, P.R. (coordinators). In: de Graciansky, P.-C., Hardenbol, J., Jacquin, Th., Vail, P.R. (eds), Mesozoic-Cenozoic Sequence Stratigraphy of European Basins, *SEPM Special Publication*, **60**: Chart 8.

Hochuli, P.A., Hermann, E., Vigran, J.O., Bucher, H., and Weissert, W., 2010, Rapid demise and recovery of plant ecosystems across the end-Permian extinction event. *Global and Planetary Change*, **74**: 144–155.

Hodych, J.P., and Dunning, G.R., 1992, Did the Manicouagan impact trigger end-of-Triassic mass extinction? *Geology*, **20**: 51–54.

Holser, W.T., and Magaritz, M., 1987, Events near the Permian–Triassic boundary. *Modern Geology*, **11**: 155–180.

Horacek, M., Brandner, R., Richoz, S., and Povoden-Karadeniz, E., 2010a, Lower Triassic sulphur isotope curve of marine sulphates from the Dolomites, N-Italy. *Palaeogeography, Palaeoclimatology, Palaeoecology*, **290**: 65–70.

Horacek, M., Povoden, E., Richoz, S., and Brandner, R., 2010b, High-resolution carbon isotope changes, litho- and magnetostratigraphy across Permian-Triassic Boundary sections in the Dolomites, N-Italy. New constraints for global correlation. *Palaeogeography, Palaeoclimatology, Palaeoecology*, **290**: 58–64.

Hornung, T., and Brandner, R., 2005, Biochronostratigraphy of the Reingraben Turnover (Hallstatt Facies Belt): local black shale events controlled by regional tectonics, climatic change and plate tectonics. *Facies*, **51**: 460–479.

Hounslow, M.K., and Muttoni, G., 2010, The geomagnetic polarity timescale for the Triassic: linkage to stage boundary definitions. In: Lucas, S.G. (ed), The Triassic Timescale, *The Geological Society of London Special Publications*, **334**: 61–102.

Hounslow, M.W., Posen, P.E., and Warrington, G., 2004, Magnetostratigraphy and biostratigraphy of the Upper Triassic and lowermost Jurassic succession, St. Audrie's Bay, UK. *Palaeogeography, Palaeoclimatology, Palaeoecology*, **213**: 331–358.

Hounslow, M.K., Szurlies, M., Muttoni, G., and Nawrocki, J., 2007, The magnetostratigraphy of the Olenekian-Anisian boundary and a proposal to define the base of the Anisian using a magnetozone datum. *Albertiana*, **36**: 72–77.

Hounslow, M.K., Peters, C., Mørk, A., Weitschat, W., and Vigran, J.O., 2008a, Biomagnetostratigraphy of the Vikinghøgda Formation, Svalbard (arctic Norway) and the geomagnetic polarity timescale for the Lower Triassic. *Geological Society of America Bulletin*, **120**: 1305–1325.

Hounslow, M.K., Hu, M., Mørk, A., Weitschat, W., Vigran, J.O., Karloukovski, V., et al., 2008b, Intercalibration of Boreal and Tethyan timescales: the magneto-biostratigraphy of the Middle Triassic and the latest Early Triassic, central Spitsbergen (arctic Norway). *Polar Research*, **27**: 469–490.

Huang, C.J., 2018. Astronomical time scale for the Mesozoic. *Stratigraphy and Time Scales*, Elsevier, **Vol. 3**, p. 81–150. https://doi.org/10.1016/bs.sats.2018.08.005.

Hüsing, S.K., Deenen, M.H.L., Koopmans, J.G., and Krijgsman, W., 2011, Magnetostratigraphic dating of the proposed Rhaetian GSSP at Steinbergkogel (Upper Triassic, Austria): implications for the Late Triassic time scale. *Earth and Planetary Science Letters*, **302**: 203–216.

Ikeda, M., and Tada, R., 2014, A 70 million year astronomical time scale for the deep-sea bedded chert sequence (Inuyama, Japan): implications for Triassic-Jurassic geochronology. *Earth and Planetary Science Letters*, **399**: 30–43 <https://doi.org/10.1016/j.epsl.2014.04.031>.

Ikeda, M., Tada, R., and Sakuma, H., 2010, Astronomical cycle origin of bedded chert: a middle Triassic bedded chert sequence, Inuyama, Japan. *Earth and Planetary Science Letters*, **297**: 369–378.

Ikeda, M., Tada, R., and Ozaki, K., 2017, Astronomical pacing of the global silica cycle recorded in Mesozoic bedded cherts. *Nature Communications*, **8**: 15532. https://doi.org/10.1038/ncomms15532.

Irmis, R.B., Martz, J.W., Parker, W.G., and Nesbitt, S.J., 2010, Re-evaluating the correlation between Late Triassic terrestrial vertebrate biostratigraphy and the GSSP-defined marine stages. *Albertiana*, **38**: 40–53.

Isozaki, Y., 2009, Integrated "plume winter" scenario for the double-phased extinction during the Paleozoic–Mesozoic transition: the G-LB and P-TB events from a Panthalassan perspective. In: Metcalfe, I., Isozaki, Y. (eds), End-Permian mass extinction: events & processes, age & timescale, causative mechanism(s) & recovery, *Journal of Asian Earth Sciences*, **36**(6): 459–480.

Jacquin, Th., and Vail, P.R. (coordinators), 1998, Sequence chronostratigraphy. Columns for Triassic chart, Mesozoic and Cenozoic sequence chronostratigraphic framework of European basins by Hardenbol, J., Thierry, J., Farley, M.B., Jacquin, Th., de Graciansky, P.-C., and Vail, P.R. In: de Graciansky, P.-C., Hardenbol, J., Jacquin, Th., Vail, P.R. (eds), Mesozoic-Cenozoic Sequence Stratigraphy of European Basins, *SEPM Special Publication*, **60**: Chart 8.

Jenks, J.F., Monnet, C., Balini, M., Brayard, A., Meier, M., 2015, Chapter 13. Biostratigraphy of Triassic ammonoids. In: Klug, C.,

Korn, D., De Baets, K., Kruta, I., Mapes, R.H. (eds), *Ammonoid Paleobiology: From Macroevolution to Paleogeography*, Topics in Geobiology. Springer Publication, Vol. **44**: 329–371 https://doi.org/10.1007/978-94-017-9633-0_13.

Jenkyns, H.C., Jones, C.E., Gröcke, D.R., Hesselbo, S.P., and Parkinson, D.N., 2002, Chemostratigraphy of the Jurassic system: applications, limitations and implications for palaeoceanography. *Journal of the Geological Society, London*, **159**: 351–378.

Jones, C.E., and Jenkyns, H.C., 2001, Seawater strontium isotopes, oceanic anoxic events, and seafloor hydrothermal activity in the Jurassic and Cretaceous. *American Journal of Science*, **301**: 112–149.

Jourdan, F., Marzoli, A., Bertrand, H., Cirilli, S., Tanner, L.H., Kontak, D.J., et al., 2009a, $^{40}Ar/^{39}Ar$ ages of CAMP in North America: implications for the Triassic–Jurassic boundary and the $^{40}K$ decay constant bias. *Lithos*, **110**: 167–180.

Jourdan, F., Renne, P.R., and Reimold, W.U., 2009b, An appraisal of the ages of terrestrial impact structures. *Earth and Planetary Science Letters*, **286**: 1–13.

Kamo, S.L., Czamanske, G.K., and Drogh, T.E., 1996, A minimum U–Pb age for Siberian flood-basalt volcanism. *Geochimica et Cosmochimica Acta*, **60**: 3505.

Kamo, S.L., Czamanske, G.K., Amelin, Y., Fedorenko, V.A., Davis, D.W., and Trofimov, V.R., 2003, Rapid eruption of Siberian flood-volcanic rocks and evidence for coincidence with the Permian-Triassic boundary and mass extinction at 251 Ma. *Earth and Planetary Science Letters*, **214**: 75–91.

Kampschulte, A., and Strauss, H., 2004, The sulfur isotopic evolution of Phanerozoic sea water based on the analysis of structurally substituted sulfate in carbonates. *Chemical Geology*, **204**: 255–286.

Kapoor, H.M., 1996, The Guryul Ravine section, candidate of the global Stratotype and point (GSSP) of the Permian-Triassic boundary (PTB). In: Yin, H.-f. (Ed.), *The Paleozoic-Mesozoic Boundary, Candidates of the Global Stratotype Section and Point of the Permian-Triassic Boundary*. China University of Geosciences Press, Wuhan, pp. 99–110.

Kemp, D.B., and Coe, A.L., 2007, A nonmarine record of eccentricity forcing through the Upper Triassic of southwest England and its correlation with the Newark Basin astronomically calibrated geomagnetic polarity time scale from North America. *Geology*, **35**: 991–994.

Kent, D.V., and Olsen, P.E., 1999, Astronomically tuned geomagnetic polarity timescale for the Late Triassic. *Journal of Geophysical Research*, **104**: 12831–12841 Web page update (2002) posted at Newark Basin Coring Project website: <www.ldeo.columbia.edu/~polsen/nbcp/nbcp.timescale.htm> [Accessed 3 July 2010].

Kent, D.V., Olsen, P.E., and Witte, W.K., 1995, Late Triassic–earliest Jurassic geomagnetic polarity sequence and paleolatitudes from drill cores in the Newark rift basin, eastern North America. *Journal of Geophysical Research*, **100**: 14965–14998.

Kent, D.V., Muttoni, G., and Brack, P., 2004, Magnetostratigraphic confirmation of a much faster tempo for sea-level change for the Middle Triassic Latemar platform carbonates. *Earth and Planetary Science Letters*, **228**: 369–377.

Kent, D.V., Olsen, P.E., and Muttoni, G., 2017, Astrochronostratigraphic polarity time scale (APTS) for the Late Triassic and Early Jurassic from continental sediments and correlation with standard marine stages. *Earth-Science Reviews*, **166**: 153–180. https://doi.org/10.1016/j.earscirev.2016.12.014.

Kent, D.V., Olsen, P.E., Rasmussen, C., Lepre, C., Mundil, R., Irmis, R.B., et al., 2018, Empirical evidence for stability of the 405-kiloyear Jupiter-Venus eccentricity cycle over hundreds of million years. *Proceedings of the National Academy of Sciences of the United States of America*, **115** (24), 6153–6158. https://doi.org/10.1073/pnas.1800891115.

Kiessling, W., 2010, Reef expansion during the Triassic: spread of photosymbiosis balancing climatic cooling. In: Kustatscher, E., Preto, N., Wignall, P. (eds), Triassic climates, *Palaeogeography, Palaeoclimatology, Palaeoecology*, **290**: 11–19.

Kiparisova, L.D., and Popov, Y.N., 1956, Subdivision of the Lower series of the Triassic system into stages. *Doklady Akademiya Nauk USSR*, **109**: 842–845 (in Russian).

Kiparisova, L.D., and Popov, Y.N., 1964. The project of subdivision of the Lower Triassic into stages. *XXII International Geological Congress, Reports of Soviet geologists, Problem 16a* (In Russian) (pp. 91–99).

Klein, H., and Lucas, S.G., 2010, Tetrapod footprints – their use in biostratigraphy and biochronology of the Triassic. In: Lucas, S.G. (ed), The Triassic Timescale, *The Geological Society of London Special Publications*, **334**: 419–446.

Knoll, A.H., Bambach, R.K., Payne, J.L., Pruss, S., and Fischer, W.W., 2007, Paleophysiology and end-Permian mass extinction. *Earth and Planetary Science Letters*, **256**: 295–313.

Koepnick, R.B., Denison, R.E., Burke, W.H., Hetherington, E.A., and Dahl, D.A., 1990, Construction of the Triassic and Jurassic portion of the Phanerozoic curve of seawater $^{87}Sr/^{86}Sr$. *Chemical Geology*, **80**: 327–349.

Konstantinov, A.G., and Klets, T.V., 2009, Stage boundaries of the Triassic in northeast Asia. *Stratigraphy and Geological Correlation*, **17**: 173–191. https://doi.org/10.1134/S0869593809020063.

Korte, C., and Kozur, H.W., 2010, Carbon-isotope stratigraphy across the Permian-Triassic boundary: a review. *Journal of Asian Earth Sciences*, **39**: 215–235.

Korte, C., Kozur, H.W., Bruckschen, P., and Veizer, J., 2003, Strontium isotope evolution of late Permian and Triassic seawater. *Geochimica et Cosmochimica Acta*, **67**: 47–62.

Korte, C., Kozur, H.W., and Veizer, J., 2005, $\partial^{13}C$ and $\partial^{18}O$ values of Triassic brachiopods and carbonate rocks as proxies for coeval seawater and palaeotemperature. *Palaeogeography, Palaeoclimatology, Palaeoecology*, **226**: 287–306.

Korte, C., Pande, P., Kalia, P., Kozur, H.W., Joachimski, M.M., and Oberhänsli, 2010, Massive volcanism at the Permian–Triassic boundary and its impact on the isotopic composition of the ocean and atmosphere. *Journal of Asian Earth Sciences*, **37**: 293–311.

Kozur, H.W., 1998, Some aspects of the Permian–Triassic boundary (PTB) and of the possible causes for the biotic crisis around this boundary. *Palaeogeography, Palaeoclimatology, Palaeoecology*, **143**: 227–272.

Kozur, H.W., 1999, Remarks on the position of the Norian-Rhaetian boundary. Proceedings of the Epicontinental Triassic International Symposium, Halle (Germany), 21–23 Sept., 1998. *Zentralblatt für Geologie und Paläontologie*, **I** (7–8): 523–535.

Kozur, H.W., 2003, Integrated ammonoid, conodont and radiolarian zonation of the Triassic. *Hallesches Jahrbuch fur Geowissenschaften*, **B25**: 49–79.

Kozur, H.W., 2007, Biostratigraphy and event stratigraphy in Iran around the Permian–Triassic boundary (PTB): implications for the causes of the PTB biotic crisis. *Global and Planetary Change*, **55**: 155–176.

Kozur, H.W., and Bachmann, G.H., 2005, Correlation of the Germanic Triassic with the international scale. *Albertiana*, **32**: 21–35.

Kozur, H.W., and Mostler, H., 1994, Anisian to Middle Carnian radiolarian zonation and description of some stratigraphically important radiolarians. *Geologisch-Paläontologische Mitteilungen Innsbruck, Sonderband*, **3**: 39–255.

Kozur, H.W., and Bachmann, G.H., 2008, Updated correlation of the Germanic Triassic with the Tethyan scale and assigned numeric ages. *Berichte der Geologischen Bundesanstalt*, **76**: 53–58.

Kozur, H.W., and Bachmann, G.H., 2010, The Middle Carnian Wet Intermezzo of the Stuttgart Formation (Schilfsandstein), Germanic Basin. In: Kustatscher, E., Preto, N., and Wignall, P. (eds), Triassic climates, *Palaeogeography, Palaeoclimatology, Palaeoecology*, **290**: 107–119.

Kozur, H.W., and Weems, R.E., 2005, Conchostracan evidence for a late Rhaetian to early Hettangian age for the CAMP volcanic event in the Newark Supergroup, and a Sevatian (late Norian) age for the immediately underlying beds. *Hallesches Jahrbuch für Geowissenschaften, Reihe B: Geologie, Paläontologie, Mineralogie*, **27**: 21–51.

Kozur, H.W., and Weems, R.E., 2010, The biostratigraphic importance of conchostracans in the continental Triassic of the northern hemisphere. In: Lucas, S.G. (ed), The Triassic Timescale, *The Geological Society of London Special Publications*, **334**: 315–417.

Kozur, H.W., and Weems, R.E., 2011, Detailed correlation and age of continental late Changhsingian and earliest Triassic beds: implications for the role of the Siberian Trap in the Permian-Triassic biotic crisis. *Palaeogeography, Palaeoclimatology, Palaeoecology*, **308**: 22–40 <https://doi.org/10.1016/j.palaeo.2011.02.020>.

Krull, E.S., and Retallack, G.J., 2000, $\delta^{13}C$ depth profiles from paleosols across the Permian-Triassic boundary: evidence for methane release. *Geological Society of America Bulletin*, **112**: 1459–1472.

Krystyn, L., 1980, Triassic conodont localities of the Salzkammergut region (northern Calcareous Alps). In: Schonlaub, H.P. (ed.), Second European Conodont Symposium ECOS II: Guidebook and Abstracts, *Abhandlungen der Geologischen Bundesanstalt*, **35**: 61–98.

Krystyn, L., 2010, Decision report on the defining event for the base of the Rhaetian stage. *Albertiana*, **38**: 11–12.

Krystyn, L., and Orchard, M.J., 1996, Lowermost Triassic ammonoid and conodont biostratigraphy of Spiti, India. *Albertiana*, **17**: 10–21.

Krystyn, L., Gallet, Y., Besse, J., and Marcoux, J., 2002, Integrated Upper Carnian to Lower Norian biochronology and implications for the Upper Triassic magnetic polarity time scale. *Earth and Planetary Science Letters*, **203**: 343–351.

Krystyn, L., Richoz, S., and Bhargava, O.N., 2007a, The Induan-Olenekian Boundary (IOB) in Mud – an update of the candidate GSSP section M04. *Albertiana*, **36**: 33–49.

Krystyn, L., Bhargava, O.N., and Richoz, S., 2007b, A candidate GSSP for the base of the Olenekian Stage: mud at Pin Valley; district Lahul & Spiti, Himachal Pradesh (Western Himalaya, India). *Albertiana*, **35**: 5–29.

Krystyn, L., Boquerel, H., Kuerschner, W., Richoz, S., and Gallet, Y., 2007c, Proposal for a candidate GSSP for the base of the Rhaetian Stage. *New Mexico Museum of Natural History and Science Bulletin*, **41**: 189–199.

Krystyn, L., Richoz, S., Gallet, Y., Bouquerel, H., Kürschner, W.M., and Spötl, C., 2007d, Updated bio- and magnetostratigraphy from the Steinbergkogel (Austria), candidate GSSP for the base of the Rhaetian stage. *Albertiana*, **36**: 164–173.

Kürschner, W.M., and Herngreen, G.F.W., 2010, Triassic palynology of central and northwestern Europe: a review of palynofloral diversity patterns and biostratigraphic subdivisions. In: Lucas, S.G. (Ed.), The Triassic Timescale, *The Geological Society of London Special Publications*, **334**: 263–283.

Kustatscher, E., Ash, S.R., Karasev, E., Pott, C., Vajda, V., Yu, J.X., et al., 2018, Flora of the Late Triassic. In: Tanner, L. (ed), *The Late Triassic World: Earth in a Time of Transition*. Topics in Geobiology, Springer Publication, Vol. **44**: 545–622. https://doi.org/10.1007/978-3-319-68009-5_13

Lehrmann, D.J., Ramezani, J., Bowring, S.A., Martin, M.W., Montgomery, P., Enos, P., et al., 2006, Timing of recovery from the end-Permian extinction: geochronologic and biostratigraphic constraints from south China. *Geology*, **34**: 1053–1056.

Large Igneous Provinces Commission (International Association of Volcanology and Chemistry of the Earth's Interior), 2020, *LIP record*. Internet database available at: <www.largeigneousprovinces.org>.

Lehrmann, D.J., Stepchinski, L., Altiner, D., Orchard, M.J., Montgomery, P., Enos, P., et al., 2015, An integrated biostratigraphy (conodonts and foraminifers) and chronostratigraphy (paleomagnetic reversals, magnetic susceptibility, elemental chemistry, carbon isotopes and geochronology) for the Permian-Upper Triassic strata of Guandao section, Nanpanjiang Basin, south China. *Journal of Asian Earth Sciences*, **108**: 117–135. http://dx.doi.org/10.1016/j.jseaes.2015.04.030.

Li, M.S., Ogg, J.G., Zhang, Y., Huang, C.J., Hinnov, L.A., Chen, Z.-Q., et al., 2016, Astronomical tuning of the end-Permian extinction and the Early Triassic Epoch of South China and Germany. *Earth and Planetary Science Letters*, **441**: 10–25.

Li, M.S., Zhang, Y., Huang, C.J., Ogg, J.G., Hinnov, L.A., and Wang, Y.D., 2017a, Astronomical tuning and magnetostratigraphy of the Upper Triassic Xujiahe Formation of South China and Newark Supergroup of North America: implications for the Late Triassic time scale. *Earth and Planetary Science Letters*, **475**: 207–223.

Li, M.S., Zhang, Y., Huang, C.J., Ogg, J.G., Hinnov, L.A., Wang, Y.D., et al., 2017b, Astrochronology and magnetostratigraphy of the Xujiahe Formation of South China and Newark Supergroup of North America: implications for the Late Triassic time scale. *AGU Fall Meeting, New Orleans, LA*.

Li, M.S., Huang, C.J., Hinnov, L.A., Chen, W.Z., Ogg, J.G., and Tian, W., 2018, Astrochronology of the Anisian Stage (Middle Triassic) at the Guandao reference section, South China. *Earth and Planetary Science Letters*, **482**: 591–606.

Litwin, R.J., Traverse, A., and Ash, S.R., 1991, Preliminary palynological zonation of the Chinle Formation, southwestern U.S.A., and its correlation to the Newark Supergroup (eastern U.S.A.). *Review of Palaeobotany and Palynology*, **68**: 269–287.

Lucas, S.G., 1998, Global Triassic tetrapod biostratigraphy and biochronology. *Palaeogeography, Palaeoclimatology, Palaeoecology*, **143**: 345–382.

Lucas, S.G., 1999, A tetrapod-based Triassic timescale. *Albertiana*, **22**: 31–40.

Lucas, S.G., 2008, *Triassic New Mexico: Dawn of the Dinosaurs*. Albuquerque: New Mexico Museum of Natural History and Science 48 pp.

Lucas, S.G., 2009, Timing and magnitude of tetrapod extinctions across the Permo-Triassic boundary. In: Metcalfe, I., Isozaki, Y. (eds), End-Permian mass extinction: events & processes, age & timescale,

causative mechanism(s) & recovery, *Journal of Asian Earth Sciences*, **36**(6): 491–502.

Lucas, S.G., 2010a, The Triassic Timescale. *The Geological Society of London Special Publications*, **334**, 500 pp.

Lucas, S.G., 2010b, The Triassic chronostratigraphy scale: history and status. In: Lucas, S.G. (ed.), The Triassic Timescale, *The Geological Society of London Special Publications*, **334**: 447–500.

Lucas, S.G., 2010c, The Triassic timescale: an introduction. In: Lucas, S. G. (ed), The Triassic Timescale, *The Geological Society of London Special Publications*, **334**: 1–16.

Lucas, S.G., 2010d, The Triassic timescale based on nonmarine tetrapod biostratigraphy and biochronology. In: Lucas, S.G. (ed), The Triassic Timescale, *The Geological Society of London Special Publications*, **334**: 17–39.

Lucas, S.G., 2016, Base of the Rhaetian and a critique of Triassic conodont-based biostratigraphy. *Albertiana*, **43**: 24–27 Available at: <http://paleo.cortland.edu/albertiana/> [and his "Base of the Rhaetian and a critique of Triassic conodont-based biostratigraphy: reply". *Albertiana*, **43**: 32].

Lucas, S.G., 2018a, The Late Triassic Timescale. In: Tanner, L.H. (ed), *The Late Triassic World: Earth in a Time of Transition*, Topics in Geobiology. Springer Publications, Vol. **46**: 351–405. https://doi.org/10.1007/978-3-319-68009-5_10.

Lucas, S.G., 2018b, Late Triassic terrestrial tetrapods: biostratigraphy, biochronology and biotic events. In: Tanner, L.H. (ed), *The Late Triassic World: Earth in a Time of Transition*, Topics in Geobiology. Springer Publications, Vol. **46**: 351–405. https://doi.org/10.1007/978-3-319-68009-5_10.

Lucas, S.G., 2018c, Permian-Triassic charophytes: distribution, biostratigraphy and biotic events. *Journal of Earth Science*, **29**: 778–793. https://doi.org/10.1007/s12583-018-0786-4.

Lucas, S.G., and Tanner, L.H., 2014, Triassic timescale based on tetrapod biostratigraphy and biochronology. *In* Rocha, R., et al. (eds), *STRATI 2013*. Springer Geology, pp. 1013–1016. https://doi.org/10.1007/978-3-319-04364-7_192.

Lucas, S.G., Tanner, L.H., Kozur, H.W., Weems, R.E., and Heckert, A. B., 2012, The Late Triassic timescale: age and correlation of the Carnian-Norian boundary. *Earth-Science Reviews*, **114**: 1–18.

Luo, G.M., Kump, L.R., Wang, Y.B., Tong, J.N., Arthur, M.A., Yang, H., et al., 2010, Isotopic evidence for an anomalously low oceanic sulfate concentration following end-Permian mass extinction. *Earth and Planetary Science Letters*, **300**: 101–111.

Luo, G.M., Wang, Y.B., Yang, H., Algeo, T.J., Kump, L.R., Huang, J.H., et al., 2011, Stepwise and large-magnitude negative shift in delta C-13 (carb) preceded the main marine mass extinction of the Permian-Triassic crisis interval. *Palaeogeography, Palaeoclimatology, Palaeoecology*, **299**: 70–82.

Lyu, Z.Y., Orchard, M.J., Chen, Z.Q., Zhao, L.S., Zhang, L., Zhang, X.M., 2018, A taxonomic re-assessment of the *Novispathodus waageni* group and its role in defining the base of the Olenekian (lower Triassic). *Journal of Earth Science*, **29**: 824–836.

Lyu, Z.Y., Orchard, M.J., Chen, Z.Q., Wang, X.D., Zhao, L.S., and Han, C., 2019, Uppermost Permian to Lower Triassic conodont successions from the Enshi area, western Hubei Province, South China. *Palaeogeography, Palaeoclimatology, Palaeoecology*, **519**: 49–64.

Lyu, Z.Y., Orchard, M.J., Chen, Z.Q., Henderson, C.M., and Zhao, L.S., 2020. A proposed ontogenesis and evolutionary lineage of conodont *Eurygnathodus costatus* and its role in defining the base of the Olenekian (Lower Triassic). *Palaeogeography, Palaeoclimatology, Palaeoecology*, article #109916: 18 pp. https://doi.org/10.1016/j.palaeo.2020.109916.

Maron, M., Rigo, M., Bertinelli, A., Katz, M.E., Godfrey, L., Zaffani, M., et al., 2015, Magnetostratigraphy, biostratigraphy, and chemostratigraphy of the Pignola-Abriola section: new constraints for the Norian-Rhaetian boundary. *Geological Society of America Bulletin*, **127** (7–8), 962–974. https://doi.org/10.1130/B31106.1.

Maron, M., Muttoni, G., Dekkers, M.J., Mazza, M., Roghi, G., Breda, A., et al., 2017, Contribution to the magnetostratigraphy of the Carnian: new magneto-biostratigraphic constraints from Pignola-2 and Dibona marine sections, Italy. *Newsletters on Stratigraphy*, **50** (2), 187–203. https://doi.org/10.1127/nos/2017/0291.

Maron, M., Muttoni, G., Rigo, M., Gianolla, P., and Kent, D.V., 2019, New magnetobiostratigraphic results from the Ladinian of the Dolomites and implications for the Triassic geomagnetic polarity timescale. *Palaeogeography, Palaeoclimatology, Palaeoecology*, **517**: 52–73. https://doi.org/10.1016/j.palaeo.2018.11.024.

Marshall, C.R., and Jacobs, D.K., 2009, Flourishing after the end-Permian mass extinction. *Science*, **325**: 1079–1080.

Martin, E.E., and Macdougall, J.D., 1995, Sr and Nd isotopes at the Permian/Triassic boundary: a record of climate change. *Chemical Geology*, **125**: 73–95.

Marzoli, A., Renne, P.R., Piccirillo, E.M., Ernesto, M., Bellieni, G., and De Min, A., 1999, Extensive 200-million-year-old continental flood basalts of the Central Atlantic Magmatic Province. *Science*, **284**: 616–618.

Mazza, M., Furin, S., Spöti, C., and Rigo, M., 2010, Generic turnovers of Carnian/Norian conodonts: climatic control or competition?. In: Kustatscher, E., Preto, N., Wignall, P. (eds), Triassic climates, *Palaeogeography, Palaeoclimatology, Palaeoecology*, **290**: 120–137.

Marzoli, A., Jourdan, F., Puffer, J.H., Cuppone, T., Tanner, L.H., Weems, R.E., et al., 2011, Timing and duration of the Central Atlantic magmatic province in the Newark and Culpeper basins, eastern U.S.A. *Lithos*, **122**: 175–188.

Mazza, M., Rigo, M., and Gullo, M., 2012, Taxonomy and biostratigraphic record of the Upper Triassic conodonts of the Pizzo Mondello section (western Sicily, Italy). *Rivista Italiana di Paleontologia e Stratigrafia*, **118**: 85–130.

Mazza, M., Nicora, A., and Rigo, M., 2018, *Metapolygnathus parvus* Kozur, 1972 (Conodonta): a potential primary marker for the Norian GSSP (Upper Triassic). *Bollettino della Società Paleontologica Italiana*, **57** (2), 81–101. https://doi.org/10.4435/BSPI.2018.06.

McArthur, J.M., 2008, Comment on 'The impact of the Central Atlantic Magmatic Province on climate and on the Sr- and Os-isotope evolution of seawater' by Cohen, A.S. and Coe, A.L. 2007. Palaeogeography, Palaeoclimatology, Palaeoecology, 244. 374–390. *Palaeogeography, Palaeoclimatology, Palaeoecology*, **263**: 146–149.

McArthur, J.M., 2010, Correlation and dating with strontium-isotope stratigraphy. In: Whitaker, J.E., Hart, M.B. (eds), Micropalaeontology, sedimentary environments and stratigraphy: a tribute to Dennis Curry (1912–2001), *The Micropalaeontological Society Special Publication*, **TSM004**: 133–145.

McArthur, J.M., Howarth, R.J., and Bailey, T.R., 2001, Strontium isotope stratigraphy: LOWESS Version 3: best fit to the marine Sr-isotope curve for 0–509 Ma and accompanying look-up table for deriving numerical age. *Journal of Geology*, **109**: 155–170.

McArthur, J.M., Howarth, R.J., Shields, G.A., and Zhou, Y., 2020, Chapter 7 - Strontium isotope stratigraphy. *In* Gradstein, F.M., Ogg, J.G., Schmitz, M.D., and Ogg, G.M. (eds), *The Geologic Time Scale 2020*. **Vol. 1** (this book). Elsevier, Boston, MA.

McRoberts, C.A., 2007, The halobid bivalve succession across a potential Carnian/Norian GSSP at Black Bear Ridge, Williston Lake, northeast British Columbia, Canada. *Albertiana*, **36**: 142–145.

McRoberts, C.A., 2010, Biochronology of Triassic pelagic bivalves. In: Lucas, S.G. (Ed.), The Triassic Timescale, *The Geological Society of London Special Publications*, **334**: 201–219.

McRoberts, C.A., Krystyn, L., and Shea, A., 2008, Rhaetian (Late Triassic *Monotis* (Bivalvia: Pectinacea) from the Northern Calcareous Alps (Austria) and the end-Norian crisis in pelagic faunas. *Journal of Paleontology*, **51**: 721–735.

Menning, M., Gast, R., Hagdorn, H., Kading, K.-C., Simon, T., Szurlies, M., et al., 2005, Zeitskala für Perm und Trias in der Stratigraphischen Tabelle von Deutschland 2002. Zyklostratigraphische Kalibrierung von höherer Dyas und Germanischer Trias und das Alter der Stufen Roadium bis Rhaetium 2005. In: Menning M., Hendrich, A. (eds), Erläuterungen zur Stratigraphischen Tabelle von Deutschland, *Newsletters of Stratigraphy*, **41**(1/3): 173–210.

Metcalfe, I., and Isozaki, Y. (eds), 2009a. End-Permian mass extinction: events & processes, age & timescale, causative mechanism(s) & recovery. *Journal of Asian Earth Sciences* **36** (6), 407–540.

Metcalfe, I., and Isozaki, Y., 2009b, Current perspectives on the Permian–Triassic boundary and end-Permian mass extinction: preface. In: Metcalfe, I., Isozaki, Y. (eds), End-Permian mass extinction: events & processes, age & timescale, causative mechanism(s) & recovery, *Journal of Asian Earth Sciences*, **36**(6): 407–412.

Metcalfe, I., Nicoll, R.S., Black, L.P., Mundil, R., Renne, P., Jagodzinski, E.A., et al., 1999, Isotope geochronology of the Permian–Triassic boundary and mass extinction in South China. *In* Yin, H.F., and Tong, J.N. (eds), *Pangea and the Paleozoic-Mesozoic Transition*. Wuhan: China University of Geosciences Press, 134–137.

Metcalfe, I., Foster, C.B., Afonin, S.A., Nicoll, R.S., Wang X., and Lucas, S.G., 2009, Stratigraphy, biostratigraphy and C-isotopes of the Permian–Triassic non-marine sequence at Dalongkou and Lucaogou, Xinjiang Province, China. In: Metcalfe, I., Isozaki, Y. (eds), End-Permian mass extinction: events & processes, age & timescale, causative mechanism(s) & recovery, *Journal of Asian Earth Sciences*, **36**(6): 407–412.

Meyers, S.R., 2008, Resolving Milankovitchian controversies: the Triassic Latemar Limestone and the Eocene Green River Formation. *Geology*, **36**: 319–322.

Mietto, P., and Manfrin, S., 1995, A high resolution Middle Triassic ammonoid standard scale in the Tethys Realm: a preliminary report. *Bulletin de la Société Géologique de France*, **166** (5), 539–563.

Mietto, P., and Manfrin, S., 1999, A debate on the Ladinian-Carnian boundary. *Albertiana*, **22**: 23–27.

Mietto, P., Andreetta, R., Broglio Loriga, C., Buratti, N., Cirilli, S., De Zanche, V., et al., 2007, A candidate of the Global Boundary Stratotype Section and Point for the base of the Carnian Stage (Upper Triassic): GSSP at the base of the *canadensis* Subzone (FAD of *Daxatina*) in the Prati di Stuores/Stuores Wiesen section (Southern Alps, NE Italy). *Albertiana*, **36**: 78–97.

Mietto, P., Manfrin, S., Preto, N., Rigo, M., Roghi, G., Furin, S., et al., 2012, A candidate of the Global Boundary Stratotype Section and Point for the base of the Carnian Stage (Upper Triassic): GSSP at the base of the *canadensis* Subzone (FAD of *Daxatina*) in the Prati di Stuores/Stuores Wiesen section (Southern Alps, NE Italy). *Episodes*, **35**: 414–430.

Moix, P., Kozur, H.W., Stampfli, G.M., and Mostler, H., 2007, New paleontological, biostratigraphic and paleogeographic results from the Triassic of the Mersin Mélange, SE Turkey. In: Lucas, S.G., Spielmann, J.A., (eds) The Global Triassic, *New Mexico Museum of Natural History and Sciences Bulletin*, **41**: 282–311.

Mojsisovics, E.V., 1869, Über die Gliederung der oberen Triasbildungen der östlichen Alpen. *Jahrbuch Geologischen Reichsanstalt*, **19**: 91–150.

Mojsisovics, E.V., 1893, Faunistische Ergebnisse aus der Untersuchung der Ammoneen-faunen der Mediterranen Trias. *Abhandlungen der Geologischen Bundesanstalt*, **6**: 810.

Mojsisovics, E., von, Waagen, W., and Diener, C., 1895, Entwurf einer Gliederung der pelagischen Sedimente des Trias-Systems. *Sitzungberichte der Akademie der Wissenschaften in Wien*, **104**: 1271–1302.

Mørk, A., Embry, A.F., and Weitschat, W., 1989, Triassic transgressive-regressive cycles in the Sverdrup Basin, Svalbard and the Barents Shelf. *In* Collinson, J.D. (ed), *Correlation in Hydrocarbon Exploration*. London: Graham and Trotman, 113–130.

Mortensen, J.K., and Hulbert, L.J., 1992, A U-Pb zircon age for a Maple Creek gabbro sill, Tatamagouche Creek area, southwest Yukon Territory. In *Radiogenic Age and Isotopic Studies, Report 5: Geological Survey of Canada, Paper, 91-2* (pp. 175–179).

Moslow, T.F., Haverslew, B., and Henderson, C.M., 2018, Sedimentary facies, petrology, reservoir characteristics, conodont biostratigraphy and sequence stratigraphic framework of a continuous (395 m) full diameter core of the Lower Triassic Montney Formation, northeastern British Columbia. In: Euzen, T., Moslow, T.F., Caplan, M. (eds), The Montney Play: Deposition to Development, *Bulletin of Canadian Petroleum Geology*, Special Volume, **66**: 259–287.

Motani, R., 2010, Warm blooded sea dragons? *Science*, **328**: 1361–1362.

Mundil, R., and Irmis, R., 2008, New U-Pb age constraints for terrestrial sediments in the Late Triassic: implications for faunal evolution and correlations with marine environments. *33rd International Geological Congress, Oslo 2008, Abstract*. Online at: <http://www.cprm.gov.br/33IGC/1342538.html>

Mundil, R., Brack, P., Meier, M., Rieber, H., and Oberli, F., 1996, High resolution U–Pb dating of Middle Triassic volcaniclastics: time-scale calibration and verification of tuning parameters for carbonate sediments. *Earth and Planetary Science Letters*, **141**: 137–151.

Mundil, R., Metcalfe, I., Ludwig, K.R., Renne, P.R., Oberli, F., and Nicoll, R.S., 2001, Timing of the Permian–Triassic biotic crisis: implications from new zircon U/Pb age data (and their limitations). *Earth and Planetary Science Letters*, **187**: 131–145.

Mundil, R., Ludwig, K.R., Metcalfe, I., and Renne, P.R., 2004, Age and timing of the Permian mass extinctions: U/Pb dating of closed-system zircons. *Science*, **305**: 1760–1763.

Mundil, R., Pálfy, J., Renne, P.R., and Brack, P., 2010, The Triassic timescale: new constraints and a review of geochronological data. In: Lucas, S.G. (ed), The Triassic Timescale, *The Geological Society of London Special Publications*, **334**: 41–60.

Muttoni, G., Kent, D.V., Nicora, A., Rieber, H., and Brack, P., 1996a, Magneto-biostratigraphy of the 'Buchenstein Beds' at Frötschbach (western Dolomites, Italy). *Albertiana*, **17**: 51–56.

Muttoni, G., Kent, D.V., Meço, S., Nicora, A., Gaetani, M., Balini, M., et al., 1996b, Magnetobiostratigraphy of the Spathian to Anisian

(Lower to Middle Triassic) Kçira section, Albania. *Geophysical Journal International*, **127**: 503–514 <https://doi.org/10.1111/j.1365-246x.1996.tb04736.x>.

Muttoni, G., Kent, D.V., Meço, S., Balini, M., Nicora, A., Rettori, R., et al., 1998, Towards a better definition of the Middle Triassic magnetostratigraphy and biostratigraphy in the Tethyan realm. *Earth and Planetary Science Letters*, **164**: 285–302.

Muttoni, G., Kent, D.V., DiStefano, P., Gullo, M., Nicora, A., Tait, J., et al., 2001a, Magnetostratigraphy and biostratigraphy of the Carnian/Norian boundary interval from the Pizzo Mondello section (Sicani Mountains, Sicily). *Palaeogeography, Palaeoclimatology, Palaeoecology*, **166**: 383–399.

Muttoni, G., Kent, D.V., and Orchard, M.J., 2001b, Paleomagnetic reconnaissance of early Mesozoic carbonates from Williston Lake, northeastern British Columbia, Canada: evidence for late Mesozoic remagnetization. *Canadian Journal of Earth Sciences*, **38**: 1157–1168.

Muttoni, G., Nicora, A., Brack, P., and Kent, D.V., 2004a, Integrated Anisian–Ladinian boundary chronology. *Palaeogeography, Palaeoclimatology, Palaeoecology*, **208**: 85–102.

Muttoni, G., Kent, D.V., Olsen, P.E., DiStefano, P., Lowrie, W., Bernasconi, S.M., et al., 2004b, Tethyan magnetostratigraphy from Pizzo Mondello (Sicily) and correlation to the Late Triassic Newark astrochronological polarity time scale. *Geological Society of America Bulletin*, **116**: 1043–1058.

Muttoni, G., Kent, D.V., Flavio, J., Olsen, P., Rigo, M., Galli, M.T., et al., 2010, Rhaetian magnetostratigraphy from the Southern Alps (Italy): constraints on Triassic chronology. *Palaeogeography, Palaeoclimatology, Palaeoecology*, **285**: 1–16.

Muttoni, G., Mazza, M., Mosher, D., Katz, M.E., Kent, D.V., and Balini, M., 2014, A Middle-Late Triassic (Ladinian-Rhaetian) carbon and oxygen isotope record from the Tethyan Ocean. *Palaeogeography, Palaeoclimatology, Palaeoecology*, **399**: 246–259 (and on-line data repository item 2015069).

Muttoni, G., Nicora, A., Balini, M., Katz, M., Schaller, M., Kent, D., et al., 2019, A candidate GSSP for the base of the Anisian from Kçira, Albania. *Albertiana*, **45**: 39–49.

Nawrocki, J., 1997, Permian to Early Triassic magnetostratigraphy from the Central European Basin in Poland: implications on regional and worldwide correlations. *Earth and Planetary Science Letters*, **152**: 37–58.

Nawrocki, J., and Szulc, J., 2000, The Middle Triassic magnetostratigraphy from the Peri-Tethys basin in Poland. *Earth and Planetary Science Letters*, **182**: 77–92.

Nesbitt, S.J., Smith, N.D., Irmis, R.B., Turner, A.H., Downs, A., and Norell, M.A., 2009, A complete skeleton of a Late Triassic Saurischian and the early evolution of dinosaurs. *Science*, **326**: 1530–1533.

Newell, N.D., 1994, Is there a precise Permian-Triassic boundary? *Permophiles*, **24**: 46–48.

Newton, R.J., Pevitt, E.L., Wignall, P.B., and Bottrell, S.H., 2004, Large shifts in the isotopic composition of seawater sulphate across the Permo-Triassic boundary in northern Italy. *Earth and Planetary Science Letters*, **218**: 331–345.

Nicora, A., Balini, M., Bellanea, A., Bowring, S.A., Di Stefano, P., Dumitrica, P., et al., 2007, The Carnian/Norian boundary interval at Pizzo Mondello (Sicani Mountains, Sicily) and its bearing for the definition of the GSSP of the Norian Stage. *Albertiana*, **36**: 102–129.

Nowak, H., Schneebeli-Hermann, E., and Kustatscher, E., 2018, Correlations of Lopingian to Middle Triassic palynozones. *Journal of Earth Sciences*, **29**: 755–777. https://doi.org/10.1007/s12583-018-0790-8.

O'Dogherty, L., Carter, E.S., Gorican, S., and Dumitrica, P., 2010, Triassic radiolarian biostratigraphy. In: Lucas, S.G. (ed), The Triassic Timescale, *The Geological Society of London Special Publications*, **334**: 163–200.

Ogg, J.G., 2004, The Triassic Period. *In* Gradstein, F.M., Ogg, J.G., and Smith, A.L. (eds), *A Geologic Time Scale 2004*. Cambridge: Cambridge University Press, 271–306.

Ogg, J.G., 2012, Triassic. *In* Gradstein, F.M., Ogg, J.G., Schmitz, M., and Ogg, G. (eds), *The Geologic Time Scale 2012*. Elsevier Publ., 681–730.

Ogg, J.G., 2015, The mysterious Mid-Carnian "Wet Intermezzo" global event. *Journal of Earth Science*, **26** (2), 181–191.

Ogg, J.G., and Steiner, M.B., 1991, Early Triassic magnetic polarity time scale—integration of magnetostratigraphy, ammonite zonation and sequence stratigraphy from stratotype sections Canadian Arctic Archipelago). *Earth and Planetary Science Letters*, **107**: 69–89.

Ogg, J.G., Ogg, G.M., and Gradstein, F.M., 2008, Triassic Period. *In* Ogg, J.G., Ogg, G.M., and Gradstein, F.M. (eds), *Concise Geologic Time Scale*. Cambridge: Cambridge University Press, 95–106.

Ogg, J.G., Huang, C., and Hinnov, L., 2014, Triassic timescale status: a brief overview. *Albertiana*, **41**: 3–30.

Ogg, J.G., Ogg, G.M., and Gradstein, F.M., 2016, *A Concise Geologic Time Scale 2016*. Elsevier Publ. 234 pp.

Ogg, J.G., Gradinaru, E., Chen, Y., Bucher, F.R., Hounslow, M.W., 2020, Comments on defining the base of Anisian Stage. *ResearchGate*: https://www.researchgate.net/publication/336767153_Early-Middle_Triassic_boundary_interval_Integrated_chemo-bio-magneto-stratigraphy_of_potential_GSSPs_for_the_base_of_the_Anisian_Stage_in_South_China/comments.

Olesen, J., 2009, Phylogeny of Branchiopoda (Crustacea)—character evolution and contribution of uniquely preserved fossils. *Arthropod Systematics & Phylogeny*, **67** (1), 3–39.

Olsen, P.E., and Kent, D.V., 1999, Long-period Milankovitch cycles from the Late Triassic and Early Jurassic of eastern North America and their implications for the calibration of the Early Mesozoic time-scale and the long-term behaviour of the planets. *Philosophical Transactions of the Royal Society of London, Series A: Mathematical, Physical and Engineering Science*, **357**: 1761–1786 <https://doi.org/10.1098/rsta.1999.0400>.

Olsen, P.E., Kent, D.V., Cornet, B., Witte, W.K., and Schlische, R.W., 1996, High-resolution stratigraphy of the Newark rift basin (early Mesozoic, eastern North America). *Geological Society of America Bulletin*, **108**: 40–77.

Orbell, G., 1983, Palynology of the British Rhaetian. *Bulletin of the Geological Survey of Great Britain*, **44**: 1–44.

Orchard, M.J., 2007a, Conodont diversity and evolution through the latest Permian and Early Triassic upheavals. *Palaeogeography, Palaeoclimatology, Palaeoecology*, **252**: 93–117.

Orchard, M.J., 2007b, A proposed Carnian-Norian Boundary GSSP at Black Bear Ridge, northeast British Columbia, an a new conodont framework for the boundary interval. *Albertiana*, **36**: 130–141.

Orchard, M.J., 2010, Triassic conodonts and their role in stage boundary definitions. In: Lucas, S.G. (ed), The Triassic Timescale, *The Geological Society of London Special Publications*, **334**: 139–161.

Orchard, M.J., 2014, Conodonts from the Carnian-Norian boundary (Upper Triassic) of Black Bear Ridge, northeastern British Columbia, Canada. *New Mexico Museum of Natural History and Science Bulletin*, **64**: 139 pp.

Orchard, M.J., 2016, Base of the Rhaetian and a critique of Triassic conodont-based biostratigraphy: comment. *Albertiana*, **43**: 28–32.

Orchard, M.J., 2018, The lower-middle Norian (Upper Triassic) boundary: new conodont taxa and a refined biozonation. *Bulletins of American Paleontology*, **395-396**: 165–193.

Orchard, M.J., 2019, The Carnian-Norian GSSP candidate at Black Bear Ridge, British Columbia, Canada: update, correlation and conodont taxonomy. *Albertiana*, **45**: 50–68.

Orchard, M.J., and Tozer, E.T., 1997, Triassic conodont biochronology, its intercalibration with the ammonoid standard, and a biostratigraphic summary for the Western Canada Sedimentary Basin. *Bulletin of Canadian Petroleum Geology*, **45**: 675–692.

Orchard, M.J., Carter, E.S., and Tozer, E.T., 2000, Fossil data and their bearing on defining a Carnian-Norian (upper Triassic) boundary in western Canada. *Albertiana*, **24**: 43–50.

Orchard, M.J., Zonneveld, J.P., Johns, M.J., McRoberts, C.A., Sandy, M.R., Tozer, E.T., et al., 2001, Fossil succession and sequence stratigraphy of the Upper Triassic of Black Bear Ridge, northeast British Columbia, a GSSP prospect for the Carnian-Norian boundary. *Albertiana*, **25**: 10–22.

Ovtcharova, M., Bucher, H., Schaltegger, U., Galfetti, T., Brayard, A., and Guex, J., 2006, New Early to Middle Triassic U-Pb ages from South China: calibration with ammonoid biochronozones and implications for the timing of the Triassic biotic recovery. *Earth and Planetary Science Letters*, **243**: 463–475.

Ovtcharova, M., Bucher, H., Goudemand, N., Schaltegger, U., Brayard, A., and Galfetti, T., 2010, New U/Pb ages from Nanpanjiang Basin (South China): implications for the age and definition of the Early-Middle Triassic boundary. *Geophysical Research Abstracts*, **12: EGU2010-12505-3**.

Ovtcharova, M., Goudemand, N., Hammer, Ø., Guodun, K., Cordey, F., Galfetti, T., et al., 2015, Developing a strategy for accurate definition of a geological boundary through radio-isotopic and biochronological dating: the Early-Middle Triassic boundary (South China). *Earth-Science Reviews*, **146**: 65–76 <https://doi.org/10.1016/j.earscirev.2015.03.006>.

Pálfy, J., and Vörös, A., 1998, Quantitative ammonoid biochronological assessment of the Anisian–Ladinian (Middle Triassic) stage boundary proposals. *Albertiana*, **21**: 19–26.

Pálfy, J., Smith, P.L., and Mortensen, J.K., 2000a, A U–Pb and $^{40}Ar/^{39}Ar$ time scale for the Jurassic. *Canadian Journal of Earth Sciences*, **37**: 923–944.

Pálfy, J., Mortensen, J.K., Carter, E.S., Smith, P.L., Friedman, R.M., and Tipper, H.W., 2000b, Timing the end-Triassic mass extinction: first on land, then in the sea? *Geology*, **28**: 39–42.

Pálfy, J., Demeny, A., Haas, J., Hetenyi, M., Orchard, M.J., and Veto, I., 2001, Carbon isotope anomaly and other geochemical changes at the Triassic-Jurassic boundary from a marine section in Hungary. *Geology*, **29**: 1047–1050.

Pálfy, J., Parrish, R.R., David, K., and Voros, A., 2003, Mid-Triassic integrated U/Pb geochronology and ammonoid biochronology from the Balaton Highland (Hungary). *Journal of the Geological Society*, **160**: 271–284.

Palmer, A.R., 1983, *Geologic time scale, Decade of North American Geology (DNAG)*. Boulder, NV: Geological Society of America.

Parrish, R.R., and McNicoll, V.J., 1992. U/Pb age determinations from the southern Vancouver Island area, British Columbia. In *Radiogenic Age and Isotopic Studies: Geological Survey of Canada, Paper, 91-2* (pp. 79–86).

Paull, R.K., 1997, Observations on the Induan-Olenekian boundary based on conodont biostratigraphic studies in the Cordillera of the western United States. *Albertiana*, **20**: 31–32.

Payne, J.L., and Kump, L.R., 2007, Evidence for recurrent Early Triassic massive volcanism from quantitative interpretation of carbon isotope fluctuations. *Earth and Planetary Science Letters*, **256**: 264–277.

Payne, J.L., Lehrmann, D.J., Wei, J., Orchard, M.J., Schrag, D.P., and Knoll, A.H., 2004, Large perturbations of the carbon cycle during recovery from the end-Permian extinction. *Science*, **305**: 506–509.

Payne, J.L., Lehrmann, D.J., Follet, D., Seibel, M., Kump, L.R., Riccardi, A., et al., 2009, Erosional truncation of uppermost Permian shallow-marine carbonates and implications for Permian-Triassic boundary events: reply. *Geological Society of America Bulletin*, **121**: 957–959.

Paytan, A., Yao, W.Q., Faul, K., and Gray, E.T., 2020, Chapter 9 - Sulfur isotope stratigraphy. *In* Gradstein, F.M., Ogg, J.G., Schmitz, M.D., and Ogg, G.M. (eds), *The Geologic Time Scale 2020*. **Vol. 1** (this book). Elsevier, Boston, MA.

Peucker-Ehrenbrink, B., and Ravizza, G.E., 2020, Chapter 8 - Osmium isotope stratigraphy. *In* Gradstein, F.M., Ogg, J.G., Schmitz, M.D., and Ogg, G.M. (eds), *The Geologic Time Scale 2020*. **Vol. 1** (this book). Elsevier, Boston, MA.

Peybernes, B., 1998, Larger benthic foraminifer. Column for Triassic chart of Mesozoic and Cenozoic sequence chronostratigraphic framework of European basins, by Hardenbol, J., Thierry, J., Farley, M.B., Jacquin, T., de Graciansky, P.-C., and Vail, P.R. (coordinators). In: de Graciansky, P.-C., Hardenbol, J., Jacquin, T., Vail, P.R. (eds.), Mesozoic-Cenozoic Sequence Stratigraphy of European Basins, *SEPM Special Publication*, **60**: Chart 8.

Phillips, J., 1840, Palaeozoic Series. *In* Long, G. (ed), The Penny Cyclopaedia of the Society for the Diffusion of Useful Knowledge. *London: Charles Knight,* **Vol. 17**: 153–154.

Phillips, J., 1841, *Figures and Descriptions of the Palaeozoic Fossils of Cornwall, Devon and east Somerset*. London: Longman, Brown, Green and Longmans.

Pia, J., 1930, *Grundbegriffe der Stratigraphie mit ausführlicher anwendung auf die Europäische Mitteltrias*. Leipzig and Wien: Deuticke.

Preto, N., Kustatscher, E., and Wignall, P.B., 2010, Triassic climates – state of the art and perspectives. In: Kustatscher, E., Preto, N., Wignall, P. (eds), Triassic climates, *Palaeogeography, Palaeoclimatology, Palaeoecology*, **290**: 1–10.

Ramezani, J., Bowring, S.A., Pringle, M.S., Winslow III, F.D., and Rasbury, E.T. 2005. The Manicouagan impact melt rock: a proposed standard for the intercalibration of U–Pb and 40Ar/39Ar isotopic systems. *15th V.M. Goldsmidt Conference Abstract Volume, Moscow, ID*. Available online at: <http://goldschmidt.info/2005_cd/Abstract%20Volume/abs_vol.pdf>

Ramezani, J., Bowring, S.A., Martin, M.W., Lehrmann, D.J., Montgomery, P., Enos, P., et al., 2007, Timing of recovery from the end-Permian extinction: geochronologic and biostratigraphic constraints from south China: comment and reply: reply. *Geology*, **35**: e137 Online Forum.

Ramezani, J., Bowring, S.A., Fastovsky, D.E., and Hoke, G.D., 2009, U-Pb-ID-TIMS geochronology of the Late Triassic Chinle Formation, Petrified Forest National Park, Arizona. *Geological Society of America Abstracts With Programs*, **41** (7), 421 [plus copy of summary slide sent to H. Kozur].

Ramezani, J., Bowring, S.A., Fastovsky, D.E., and Hoke, G.D., 2010, Depositional history of the Late Triassic Chinle fluvial system at the Petrified Forest National Park: U-Pb geochronology, regional correlation and insights into early dinosaur evolution. *American Geophysical Union Fall meeting 2010, Abstract #V31A-2313*.

Rampino, M.,R., Prokoph, A., and Adler, A.C., 2000, Tempo of the end-Permian event: high-resolution cyclostratigraphy at the Permian-Triassic Boundary. *Geology*, **28**: 643–646.

Rampino, M.,R., Prokoph, A., Adler, A.C., and Schwindt, D.M., 2002, Abruptness of the end-Permian mass extinction as determined from biostratigraphic and cyclostratigraphic analysis of European western Tethyan sections. In: Koeberl, C., MacLeod, K.G. (eds), Catastrophic Events and mass extinctions: Impacts and Beyond, *Geological Society of America Special Paper*, **356**: 415–427.

Reichow, M.K., Saunders, A.D., Ivanov, A.V., and Puchkov, V.N., 2004, The Siberian large igneous province. *Internet Article From Large Igneous Provinces Commission, Large Igneous Province of the Month: March 2004*. Available at < www.largeigneousprovinces.org/ >

Reichow, M.K., Pringle, M.S., Al'Mukhamedov, A.I., Allen, M.B., Andreichev, V.L., Buslov, M.M., et al., 2009, The timing and extent of the eruption of the Siberian Traps large igneous province: implications for the end-Permian environmental crisis. *Earth and Planetary Science Letters*, **27**: 9–20.

Renesto, S., and Dalla Vecchio, F.M., 2018, Late Triassic marine reptiles. In: Tanner, L.H. (ed), *The Late Triassic World: Earth in a Time of Transition*, Topics in Geobiology. Springer Publication, pp. 263–313. https://doi.org/10.1007/978-3-319-68009-5_8

Renne, P.R., and Basu, A.R., 1991, Rapid eruption of the Siberian traps flood basalts at the Permo-Triassic boundary. *Science*, **253**: 176–179.

Renne, P.R., Zhang, Z., Richards, M.A., Black, M.T., and Basu, A.R., 1995, Synchrony and causal relations between Permian-Triassic boundary crisis and Siberian flood volcanism. *Science*, **269**: 1413–1416.

Renne, P.R., Mundil, M., Balco, G., Min, K., and Ludwig, K.R., 2010, Joint determination of $^{40}K$ decay constants and $^{40}Ar^*/^{40}K$ for the Fish Canyon sanidine standard, and improved accuracy for $^{40}Ar/^{39}Ar$ geochronology. *Geochimica et Cosmochimica Acta*, **74**: 5349–5367.

Rigo, M., Preto, N., Roghi, G., Tateo, F., and Mietto, P., 2007, A rise in the carbonate compensation depth of western Tethys in the Carnian (Late Triassic): deep-water evidence for the Carnian pluvial event. *Palaeogeography, Palaeoclimatology, Palaeoecology*, **246**: 188–205.

Rigo, M., Bertinelli, A., Concheri, G., Gattolin, G., Godfrey, L., Katz, M.E., et al., 2016, The Pignola-Abriola section (southern Apennines, Italy): a new GSSP candidate for the base of the Rhaetian Stage. *Lethaia*, **49** (3), 287–306. https://doi.org/10.1111/let.12145.

Rigo, M., Mazza, M., Karádi, V., and Nicora, A., 2018, New Upper Triassic conodont biozonation of the Tethyan Realm. In: Tanner, L.H. (ed), *The Late Triassic World: Earth in a Time of Transition*, Topics in Geobiology. Springer Publication, **Vol. 46**: 189–235. https://doi.org/10.1007/978-3-319-68009-5_6.

Rogers, R.R., Swisher III, C.C., Sereno, P.C., Monetta, A.M., Forster, C.A., and Martinez, R.N., 1993, The Ischigualasto tetrapod assemblage (Late Triassic, Argentina) and $^{40}Ar/^{39}Ar$ dating of dinosaur origins. *Science*, **260**: 794–797.

Roghi, G., Gianolla, P., Minarelli, L., Pilati, C., and Preto, N., 2010, Palynological correlation of Carnian humid pulses throughout western Tethys. In: Kustatscher, E., Preto, N., Wignall, P. (eds), Triassic climates, *Palaeogeography, Palaeoclimatology, Palaeoecology*, **290**: 89–106.

Röhling, H.-G., 1991, A lithostratigraphic subdivision of the Lower Triassic in the northwest German Lowlands and the German Sector of the North Sea, based on Gamma-Ray and Sonic Logs. *Geologisches Jahrbuch Reihe A*, **119**: 3–24.

Ruffell, A., Simms, M.J., and Wignall, P.B., 2016, The Carnian Humid Episode of the late Triassic: a review. *Geological Magazine*, **153** (Special Issue 2 (mass extinctions)), 271–284. https://doi.org/10.1017/S0016756815000424.

Ruhl, M., Kuerschner, W.M., and Krystyn, L., 2009, Triassic–Jurassic organic carbon isotope stratigraphy of key sections in the western Tethys realm (Austria). *Earth and Planetary Science Letters*, **281**: 169–187.

Satterley, A.K., 1996, The interpretation of cyclic successions of the Middle and Upper Triassic of the Northern and Southern Alps. *Earth-Science Reviews*, **40**: 181–207.

Schlager, W., and Schöllnberger, W., 1974, Das Prinzip stratigraphischer Wenden in der Schichtenfolge der Nördlichen Kalkalpen. *Mitteilungen der Österreichischen Geologischen Gesellschaft, Wien*, **66/67**: 165–193.

Schaltegger, U., Guex, J., Bartolini, A., Schoene, B., and Ovtcharova, M., 2008, Precise U-Pb age constraints for end-Triassic mass extinction, its correlation to volcanism and Hettangian post-extinction recovery. *Earth and Planetary Science Letters*, **267**: 266–275.

Schneider, J.W., and Scholze, F., 2018, Late Pennsylvanian–Early Triassic conchostracan biostratigraphy: a preliminary approach. *In* Lucas, S.G., and Shen, S.Z. (eds), *The Permian Timescale*. The Geological Society of London Special Publications, **450**: 365–386.

Schoene, B., Guex, J., Bartolini, A., Schaltegger, U., and Blackburn, T.J., 2010, Correlating the end-Triassic mass extinction and flood basalt volcanism at the 100 ka level. *Geology*, **38**: 387–390 and 13-page supplement.

Scholze, F., Schneider, J.W., and Werneburg, R., 2016, Conchostracans in continental deposits of the Zechstein-Buntsandstein transition in central Germany: taxonomy and biostratigraphic implications for the position of the Permian–Triassic boundary within the Zechstein Group. *Palaeogeography, Palaeoclimatology, Palaeoecology*, **449**: 174–193.

Scholze, F., Shen, S.Z., Backer, M., Wei, H.B., Hübner, M., Cui, Y.Y., et al., 2019, Reinvestigation of conchostracans (Crustacea: Branchiopoda) from the Permian–Triassic transition in Southwest China. *Palaeoworld*. https://doi.org/10.1016/j.palwor.2019.04.007.

Schuurman, W.M.N., 1979, Aspects of Late Triassic palynology. 3. Palynology of the latest Triassic and earliest Jurassic deposits of the Northern Limestone Alps in Austria and southern Germany, with special reference to a palynological characterization of the Rhaetian stage in Europe. *Review of Palaeobotany and Palynology*, **27**: 53–75.

Schwarzacher, W., 2005, The stratification and cyclicity of the Dachstein Limestone in Lofer, Leogang and Steinernes Meer (Northern Calcareous Alps, Austria). *Sedimentary Geology*, **181**: 93–106.

Scotese, C.R., 2014, *Atlas of Middle & Late Permian and Triassic Paleogeographic Maps, Maps 43–52, Volumes 3 & 4, PALEOMAP PaleoAtlas for ArcGIS, PALEOMAP Project, Evanston, IL, 2014*.

Sedlacek, A.R., Saltzman, M.R., Algeo, T.J., Horacek, M., Brandner, R., Foland, K., et al., 2014, $^{87}Sr/^{86}Sr$ stratigraphy from the Early Triassic of Zal, Iran: linking temperature to weathering rates and the tempo of ecosystem recovery. *Geology*, **42**: 779–782.

Sephton, M.A., Looy, C.V., Veefkind, R.J., Brinkhuis, H., De Leeuw, J. W., and Visscher, H., 2002a, Synchronous record of $\partial^{13}C$ shifts in the oceans and atmosphere at the end of the Permian. In: Koeberl, C., MacLeod, K.G. (eds), Catastrophic Events and mass extinctions: Impacts and Beyond, *Geological Society of America Special Paper*, **356**: 455–462.

Sephton, M.A., Amor, K., Franchi, I.A., Wignall, P.B., Newton, R., and Zonneveld, J.-P., 2002b, Carbon and nitrogen isotope disturbances and an end-Norian (Late Triassic) extinction event. *Geology*, **30**: 1119–1122.

Shen, C., 2018, Astronomical tuning, astronomical forcing and environmental conditions of the Lower Triassic Montney Formation, northeastern British Columbia, Canada. *Thesis*. University of Calgary, Graduate Program in Geology and Geophysics, 106 pp.

Shen, C., Shoepfer, S.D., and Henderson, C.M., 2017, Astronomical tuning of the Early Triassic Induan Stage in the distal Montney Formation, NE British Columbia, Canada. *Geological Society of America Abstracts With Programs*, **(6)**: 49. https://doi.org/10.1130/abs/2017AM-300972.

Shen, S.Z., Henderson, C.M., Bowring, S.A., Cau, C.Q., Wang, Y., Wang, W., et al., 2010, High-resolution Lopingian (Late Permian) timescale of South China. *Geological Journal*, **45**: 122–134.

Shen, S.Z., Ramezani, J., Chen, J., Cao, C.Q., Erwin, D.H., Zhang, H., et al., 2019, A sudden end-Permian mass extinction in South China. *Geological Society of America Bulletin*, **131**: 205–223. https://doi.org/10.1130/B31909.1.

Silberling, N.J., and Tozer, E.T., 1968, Biostratigraphic classification of the marine Triassic in North America. *Geological Society of America Special Papers*, **10**: 1–63.

Simms, M.J., and Ruffel, A.H., 1989, Synchroneity of climate change and extinctions in the Late Triassic. *Geology*, **17**: 265–268.

Simmons, M.D., Sharland, P.R., Casey, D.M., Davies, R.B., and Sutcliffe, O.E., 2007, Arabian Plate sequence stratigraphy: potential implications for global chronostratigraphy. *GeoArabia*, **12** (4), 101–130.

Simmons, M.S., Miller, K.G., Ray, D.C., Davies, A., van Buchem, F.S.P., and Gréselle, B., 2020, Chapter 13 - Phanerozoic eustasy. *In* Gradstein, F.M., Ogg, J.G., Schmitz, M.D., and Ogg, G.M. (eds), *The Geologic Time Scale 2020*. **Vol. 1** (this book). Elsevier, Boston, MA.

Skjold, L.J., Van Veen, P.M., Kristensen, S.-E., and Rasmussen, A.R., 1998, Triassic sequence stratigraphy of the southwestern Barents Sea. In: de Graciansky, P.-C., Hardenbol, J., Jacquin, T., Vail, P.R. (eds), Mesozoic-Cenozoic Sequence Stratigraphy of European Basins, *SEPM Special Publication*, **60**: 651–666.

Song, H.Y., Tong, J.N., Algeo, T.J., Horacek, M., Qiu, H.O., Song, H.J., et al., 2013, Large vertical delta C-13(DIC) gradients in Early Triassic seas of the South China craton: Implications for oceanographic changes related to Siberian Traps volcanism. *Global and Planetary Change*, **105**: 7–20. https://doi.org/10.1016/j.gloplacha.2012.10.023.

Stefani, M., Furin, S., and Gianolla, P., 2010, The changing climate framework and depositional dynamics of Triassic carbonate platforms from the Dolomites. In: Kustatscher, E., Preto, N., Wignall, P. (eds.), Triassic climates, *Palaeogeography, Palaeoclimatology, Palaeoecology*, **290**: 43–57.

Steiner, M.B., 2006, The magnetic polarity time scale across the Permian–Triassic boundary. In: Lucas, S.G., Cassinis, G., and Schneider, J.W. (eds), Non-Marine Permian Biostratigraphy and Biochronology, *The Geological Society of London Special Publications*, **265**: 15–38.

Steiner, M.B., Ogg, J.G., Zhang, Z., and Sun, S., 1989, The Late Permian/Early Triassic magnetic polarity time scale and plate motions of south China. *Journal of Geophysical Research*, **94**: 7343–7363.

Sugiyama, K., 1997, Triassic and Lower Jurassic radiolarian biostratigraphy in the siliceous claystone and bedded chert units of the southeastern Mino Terrane, Central Japan. *Bulletin of the Mizunami Fossil Museum*, **24**: 79–193.

Sun, Y.D., Joachimski, M.M., Wignall, P.B., Yan, C., Chen, Y., Jiang, H., et al., 2012, Lethally hot temperatures during the Early Triassic Greenhouse. *Science*, **338**: 366–370.

Sun, Z.M., Hounslow, M.W., Pei, J., Zhao, L., Tong, J.N., and Ogg, J.G., 2007, Magnetostratigraphy of the West Pingdingshan section, Chaohu, Anhui Province: relevance for base Olenekian GSSP selection. *Albertiana*, **36**: 22–32.

Szurlies, M., 2004, Magnetostratigraphy: the key to global correlation of the classic Germanic Trias – case study Volpriehausen Formation (Middle Buntsandstein), Central Germany. *Earth and Planetary Science Letters*, **227**: 395–410.

Szurlies, M., 2007, Latest Permian to Middle Triassic cyclo-magnetostratigraphy from the Central European Basin, Germany: implications for the geomagnetic polarity timescale. *Earth and Planetary Science Letters*, **261**: 602–619.

Tanner, L.H., 2010a, The Triassic isotope record. In: Lucas, S.G. (ed), The Triassic Timescale, *The Geological Society of London Special Publications*, **334**: 103–118.

Tanner, L.H., 2010b, Cyclostratigraphy record of the Triassic: a critical examination. In: Lucas, S.G. (ed), The Triassic Timescale, *The Geological Society of London Special Publications*, **334**: 119–137.

Tanner, L.H., 2018, *The Late Triassic World: Earth in a Time of Transition*. Topics in Geobiology, Springer Publications, Vol. 46: 805 pp. https://doi.org/10.1007/978-3-319-68009-5

Tong, J.N., Zakharov, Y.D., Orchard, M.J., Yin, H.F., and Hansen, H.J., 2004, Proposal of the Chaohu section as the GSSP candidate of the I/O boundary. *Albertiana*, **29**: 13–28.

Tong, J.N., Chu, D.L., Liang, L., Shu, W.C., Song, H.J., Song, T., et al., 2019, Triassic integrative stratigraphy and timescale of China. *Science China Earth Sciences*, **62**: 189–222. https://doi.org/10.1007/s11430-018-9278-0.

Tozer, E.T., 1965, *Lower Triassic stages and ammonoid zones of Arctic Canada*, Geological Survey of Canada Paper, 65-12. pp. 1–14.

Tozer, E.T., 1967, *A standard for Triassic Time*. *Geological Survey of Canada Bulletin*, **156**: 104 pp.

Tozer, E.T., 1984, The Trias and its Ammonites: the evolution of a time scale. *Geological Survey of Canada Miscellaneous Report*, **35**: 171 pp.

Tozer, E.T., 1986, Definition of the Permian–Triassic (P–T) boundary: the question of the age of the *Otoceras* beds. *Memorie della Società Geologica Italiana*, **34**: 291–301.

Tozer, E.T., 1990, How many Rhaetians? *Albertiana*, **8**: 10–13.

Tozer, E.T., 1994, Age and correlation of the *Otoceras* beds at the Permian–Triassic Boundary. *Albertiana*, **14**: 31–37.

Traverse, A., 2007, *Paleopalynology*, second ed. Dordrecht: Springer, 813 pp.

Trotter, J.A., Williams, I.S., Nicora, A., Mazza, M., and Rigo, M., 2015, Long-term cycles of Triassic climate change: a new $\delta^{18}O$ record

from conodont apatite. *Earth and Planetary Science Letters*, **415**: 165–174.

Van Veen, P.M., 1995, Time calibration of Triassic/Jurassic microfloral turnover, eastern North America—Comment. *Tectonophysics*, **245**: 93–95.

Van Veen, P., Hochuli, P.A., and Vigran, J.O., 1998, Arctic spores/pollen. Column for Triassic chart of Mesozoic and Cenozoic sequence chronostratigraphic framework of European basins, by Hardenbol, J., Thierry, J., Farley, M.B., Jacquin, Th., de Graciansky, P.-C., and Vail, P.R. (coordinators). In: de Graciansky, P.-C., Hardenbol, J., Jacquin, Th., and Vail, P.R. (eds), Mesozoic-Cenozoic Sequence Stratigraphy of European Basins, *SEPM Special Publication*, **60**: Chart 8.

Veizer, J., and Prokoph, A., 2015, Temperatures and oxygen isotopic composition of Phanerozoic oceans. *Earth-Science Reviews*, **146**: 92–104.

Veizer, J., Ala, D., Azmy, K., Bruckschen, P., Buhl, D., Bruhn, F., et al., 1999, $^{87}Sr/^{86}Sr$, $\partial^{13}C$ and $\partial^{18}O$ evolution of Phanerozoic seawater. *Chemical Geology*, **161**: 59–88 Datasets available at: <http://www.science.uottawa.ca/geology/isotope_data/>.

Veizer, J., Godderis, Y., and François, L.M., 2000, Evidence for decoupling of atmospheric $CO_2$ and global climate during the Phanerozoic eon. *Nature*, **408**: 698–701.

Visscher, H., 1992, The new STS Triassic stage nomenclature. *Albertiana*, **10**: 1–2.

Visscher, H., and Brügman, W.A., 1981, Ranges of selected palynomorphs in the Alpine Triassic of Europe. *Review of Palaeobotany and Palynology*, **34**: 115–128.

Visscher, H., Van Houte, M., Brugman, W.A., and Poort, R.J., 1994, Rejection of a Carnian (Late Triassic) 'pluvial event' in Europe. *Review of Palaeobotany and Palynology*, **83**: 217–226.

von Alberti, F.A., 1834, *Beitrag zu einer Monographie des Bunter Sandsteins, Muschelkalks und Keupers und die Verbindung dieser Gebilde zu einer Formation*. Stuttgart and Tübingen: Verlag der J.G. Cottaíshen Buchhandlung 326 pp.

von Gümbel, C.W., 1861, *Geognostische Beschreibung des bayerischen Alpengebirges und seines Vorlands*. Perthes: Gotha 950 pp.

von Salis, K., 1998, Calcareous nannofossils. Column for Triassic chart of Mesozoic and Cenozoic sequence chronostratigraphic framework of European basins, by Hardenbol, J., Thierry, J., Farley, M.B., Jacquin, Th., de Graciansky, P.-C., and Vail, P.R. (coordinators). In: de Graciansky, P.-C., Hardenbol, J., Jacquin, Th., Vail, P.R. (eds), Mesozoic-Cenozoic Sequence Stratigraphy of European Basins, *SEPM Special Publication*, **60**: Chart 8.

Vörös, A., Szabó, I., Kovács, S., Dosztály, L., and Budai, T., 1996, The Felsöörs section: a possible stratotype for the base of the Ladinian Stage. *Albertiana*, **17**: 25–40.

Vrielynck, B., 1998, Conodonts. Column for Triassic chart of Mesozoic and Cenozoic sequence chronostratigraphic framework of European basins, by Hardenbol, J., Thierry, J., Farley, M.B., Jacquin, Th., de Graciansky, P.-C., and Vail, P.R. (coordinators). In: de Graciansky, P.-C., Hardenbol, J., Jacquin, Th., Vail, P.R. (eds), Mesozoic-Cenozoic Sequence Stratigraphy of European Basins, *SEPM Special Publication*, **60**: Chart 8.

Vuks, V.J., 2000, Triassic foraminifers of the Crimea, Caucasus, Mangyshlak and Pamirs (biostratigraphy and correlation). *Zentralblatt für Geologie und Paläontologie, I*, **11-12**: 1353–1365.

Vuks, V.J., 2007, New data on the Late Triassic (Norian-Rhaetian) foraminiferans of the western Pre-caucasus (Russia). *New Mexico Museum of Natural History and Science Bulletin*, **41**: 411–412.

Waagen, W., and Diener, C., 1895. Untere Trias. In: Mojsisovics, E., von Waagen, W., Diener, C. (eds), Entwurf einer Gliederung der pelagischen Sedimente des Trias-Systems, *Sitzungberichte Akademie Wissenschaften Wien*, **104**: 1271–1302.

Wallman, K., 2001, The geological carbon cycle and the evolution of marine $\partial^{18}O$ values. *Geochimica et Cosmochimica Acta*, **65**: 2469–2485.

Wang, X.D., Cawood, P.A., Zhao, H., Zhao, L.S., Grasby, S.E., Chen, Z. Q., et al., 2018, Mercury anomalies across the end Permian mass extinction in South China from shallow and deep water depositional environments. *Earth and Planetary Science Letters*, **496**: 159–167. https://doi.org/10.1016/j.epsl.2018.05.044.

Wang, X.D., Cawood, P.A., Zhao, H., Zhao, L.S., Grasby, S.E., Chen, Z. Q., and Zhang, L., 2019, Global mercury cycle during the end-Permian mass extinction and subsequent Early Triassic recovery. *Earth and Planetary Science Letters*, **513**: 144–155. https://doi.org/10.1016/j.epsl.2019.02.026.

Ward, P.D., Haggart, J.W., Carter, E.S., Wilbur, D., Tipper, H.W., and Evans, T., 2001, Sudden productivity collapse associated with the Triassic-Jurassic boundary mass extinction. *Science*, **292**: 1148–1151.

Warrington, G., 2002, Triassic spores and pollen. In: Jansonius, J., McGregor, D.C. (eds), Palynology: principles and applications. 2nd ed., *American Association of Stratigraphic Palynologists Foundation*, **2**: 755–766.

Weems, R.E., and S.G. Lucas. 2015. A revision of the Norian conchostracan zonation in North America and its implication for Late Triassic North American history. In: Sullivan, R.M., Lucas, S.G. (eds), Fossil Record 4, *New Mexico Museum of Natural History and Science Bulletin*, **67**: 303–318.

Whiteside, J.H., Olsen, P.E., Kent, D.V., Fowell, S.J., and Et-Touhami, E., 2007, Synchrony between the Central Atlantic magmatic province and the Triassic–Jurassic mass-extinction event? *Palaeogeography, Palaeoclimatology, Palaeoecology*, **244**: 345–367.

Wignall, P.B., 2001, Large igneous provinces and mass extinctions. *Earth-Science Reviews*, **53**: 1–33.

Wignall, P.B., 2007, The End-Permian mass extinctions – how bad did it get? *Geobiology*, **5**: 303–309.

Wignall, P., 2015, *The Worst of Times: How Life on Earth Survived Eighty Million Years of Extinctions*. Princeton University Press 224 pp.

Wignall, P.B., and Hallam, A., 1992, Anoxia as a cause of the Permo-Triassic mass extinction: facies evidence from northern Italy and the western United States. *Palaeogeography, Palaeoclimatology, Palaeoecology*, **93**: 21–46.

Wing, S.L., and Sues, H.-D., 1992, Mesozoic and early Cenozoic terrestrial ecosystems. *In* Behrensmeyer, A.K., Damuth, J.D., DiMichele, W.A., Potts, R., Sues, H.-D., and Wing, S.L. (eds), *Terrestrial Ecosystems through Time: Evolutionary Paleoecology of Terrestrial Plants and Animals*. Chicago, IL: University of Chicago Press, 324–416.

Wotzlaw, J.-F., Guex, J., Bartolini, A., Gallet, Y., Krystyn, L., McRoberts, C.A., et al., 2014, Towards accurate numerical calibration of the Late Triassic: high-precision U-Pb geochronology constraints on the duration of the Rhaetian. *Geology*, **42**: 571–574.

Wotzlaw, J.-F., Brack, P., and Storck, J.-C., 2018, High-resolution stratigraphy and zircon U–Pb geochronology of the Middle Triassic Buchenstein Formation (Dolomites, northern Italy): precession-forcing of hemipelagic carbonate sedimentation and calibration of the Anisian-Ladinian boundary interval. *Journal of the Geological Society*, **175**: 71–85. https://doi.org/10.1144/jgs2017-052.

Xie, S.C., Pancost, R.D., Wang, Y.B., Yang, H., Wignall, P.B., Luo, G.M., et al., 2010, Cyanobacterial blooms tied to volcanism during the 5 m.y. Permo-Triassic biotic crisis. *Geology*, **38**: 447–450.

Xu, G., Hannah, J.L., Stein, H.J., Bingen, B., Yang, G., Zimmerman, A., et al., 2009, Re–Os geochronology of Arctic black shales to evaluate the Anisian-Ladinian boundary and global faunal correlations. *Earth and Planetary Science Letters*, **288**: 581–587.

Yin, H.F., Zhang, K.X., Tong, J.N., Yang, Z.Y., and Wu, S.B., 2001, The Global Stratotype Section and Point (GSSP) of the Permian-Triassic boundary. *Episodes*, **24**: 102–114.

Yin, H.F., Tong, J.N., and Zhang, K.X., 2005, A review of the global stratotype section and point of the Permian-Triassic boundary. *Acta Geologica Sinica*, **79**: 715–728.

Yin, H.F., Feng, Q., Xie, S., Yu, J., He, W., Liang, H., et al., 2007a, Recent achievements on the research of the Paleozoic–Mesozoic transitional period in South China. *Frontiers of Earth Science in China*, **1**: 129–141.

Yin, H.F., Yang, F.Q., Yu, J.X., Peng, Y.Q., Zhang, S.X., and Wang, S. Y., 2007b, An accurately delineated terrestrial Permian–Triassic Boundary and its implication. *Science in China, Series D: Earth Sciences*, **50**: 1281–1292.

Yu, J.X., Broutin, J., Chen, Z.Q., Shi, X., Li, H., Chu, D.L., and Huang, Q.S., 2015, Vegetation changeover across the Permian-Triassic Boundary in Southwest China. *Earth-Science Reviews*, **149**: 203–224. https://doi.org/10.1016/j.earscirev.2015.04.005.

Zaffani, M., Jadoul, F., and Rigo, M., 2018, A new Rhaetian $\delta^{13}C_{org}$ record: carbon cycle disturbances, volcanism, End-Triassic mass Extinction (ETE). *Earth-Science Reviews*, **178**: 92–104.

Zakharov, Y.D., 1994, Proposals on revision of the Siberian standard for the Lower Triassic and candidate stratotype section and point for the Induan–Olenekian boundary. *Albertiana*, **14**: 44–51.

Zakharov, Y.D., Shigata, Y., Popov, A.M., Sokarev, A.N., Buryi, G.I., Golozubov, V.V., et al., 2000, The candidates of global stratotype of the boundary of the Induan and Olenekian stages of the Lower Triassic in Southern Primorye. *Albertiana*, **24**: 12–26.

Zakharov, Y.D., Shigeta, Y., Popov, A.M., Buryi, G.E., Oleinikov, A.V., Dorukhovskaya, E.A., et al., 2002, Triassic ammonoid succession in South Primorye: 1. Lower Olenekian *Hedenstroemia bosphorensis* and *Anasibirites nevolini* Zones. *Albertiana*, **27**: 42–64.

Zakharov, Y.D., Shigeta, Y., and Igo, H., 2009, Correlation of the Induan-Olenekian boundary beds in the Tethys and Boreal realm: evidence from conodont and ammonoid fossils. *Albertiana*, **37**: 20–27.

Zapfe, H., 1974, Die Stratigraphie der Alpin-Mediterranen Trias. *Schriftenreihe der Erdwissenschaftlichen Kommissionen, Österreichische Akademie der Wissenschaften*, **2**: 137–144.

Zhang, L., Orchard, M.J., Brayard, A., Algeo, T.J., Zhao, L.S., Chen, Z.-Q., et al., 2019, The Smithian/Spathian boundary (late Early Triassic): a review of ammonoid, conodont, and carbon-isotopic criteria. *Earth-Science Reviews*, **195**: 7–36. https://doi.org/10.1016/j.earscirev.2019.02.014.

Zhang, Y., Li, M.S., Ogg, J.G., Montgomery, P., Huang, C., Chen, Z.Q., et al., 2015, Cycle-calibrated magnetostratigraphy of middle Carnian from South China: implications for Late Triassic time scale and termination of the Yangtze Platform. *Palaeogeography, Palaeoclimatology, Palaeoecology*, **436**: 135–166. http://dx.doi.org/10.1016/j.palaeo.2015.05.033.

Zhang, Y., Ogg, J.G., Franz, M., Bachmann, G.H., Szurlies, M., Röhling, H.-G., et al., 2020, Late Triassic magnetostratigraphy from the Germanic Basin and the global correlation of the Carnian Pluvial Episode. *Earth and Planetary Science Letters*, **541**, article #116275: 15 pp. https://doi.org/10.1016/j.epsl.2020.116275.

Zhao, L.S., Orchard, M.J., Tong, J.N., Sun, Z.M., Zuo, J., Zhang, S., et al., 2007, Lower Triassic conodont sequence in Chaohu, Anhui Province, China and its global correlation. *Palaeogeography, Palaeoclimatology, Palaeoecology*, **252**: 24–38. http://dx.doi.org/10.1016/j.palaeo.2006.11.032.

Zhao, L.S., Tong, J.N., Sun, Z.M., and Orchard, M.J., 2008, A detailed Lower Triassic conodont biostratigraphy and its implications for the GSSP candidate of the Induan-Olenekian boundary in Chaohu, Anhui Province. *Progress in Natural Scienc*, **18**: 79–90.

Zhao, L.S., Chen, Y.L., Chen, Z.Q., and Cao, L., 2013, Uppermost Permian to lower Triassic conodont zonation from Three George area, South China. *Palaios*, **28**: 509–522. http://dx.doi.org/10.2110/palo.2012.p12-107r.

Zhu, Z.C., Liu, Y.Q., Kuang, H.W., Benton, M.J., Newell, A.J., Xu, H., et al., 2019, Altered fluvial patterns in North China indicate rapid climate change linked to the Permian-Triassic mass extinction. *Science Reports*, **9**: 16818. https://doi.org/10.1038/s41598-019-53321-z.